COMPUTATIONAL THERMODYNAMICS OF
CoNiGa HIGH TEMPERATURE SHAPE MEMORY ALLOYS

A Thesis

by

ARPITA RAMESH CHARI

Submitted to the Office of Graduate Studies of
Texas A&M University
in partial fulfillment of the requirements for the degree of

MASTER OF SCIENCE

August 2011

Major Subject: Mechanical Engineering

COMPUTATIONAL THERMODYNAMICS OF
CoNiGa HIGH TEMPERATURE SHAPE MEMORY ALLOYS

A Thesis

by

ARPITA RAMESH CHARI

Submitted to the Office of Graduate Studies of
Texas A&M University
in partial fulfillment of the requirements for the degree of

MASTER OF SCIENCE

Approved by:

Chair of Committee,	Raymundo Arroyave
Committee Members,	Ibrahim Karaman
	Tahir Cagin
Head of Department,	Dennis O'Neal

August 2011

Major Subject: Mechanical Engineering

ABSTRACT

Computational Thermodynamics of
CoNiGa High Temperature Shape Memory Alloys. (August 2011)
Arpita Ramesh Chari, B.E., M.S.Ramaiah Institute of Technology
Chair of Advisory Committee: Dr. Raymundo Arroyave

Shape Memory Alloys (SMAs) are advanced materials with interesting properties such as pseudoelasticity (PE) and the shape memory effect (SME). Recently, the CoNiGa system has emerged as the basis for very promising High Temperature Shape Memory Alloys (HTSMAs),with possible applications in the aerospace and automotive industries. Although the CoNiGa system shows significant promise for it's use as HTSMAs, limited studies are available on them. Hence, a more intensive investigation of these alloys is necessary to understand their phase stability over a wide range of temperature and compositions in order for further development of CoNiGa-based HTSMAs and future use of the model in alloy design. This formed the basis of motivation for the present work.

In this work, a thermodynamic model of the ternary system is calculated based on the CALPHAD approach, to investigate the thermodynamic properties, phase stability and shape memory properties of these alloys. The CALPHAD approach is a computational method that enables the calculations of thermodynamic properties of systems. This method uses all available experimental and theoretical data in order to calculate the Gibbs energies of the phases in the system. The software used to carry out the calculations is "ThermoCalc", which is a computational software using CALPHAD principles, based on the minimization of Gibbs energy, and is enhanced by a global minimization technique on the system. The stability of the β phase at high temperatures was enforced accurately by remodeling the CoGa system. The binary

CoGa system that makes up the ternary was remodeled, as the β phase (which is very important as it dominates the central region of the ternary CoNiGa system where the shape memory effect is observed), re-stabilizes as the temperature increases above the liquidus in the CoGa system.

Phase relations and thermodynamic properties of the CoNiGa system based on all experimental information were evaluated. Different properties like enthalpies, activities, sublattice site fraction of vacancies and phase fractions calculated in the system matched well compared to the experimental information used to model the system. Also, the phase equilibria among the γ (fcc), β, γ' (Ni_3Ga), δ (Ni_5Ga_3) and ϵ ($Ni_{13}Ga_9$) were determined at various temperatures.

To Mom, Dad and Rach

ACKNOWLEDGMENTS

I would like to thank Dr. Raymundo Arroyave, my professor, mentor and guide, for this wonderful experience of doing thermodynamics materials research, and for giving me the opportunity to learn in our Computational Materials Science group. My learning curve has been increased exponentially since I started working under him. I thank him for his patience and help throughout my master's studies. I would not have been able to finish writing my thesis on time, if not for his timely replies to all the countless number of emails I sent to him for approvals and advice on my thesis and paper, when I was away on my internship overseas. It has been a rough, albeit enlightening journey of pursuing my masters. For this, I would like to thank my husband Rachith for putting up with me when I stayed away from him for almost a year after being married. I really appreciate the support I got from him through the difficult times of being away from my home in India for the first time. Thanks for everything Rachith, I couldn't have done this without you. I thank my parents for their unconditional love and support and for being there for me every step of the way. Without them, I would not be where I am today. I am grateful to God for everything he has given me, for I have learned and matured as a human being in the last 3 years.

TABLE OF CONTENTS

CHAPTER Page

LIST OF TABLES

LIST OF FIGURES

FIGURE Page

CHAPTER I

INTRODUCTION

Shape Memory Alloys (SMAs) are advanced materials with interesting properties such as pseudoelasticity (PE) and the shape memory effect (SME). The most widely used alloys are NiTi (Nickel - Titanium), CuZnAl, CuAlNi [1] and more recently, CoNiGa (this work). The unique properties of these alloys are due to a solid-state phase transformation, which results in a short- range atomic rearrangement leading to structural (martensitic) transformations. SMAs are unique in that they are able to produce very high recoverable shape changes that can be brought about by changes in temperature, stress or magnetic fields. Their distinct shape memory properties (in some cases accompanied by significant pseudoelastic behavior) make SMAs very attractive functional materials widely used in the aerospace and medical device industries, as well as in more general applications in which the SM effect is used for the purposes of sensing and/or actuating. Recently, the CoNiGa system has emerged as the basis for very promising High Temperature Shape Memory Alloys (HTSMAs) [2, 3].

Compared to other systems such as NiTi based alloys, the CoNiGa was chosen because they can be made more ductile with the precipitation of γ phase [4–6] and show higher PE. CoNiGa is a potential HTSMA due to its use at temperatures above 200 °C [7, 8], PE upto 450 °C [7], stability over a wide range of stress and temperature [4, 9] among others. An ideal HTSMA should have high martensitic transformation (M_s), good ductility, low cost, resistance to oxidation, etc and if the ternary CoNiGa alloy is properly designed, then it is possible to achieve most of the above characteristics, if not all.

This thesis follows the style of the journal model CALPHAD:Computer Coupling of Phase Diagrams and Thermochemistry.

Although the CoNiGa system shows significant promise for it's use as HTSMAs, limited studies are available on them. Hence a more intensive investigation of these alloys is necessary to understand their phase stability over a wide range of temperature and composition in order for further development of CoNiGa-based HTSMAs and future use of the model in alloy design.

In the present work, the thermodynamic model of the ternary CoNiGa Shape Memory Alloy has been calculated using the CALPHAD (CALculation of PHase Diagrams) method.

The CALPHAD approach is a computational method that enables the calculations of thermodynamic properties of systems [10]. This method uses all available experimental and theoretical data in order to calculate the Gibbs energies of the phases in the system. Phase equilibrium is defined by a minimum of the Gibbs Energy of all the phases that are taking part in the equilibrium process. When a system reaches the equilibrium condition at constant pressure and temperature, it is said to have attained a minimum in its Gibbs Energy. The calculated results when combined with experimental data in this approach, provide a much better description of the model which later becomes useful in applications with required levels of accuracy. The technique is useful when there are many components involved as it provides consistent results.

The phases that dominate the ternary at higher temperatures are β (B2), γ (L12) (ductile phase) and the γ' (hard precipitates) phases. These phases are found in different amounts in the ternary and vary according to composition of the combining elements of the ternary and temperature.

The elements that make up this ternary HTSMA are Co, Ni and Ga. The symmetry of a system is described by the space group. There are 230 space groups that are ordered according to crystal structure. The cell parameters are the dimensions of the lattice (3-D arrangement of atoms in a periodic manner in a cell) in terms of lengths of axes of the unit cell and angles in between them.

The crystal structure of the three elements in the ternary is as summarized in Table I [11].

The crystal structure of the cell is important to model the Gibbs energies of the system. Each set of atoms in a cell that are at equivalent positions can be considered a sublattice. Crystal structures with multiple sublattices can be modeled using the sublattice formalism where the phase constitution is represented by distinct sublattices. Here, mutually soluble elements can combine on the distinct sublattices that make up the structure, thus allowing extrapolation to higher order systems.

The structure of a simple cubic sublattice structure is shown in Fig. 1 [12].

A. Structure of thesis

The thesis has been divided into 7 chapters in this order: Introduction, Literature review of Shape Memory Alloys, CALPHAD approach, Calculation of thermodynamic properties in the NiGa system, Thermodynamic remodeling of the CoGa system, Thermodynamic modeling of the CoNiGa system, Conclusions.

Chapter II gives a brief summary on the literature review of SMAs including the important properties they exhibit.

Chapter III outlines the basic principles in the CALPHAD approach.The CALPHAD technique combines the basic principles of thermodynamics with mathematical formulations in order to describe the thermodynamic properties of the different phases in a system. With this approach, it is possible to predict stabilities and calculate equilibria of phases in alloys [10]. Thermodynamics defines the state of a system subject to external constraints, once it reaches equilibrium. The equilibrium state

Table I.: Crystal structure of Co, Ni and Ga in the ternary CoNiGa System

Element	Space Group	Structure	Cell Parameters					
			a	b	c	α	β	γ
Cobalt	P63/mmc	hcp	250.71 pm	250.71 pm	406.95 pm	90°	90°	120°
Nickel	Fm3m	ccp	352.4 pm	352.4 pm	352.4 pm	90°	90°	90°
Gallium	Cmca	ort	451.97 pm	766.33 pm	452.6 pm	90°	90°	90°

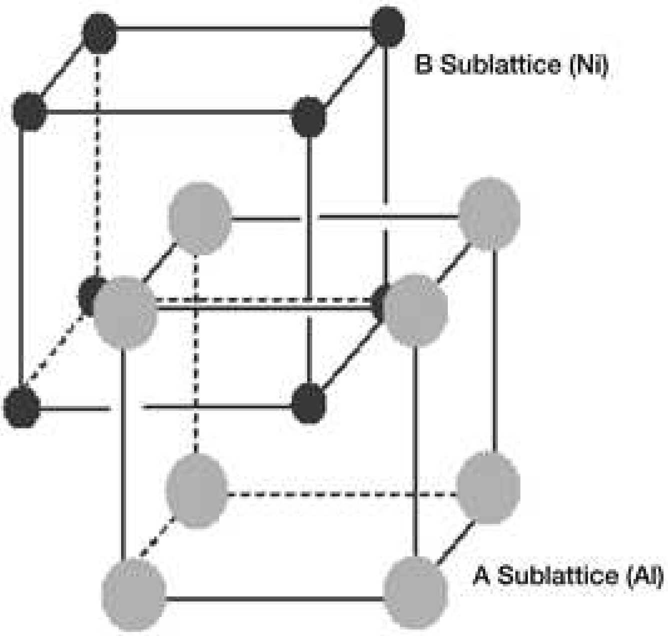

Fig. 1.: Structure of simple cubic interpenetrating sublattices of B2 (NiAl taken as an example). [12]

of a system is calculated by minimization of a state function called Gibbs Energy, which depends on the external conditions imposed on the system. The CALPHAD method is adopted to calculate/model the Gibbs free energies which can then be used to calculate the thermodynamic properties of several materials. The technique is also useful for a system that needs an accurate thermodynamic description. For the simulations that are hence carried out, experimental data like fractional components of phases and components, energies of states, enthalpies, activities, etc., are used.

Chapter IV describes the calculation of thermodynamic properties in one of the binary systems that make up the ternary CoNiGa system, which is the NiGa system. The phase stability of the NiGa system throughout the composition range via *ab initio* methods have also been investigated in this work. The ground state of the NiGa binary was determined through a DFT-based high-throughput ground state search [13] over hundreds of possible binary crystal structures. The NiGa system is of considerable importance due to its use in CoNiGa as High Temperature Shape Memory Alloys(HTSMAs). The two phases chosen for this study were the β (B2) and γ (L12) phases. The β phase dominates the central region of the ternary (and is the one that undergoes the martensitic transformation) and the cubic L12 structure has been known to increase ductility [4–6]in the ternary. From the studies, it shows that the γ phase increases ductility if it precipitates along grain boundaries. L12 phase is a hard intermetallic that can be used to reduce the hysteresis of the transformation as the γ phase is too soft and without L12 it would dissipate a lot of energy during the austenite-martensite transformation of the β phase. In order to study the thermodynamic properties in this system which will then help to better understand the ternary, finite temperature thermodynamic properties were calculated using lattice dynamics of B2 and L12 phases in NiGa.

The low temperature phase study and ground state calculations is a paper that will be published and due recognition is given to Avinash Chivukula and Professor Stefano Curtarolo [14] at Duke University for their contribution to this work.

Chapter V gives an outline on the remodeling of the CoGa system, one of the other binary systems that make up the ternary. The focus in the study was to overcome the limitations found in previously developed models for the CoGa system, especially with regards to the stability of the β phase. The correct description of the β phase is very important, as it dominates the central region of the ternary CoNiGa system where the shape memory effect is observed [3]. An accurate thermodynamic model for the CoGa system is essential for the development of reliable thermodynamic descriptions of the CoNiGa ternary.

Chapter VI, the most important chapter in this thesis, illustrates the computational design of the ternary CoNiGa system using the CALPHAD approach coupled with experimental work. Limited experimental information is available for this system for a wide range of composition, and temperature regions [4, 5, 9] A reliable and consistent thermodynamic model of the CoNiGa system has not been calculated using a computational approach thus far, and it would be useful to have a complete description of phase stability over a wide range of compositions and temperatures. The main aim of this work is to develop a model for the Shape Memory Alloy with accurate descriptions of the Gibbs energies of its phases. This system should then be able to demonstrate required characteristics such as perfect Shape Memory Effect(SME) and pseudoelasticity (PE) for temperatures of 500 °C and above, have a broad range of M_s temperatures, high Curie Temperature (T_c) and provide a better understanding of how the martensitic transformation temperature M_s changes with composition. The ternary model developed was then used to calculate isothermal sections at various temperatures, activities, enthalpy of formation and vertical sections. Experiments were conducted to corroborate the results obtained from the calculated thermodynamic model. It has been shown that the ductility of the brittle CoNiGa β alloys can be improved by the addition of the γ (fcc) phase [4]. Hence, the study of the stability of the β phase (which undergoes the martensitic transformation in the ternary and has a wide range of stability in the NiGa and CoGa binaries), along with the existence of the two-phase $\beta + \gamma$ equilibrium in the Co-rich and Ni-rich regions in the binaries, is important in this investigation in order for the ternary alloy system to be used as a ductile ferromagnetic Shape Memory Alloy.

In order to validate the thermodynamic model of the ternary developed in this work, experimental studies were also performed by Dr. Karaman's group. Different alloy buttons of varying compositions (taken from different regions of the ternary) were prepared. The experimental results were then compared to the results obtained from the ternary model to corroborate the latter, and this has been described in Chapter VI as well.

Lastly, Chapter VII summarizes the conclusions and overall results of the present work. Thermodynamic properties like enthalpies, activities, phase fractions, site fractions of vacancies in the β phase, etc were calculated and compared with experimental data. The results compared well with the experimental data used, thus corroborating the present work. The same defect structure of the β phase in the binary CoGa and NiGa systems was used in the ternary. Similar results while calculating site fractions of vacancies were obtained in the ternary when compared to the binary systems, giving rise to a speculation that point defects exist in the ternary as well.

CHAPTER II

LITERATURE REVIEW OF SHAPE MEMORY ALLOYS

A. Introduction

Shape Memory Alloys (SMAs) are advanced materials with interesting properties such as PseudoElasticity (PE) and the Shape Memory Effect (SME). The most widely used alloys are NiTi (Nickel - Titanium), CuZnAl, and CuAlNi [1] The unique properties as mentioned, are due to a solid-state phase transformation, resulting in a short-range molecular rearrangement, leading to martensitic transformation. What makes SMAs unique is that they are able to produce very high recoverable shape changes that can be brought about by changes in temperature, stress or magnetic fields.

There are two phases seen in SMAs - Martensite and Austenite. Martensite is the low temperature, lower symmetry phase and austenite is the high temperature phase with a cubic crystal structure (as seen to the left of Fig. 2 [15]). In most cases this cubic crystal structure is seen, although this is not universal. What is truly universal is that the austenite phase has a higher symmetry than martensite. In Fig. 2 we see a *twinned* molecular structure of martensite. In the CoNiGa SMA, martensite has a BCT (Body Centered Tetragonal) crystal structure.

Martensitic transformation is a diffusionless transformation which involves the movement of atoms over short distances (which are less than their inter-atomic distances) with a shear-like mechanism. Martensitic transformation occurs due to a cooperative movement of atoms and hence also known as military or displacive transformation [16]. In order to fully understand the Shape Memory Effect and PseudoElasticity that are seen in SMAs, it is important to know the process of martensitic transformation. SME and PE effects are clearly observed in SMAs due to a macro-

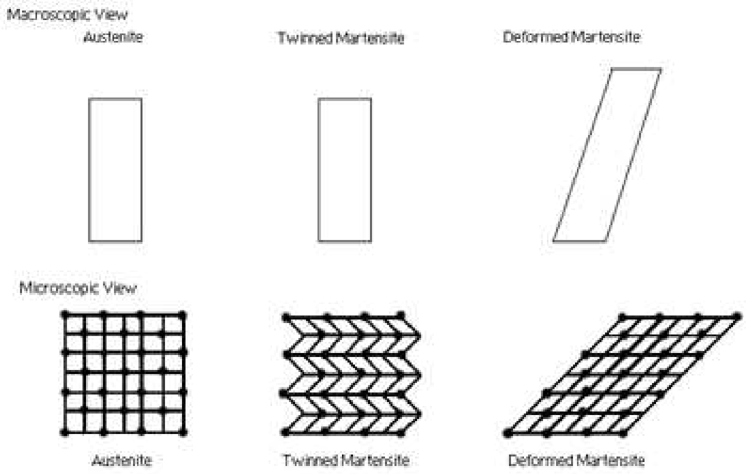

Fig. 2.: Microscopic and macroscopic views of the two phases of Shape Memory Alloys. [17]

scopic shape change that occurs as a result of martensitic transformation.

The shear-like movement of atoms in martensitic transformation starts when the temperature of the parent phase is lowered below a critical temperature. This is called the martensitic start temperature (M_s). A model depicting the martensitic transformation is as shown in Fig. 3 [16]. Here we see that the atoms in region A and B which are displaced due to shear, have the same crystal structure but different orientations. These are called variants of the martensitic phase and since martensite has a lower symmetry, many variants can exist in the parent phase. Reverse martensitic transformation occurs when the temperature is increased and martensite becomes unstable.

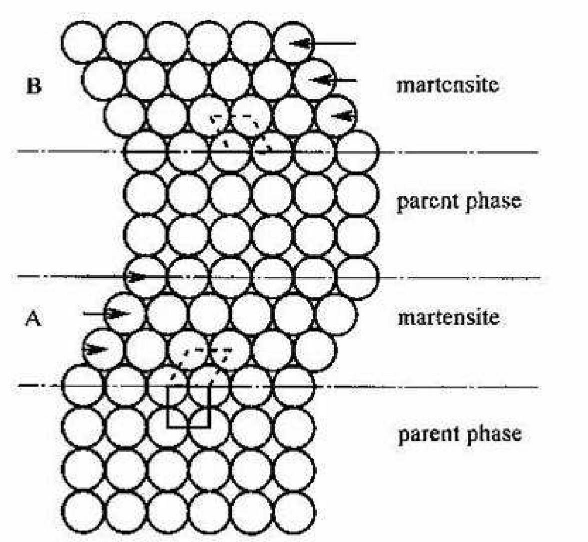

Fig. 3.: Model depicting martensitic transformation. [16]

B. Transformation temperatures

The four characteristic temperatures that are involved in a thermoelastic martensitic transformation are:

- The martensite start temperature, M_s, is the temperature when martensite first appears in the austenite, i.e., when the parent austenite becomes mechanically unstable. At a constant temperature below M_s, a fraction of the parent austenite transforms to martensite, after which there is no further transformation.
- A_s the martensite is cooled further, the transformation continues till the martensite finish temperature M_f. Below M_f, the whole specimen is in the martensite phase, and it consists of many regions that have a different variant of martensite.

- The austenite start temperature, A_s, is the temperature at which austenite first appears in the martensite. By heating the specimen further, the remaining martensite transforms into austenite.
- The reverse transformation is complete at the austenite finish temperature, A_f.

1. Differential Scanning Calorimetry (DSC)

Differential scanning calorimetry is a technique that is used to measure the transformation temperatures of the Shape Memory Alloy.

In this method, the Shape Memory Alloy in the twinned martensitic state, is heated to begin the transformation to austenite at A_s. This reaction is endothermic, i.e., during the reverse transformation, additional heat is supplied to the specimen so that the prescribed constant heating rate is maintained. This heat supplied is seen as a transformation "peak" during heating, as shown in Fig 4 [17]. A similar peak is seen during the cooling process during which the exothermic transformation takes place from austenite to martensite. The transformation temperatures from the data are computed by drawing tangents to the start and end regions of the peaks and the baseline of the heating and cooling curves. This is shown in the figure below [17]. These temperatures are significantly affected by stored mechanical energy (precipitates, dislocations produced by cutting, detwinning, etc), and hence, the initial state of the material is very important.

Shape Memory Alloys show a hysteresis of strain upon heating and cooling through the transformation temperatures. Plotting strain vs. temperature during forward and reverse transformation also helps to determine the four characteristic transformation temperatures [Fig. 5]. These property changes with temperature can also be used to determine the fraction of a phase that has transformed [17].

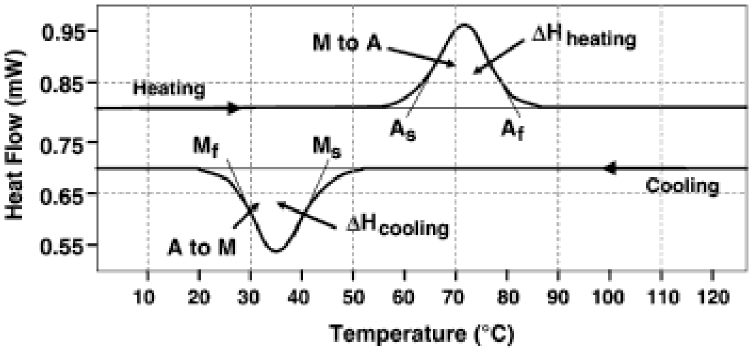

Fig. 4.: Typical DSC curve for a Shape Memory Alloy. Note that the transformation temperatures are measured from this data. [17]

2. Lattice Invariant Shear Mechanisms

The transformation from austenite to martensite is a diffusionless transformation that takes place by shear distortion of the lattice structure. What makes this martensitic transformation different from other transformations is that it possesses well-defined characteristics. Within a single crystal, i.e., single grain in a polycrystalline material, the shear distortion occurs along a specific plane called the habit plane, which is the interface between the martensitic and the austenitic phases. The habit plane does

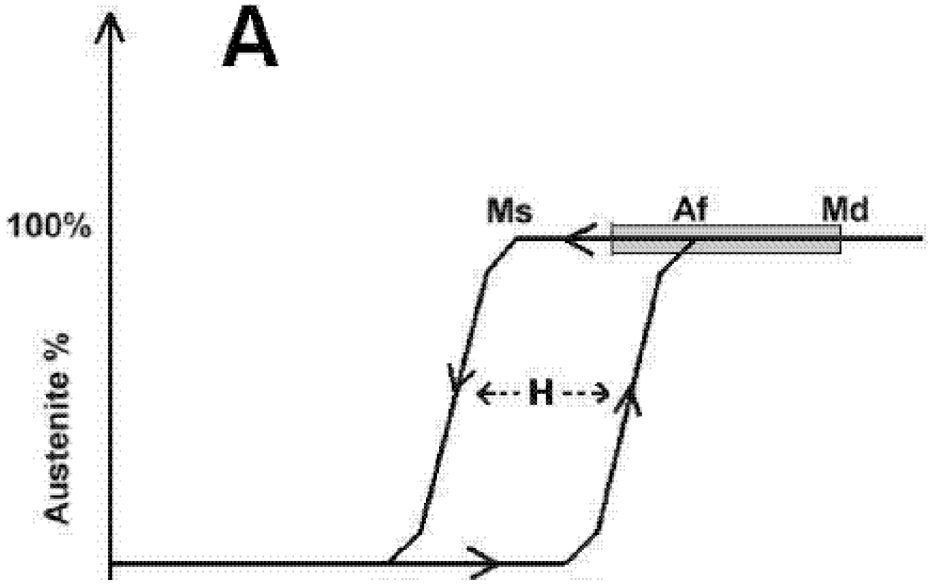

Fig. 5.: Transformation temperature as seen from the temperature-strain plot. [17]

not deform during the process of the transformation, and hence it is also called the "lattice invariant plane" [17].

As martensitic transformation occurs due to a shape change, strains develop around the regions of the martensite formation. In order to reduce these induced strains, it is necessary to introduce slip or twins along the habit plane. These mechanisms are called lattice invariant shear mechanisms [16]. Slip is a process by which atoms move by one or more atomic space and twinning is a mirror symmetry displacement of atoms across a particular atom plane called the twinning plane. In SMAs, twinning is the most common mechanism of lattice invariant shear [16].

Shape Memory Alloys are capable of recovering from large amounts of bending and torsional deformations as well as small amounts of strain. As long as these deformations are within recoverable ranges, the process of deformation and shape recovery can be repeated millions of times.

C. Superelasticity or PseudoElasticity (PE)

Pseudoelasticity is the ability of a material to exhibit large recoverable strains when deformed within a range of temperatures, and this property is a characteristic of this particular type of alloys. The superelastic effect is a stress-induced transformation, which leads to a strain recovery on loading and unloading. Strains of up to 12% are seen in superelastic response of Shape Memory Alloys [18] before plastic deformation can be seen. This is much higher in comparison to materials like stainless steel or even aluminum. This strain is completely recovered on unloading and so this phenomenon is also called pseudoelastic effect. A superelastic loading generally starts at a temperature higher than A_f and is done at a constant temperature where the starting phase is austenite. This process is a stress-induced phase transformation, where the initially austenitic SMA transforms to martensite on loading it beyond a particular stress level. On reversal of the direction of loading (i.e. unloading) the martensite transforms back into austenite.

It can be seen that the superelastic response has two predominant effects, which can be seen in Fig. 6. One is the flat plateau, which corresponds to the large deformation under a minor change in stress and the other one is the hysteresis that is observed while loading and unloading. Though the strain is completely recovered, it is done so with a hysteretic energy loss and this energy loss can be used for a variety of applications, particularly in damping [19]. The hysteresis that is observed is basically a dissipation of energy by the Shape Memory Alloy. This dissipation can be used to dampen out vibrations by absorbing the vibrational energy in, say a structure, and dissipating away as heat thus reducing the energy content in the vibrating member, thus reducing the vibration as such.

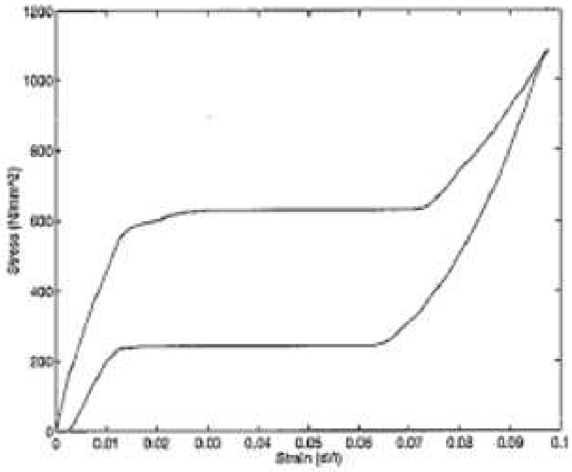

Fig. 6.: The experimental piecewise linear approximation of a superelastic SMA stress-strain response. Notice the hysteresis that is observed, though strain is completely reversed. [19]

D. Shape Memory Effect (SME)

This effect is seen as a result of a reversible phase transformation occurring in the solid state from martensite to austenite. Although there are various orientations that martensite can form upon cooling from austenite [20], there is only one preferred variant which grows at the expense of the others. This is due to crystallographic limitations that permit the formation of the variant only if the strain direction is parallel to the tensile axis, resulting in maximum elongation.

The shape memory effect is observed when the SMA is deformed in the twinned martensite state and then heated beyond the temperature A_s. The shape memory effect is a response of heat stimulus, although this effect can also be activated through the application of stress or magnetic field (in the particular case of ferromagnetic SMAs). Starting from the austenite state and cooling below M_f reach the twinned martensite state. On applying a stress, the twinned martensite deforms elastically and when the applied stress reaches , certain variants of the martensite phase start to grow, and at a stress , the detwinning process is complete. On unloading from this stress, the material shows a permanent deformation. It is to be noted that the stress is far lower than the stress required for the plastic deformation of the martensite phase [17]. On heating the specimen above the temperature A_f, it recovers the strain completely, thus reverting back to its original shape. It is to be noted that cooling the SMA to get another shape is not seen if the wire is a one-way Shape Memory Alloy. Fig. 7 shows schematically, a thermo-mechanical cycle that is typical of one-way shape memory effect [17] and Fig. 8 shows the microstructure variations during SME [21].

The strain that is recovered in such a process is called the transformation strain (ϵ_t). In the absence of permanent plastic strain, the original shape is completely recovered. This entire phenomenon is termed as one-way shape memory effect since the direction of recovery is one-way (only while heating). Typical transformation strains in such shape memory responses are of the order of 4% [17].

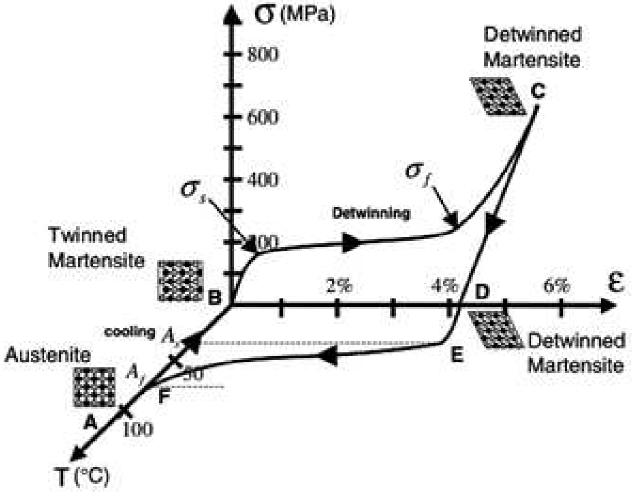

Fig. 7.: Shape memory effect in Shape Memory Alloys. Notice that typical strain recovery is of the order of 4%. [17]

E. Motivation and Background

The system under study is the CoNiGa system which is being used as a High Temperature Shape Memory Alloy (HTSMA). The primary applications are in those fields where the M_s temperatures are between 100-250 °C. These magnetic Shape Memory Alloys have a good ductility and is less costly when compared to NiTi alloys [2,3].

This system is chosen as it has high M_s, pseudoelasticity at high temperatures, wide range of composition of the beta phase exhibiting ductility in the binary CoGa and NiGa systems and the presence of $\beta+\gamma$ equilibrium in the Co-rich and Ga-rich

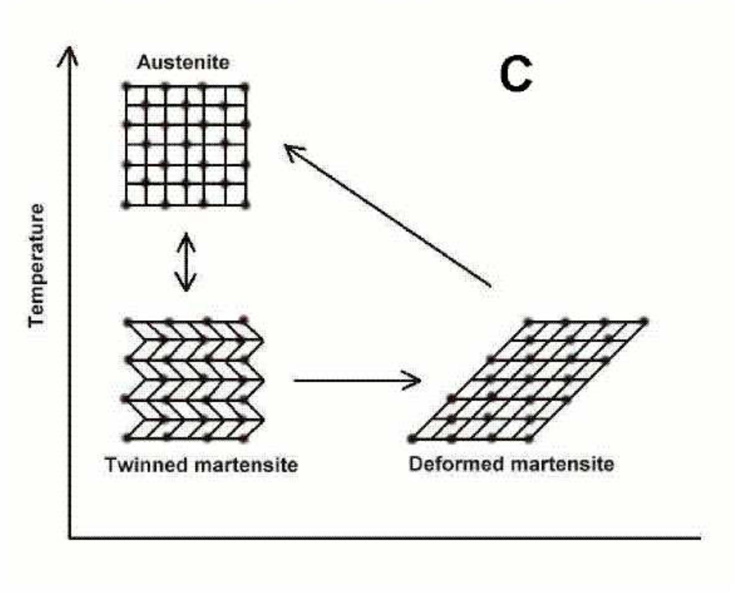

Fig. 8.: The microstructure variations during shape memory effect. Note that the twinned martensite phase is reached by cooling the austenite and that heating from the deformed martensite leads to the ordered austenite state. [21]

regions, when compared to CoNiAl alloys.

Phase stability of the CoNiGa system is of prime importance as the behavior of the alloy depends on the microstructural composition which can vary drastically with temperature. An ideal HTSMA has high M_s, good ductility including formability, low cost and resistance to structural and functional fatigue, oxidation, plasticity and creep during operation [2, 3]. The CoNiGa Shape Memory Alloy is believed to have several of these properties if they are designed well.

Information on the microstructure of the phases present in this system has not been extensively studied in the past which makes it all the more necessary to get a better understanding of these materials for high temperature applications. The

CALPHAD approach has been used in this work in order to model the system. This approach helps in evaluating the system parameters for the Gibbs energies of all the phases in the system, by applying thermodynamic optimization of the data. The model developed will then be used to find compositions and temperatures of the precipitates. This is verified with experimental results and refined to produce a better description of the phases.

CHAPTER III

THE CALPHAD APPROACH

A. Introduction

The CALPHAD technique (CALculation of PHAse Diagrams), combines the basic principles of thermodynamics with mathematical formulations in order to describe the thermodynamic properties of the different phases in a system. With this approach, it is possible to predict stabilities and calculate equilibria of phases in alloys [10]. This method is adopted to calculate/model the Gibbs free energies which can then be used to calculate the thermodynamic properties of several materials. The technique is also useful for a system that needs an accurate thermodynamic description. For the simulations that are hence carried out, experimental data like fractional components of phases and components, energies of states, enthalpies, activities, etc., are used to fit the model parameters used to describe the Gibbs energies of the phases. [22]

Phase equilibrium is defined by a minimum of the Gibbs Energy of all the phases that are taking part in the equilibrium process, given by:

$$G = \sum_{i=1}^{p} n_i G_i^{\phi} = minimum \tag{3.1}$$

where n_i is the number of moles and G_i^{ϕ} is the Gibbs energy of the phase i.

When a system reaches the equilibrium condition at constant pressure and temperature, it is said to have attained a minimum in its chemical potential, also known as Gibbs Energy. The CALPHAD method uses all data available from experimental procedures as well as theoretical data in order to model the parameters for the Gibbs energy functions for each phase. The calculated results when combined with experimental data in this approach, provide a much better description of the model which later becomes useful in applications with required levels of accuracy. The technique is useful when there are many components involved as it provides consistent results. The CALPHAD technique helps to provide an overall consistent description of all the phases in the system, with reliable accuracy.

For multicomponent systems, the Scientific Group Thermodata Europe (SGTE) define Gibbs Energy as a power series of T [10]. This refers to the need to have a common reference state so that the models are consistent:

$$G_m(T) - H_m^{SER} = a + bT + cTln(T) + \sum_{2}^{n} d_n T^n \tag{3.2}$$

The left hand side of Eq. (3.2)is the Gibbs energy relative to a standard reference state of the element (SER). H_m^{SER} is the enthalpy of the element in its reference state at 298.15 K.

a, b, c, d are co-efficients and n is a set of integers with values of 2,3, -1.

B. Methodology

Data obtained from experiments relating the structure of the system, thermodynamics and phase equilibria are described using a mathematical model. The parameters in the Gibbs energy functions that are used to describe such a model are then found by optimization procedures, where error between experimental and calculated results are minimized. The models developed can be used to extrapolate to higher order systems in multi-component alloys. They help in determining the thermodynamic properties of the system in order to calculate the phase diagram accurately. There are several computational software available today to help in thermodynamic modeling, one of which is ThermoCalc, and is used in the present work.

C. Thermodynamic modeling of the phases

1. Stoichiometric compounds

Stoichiometric compounds are those in which the composition of the elements that make up the substance are represented by whole numbers. For such compounds, the Gibbs energy function is given by [10]:

$$G_{(T,P)} = H_{(T,P)} - TS_{(T,P)} \tag{3.3}$$

where H and S is the enthalpy and entropy, which are functions of temperature and pressure.

2. Solution and compound phases

Thermodynamic calculations of complex systems involving stoichiometric as well as non-stoichiometric substances involves the solubility of various elements in the phases.

Solution phases are those in which allow the solubility of more than one compound. There are four types of solution phases [10]:

1. Random substitutional phases
2. Sublattice phases
3. Ionic phases
4. Aqueous phases

The Gibbs energy function for these phases is given by Eq. (3.4) [10]:

$$G = G^0 + G_{mix}^{ideal} + G_{mix}^{xs} \tag{3.4}$$

where G^0 is the contribution of the pure components of the phase, G_{mix}^{ideal} is the contribution from ideal mixing and G_{mix}^{xs} is contribution due to non-ideal interactions between the compounds, giving rise to excess energy of mixing. The last two terms on the right hand side of the equation depend on site occupation by the components on the sublattices and not on the global concentration of the components.

The first two types of phases will be described in detail in this section as they are of importance in the modeling procedure carried out in the present work. The ionic model for phase description is used for liquids such as slags, molten salts, etc which need more number of co-efficients to describe the changes in enthalpy at the critical compositions. Although many models have been suggested in the past to model ionic solutions, the most important ones that have been successful to describe multicomponent systems are the following [10]:

1. Cellular model
2. Modified quasichemical model
3. Sublattice model
4. Associated solution model

Aqueous solutions are dilute solutions and the models developed for these phases have been used for the development in areas such as corrosion and geochemistry. Instead of defining units in terms of mole fractions, as is done in all the other models described so far, the aqueous solution model uses units of molarity and molality. The extended UNIQUAC model has been used to model aqueous solutions of electrolytes and non-electrolytes. The parameters optimized in this model lie within the temperature range of freezing point and boiling point of the solutions. The model is an example of achieving high accuracy of calculations when compared to experimental data [10].

a. Random substitutional phases

Here, there is a random occupation of alloys on the sites and it is generally considered to be a single-sublattice phase. Examples of this type of phase is a gas phase or a simple solid solution, where the atomic positions are not position specific and there is no 'preferred' site occupation by the atoms. They can be classified as follows [10]:

1. Dilute solutions
2. Ideal solutions
3. Non-Ideal solutions

The dilute solution model has fewer practical applications due to limitations over a wider range of compositions. In the ideal solution model, the atoms randomly distribute in the lattice sites and the interchange energy between them is zero. Hence, atoms can be randomly substituted without changing the energy of the state. The Gibbs energy of mixing is given by Eq. (3.5) [10]:

$$G_{\text{mix}}^{\text{ideal}} = -TS_{\text{mix}}^{\text{ideal}} = RT \sum_i x_i \log_e x_i \tag{3.5}$$

And hence from Eq. (3.4), we have the Gibbs energy of an ideal solution phase to be [10]:

$$G_m = \sum_i x_i G_i^0 + RT \sum_i x_i \log_e x_i \tag{3.6}$$

The regular and non-regular solution models are non-ideal solution models, the former being the simpler form of the two. A non-ideal solution is one in which the

ΔH_{mix} is not equal to zero or ΔS_{mix} is deviating from its ideal value. The equation for chemical potential is given by [10]:

$$\mu = \mu^0 + RTlnx + F(x) \tag{3.7}$$

where μ^0 is the contribution from the pure component and $F(x)$ is the difference between the real and ideal chemical potentials.

In this work, the binary solution phases such as liquid and solid solutions have been described by the regular solution model given by the Redlich Kister expansion [10]:

$$G_m = \sum_i x_i G_i^0 + RT \sum_i x_i \ln x_i + \sum_i \sum_{j>1} x_i x_j \sum_v \Omega_{ij}^v (x_i - x_j)^v \tag{3.8}$$

where Ω_{ij}^v is a temperature dependent binary interaction parameter which depends on the value of v. When v=0, the above equation corresponds to a regular solution and when v=1, it becomes sub-regular. If $v > 2$, the model chosen to represent the phase is incorrect and should be changed. The sum $(x_i - x_j)$ is called the Redlich-Kister polynomial, used most frequently in solution models.

b. Sublattice phases

A sublattice phase is one in which there are interpenetrating sublattices, each of which have atoms that are distributed throughout the sublattice. If the atoms randomly occupy sites, the crystal structure is said to be disordered. This generally occurs at high temperatures. If the interpenetrating sublattices each have only one type of atom then the structure is completely ordered. If this ordering extends over a large order of atom diameter spanning thousands, then this would represent ”long-range” order.

The energy of a ordered state is lower than that of the disordered state and the entropy of a disordered state is larger than that of ordered systems. The probability that a given site is occupied by a certain type of atom in the disordered state is given by the site fractions. For example a two sublattice model with the formalism: $(A, B, ...)_u(X, Y, ...)_v$, where u and v represent the number of sites in the two sublattices respectively. A, B etc. are the components that can mix in the first sublattice, and X, Y etc. in the second sublattice [10].

The fractional site occupancy of each component on the sublattices is given by [10]:

$$y_i^{\mathrm{s}} = \frac{n_i^{\mathrm{s}}}{N^{\mathrm{s}}} \tag{3.9}$$

Here, n_i^{s} denotes the number of atoms of component i that occupy a sublattice s and N^{s} is the total number of sites in the given sublattice.

The sublattices can also be occupied by vacancies. Incorporating this into Eq. (3.9), we now have [10]:

$$y_i^{\mathrm{s}} = \frac{n_i^{\mathrm{s}}}{n_{Va}^{\mathrm{s}} + \sum_i n_i^{\mathrm{s}}} \tag{3.10}$$

The structure of a simple cubic sublattice structure is shown in Fig. 9 [12].

Intermetallic line compounds. These phases are considered to be stoichiometric in binary systems, with complete or partial solubility of components other than the elements in the binary, thus substituting the binary components preferentially. The site occupation of components display a definite stoichiometry. A general formalism

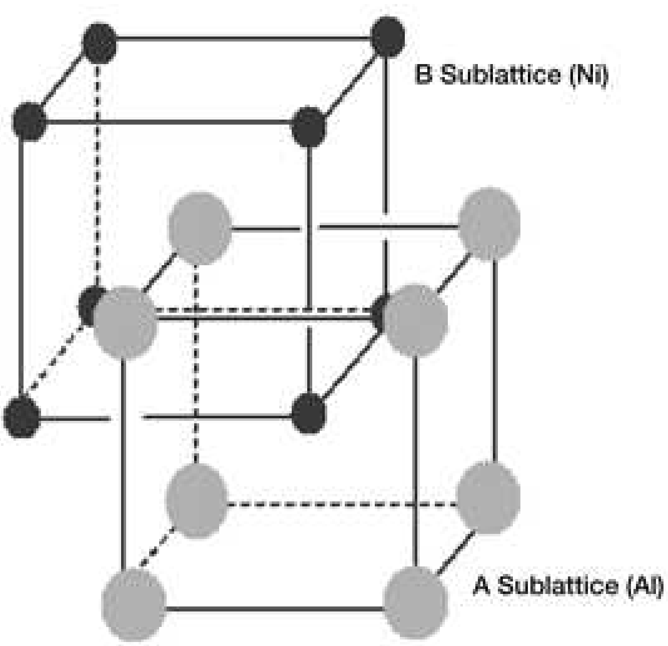

Fig. 9.: Structure of simple cubic interpenetrating sublattices of B2 (NiAl taken as an example). [12]

of the sublattice occupation is given by: $(A, B, ...)_u(Z)_v$ where A, B etc. are the components that can mix on the first sublattice and the Z is the component that has a fixed stoichiometry.

Interstitial compounds. These compounds are metallic and have two sublattices- one occupied by the substitutional elements and the other occupied by interstitial elements (They are relatively smaller atoms when compared to the substitutional elements). These have a narrow range of composition, have high melting points and are very hard materials. The sublattice formation is given by: $(A, B, ...)_u(X, Y, Va, ..)_v$ where A, B etc. are generally metals, X, Y etc. are interstitial elements, and Va

represents the interstitial vacancies.

D. ThermoCalc

ThermoCalc is a computational software that provides an interface to calculate many different thermodynamic properties for designing and creating materials. A computational approach thus helps in saving the time and costs to perform ad-hoc experiments to achieve material properties in a system. Calculation of phase diagrams, property diagrams, driving forces, equilibria, etc are handled very effectively for multicomponent systems containing up to 40 elements [23–26].

The main principle of ThermoCalc is based on the minimization of Gibbs energy and is enhanced by a global minimization technique on the system. The modules present in ThermoCalc can be seen in Fig.10. The type of files present in these modules can be seen in Fig. 11 [26]

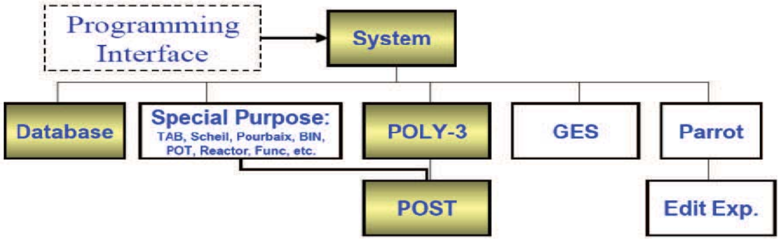

Fig. 10.: Modules present in ThermoCalc. [26]

ThermoCalc always begins from the SYS module which is system defined. It acts as an interface to all the other modules present in ThermoCalc.

A brief description of the modules of importance to the present work have been described here.

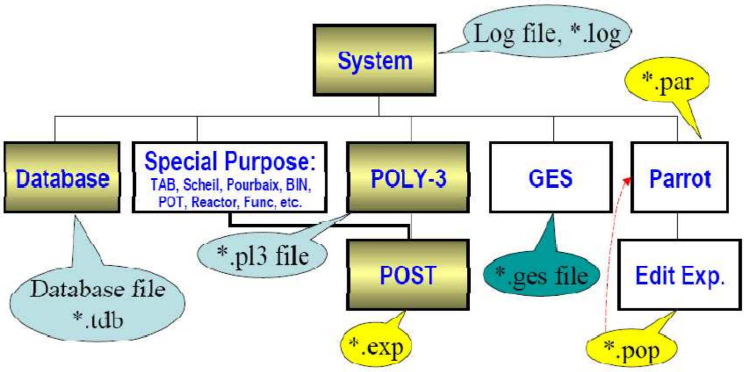

Fig. 11.: Files present in the modules of ThermoCalc. [26]

1. The TDB database module is useful to retrieve data that has already been defined.

2. The GES module handles data and phase descriptions.

3. The PARROT module, is used to compile experimental data and optimize parameters in order to assess the input data.

4. The ED_EXP module, a sub-module of the PARROT module, is used to edit experimental data present in the compiled .POP file (this file contains all the experimental information used for parameter optimization) and calculate equilibrium of the experiments by assigning suitable weights to them.

5. The POLY module is an most important module used to define phase equilibria and calculate equilibrium for heterogeneous systems using stepping and mapping.

6. The POST module generally regarded to be a sub-module of the POLY module is used for post-processing of the phase diagrams and property diagrams. There

is a link between the ED_EXP and PARROT modules and between the POLY AND POST modules.

The special modules namely the BIN and TERN modules are useful when specific calculations of diagrams are required and are reproduced in high quality standards. If one does not want to access the in-built models present in these modules, one can switch to a user defined database for example and calculate the property diagrams from there.

CHAPTER IV

CALCULATION OF THERMODYNAMIC PROPERTIES OF L12 AND B2 PHASES, LOW TEMPERATURE PHASE STUDY AND GROUND STATE CALCULATIONS IN THE BINARY NiGa SYSTEM

A. Overview

The NiGa binary system is an important component of higher order technologically important systems, such as materials for semiconductor applications (GaNiAs) as well as Shape Memory Alloys (CoNiGa). Recent experimental investigations [27, 28] have yielded substantial modifications to the accepted NiGa phase diagram [29]. In this work, the phase stability of the NiGa system throughout the composition range via *ab initio* methods have been investigated. The ground state of the NiGa binary was determined through a DFT-based high-throughput ground state search [13] over hundreds of possible binary crystal structures. After a preliminary candidate ground state was determined, recent experimental observations of stable and metastable phases were used to supplement the high-throughput database search. Calculated crystal structure parameters are compared to experimental data. Calorimetric measurements of the formation enthalpies of several NiGa intermetallic compounds are used to validate the formation energies calculated through *ab initio* methods. The calculations corroborate experimental results regarding the existence of Ni_3Ga_7 as well as the absence of Ga_4Ni from the ground state of the system. The B2 structure that dominates the central region of the phase diagram was found to be at best a relatively shallow ground state, in competition with several intermetallic compounds. In addition, a possible crystal structure for the recently found Ga_5Ni is proposed. The finite temperature thermodynamic properties using lattice dynamics of B2 and

L12 phases in NiGa have also been calculated in this work.

This chapter is divided into primarily two parts: The ground state calculations of the phases in the NiGa system and the finite temperature thermodynamic properties of the L12 and B2 phases.

B. Introduction

The NiGa binary system is an important component of higher order systems of significant technological importance. Ipser and collaborators have investigated this binary because it is an important constituent of the NiGaAs and NiGaSb ternaries, which are in turn important materials for the semiconductor industry [28]. Complete characterization of the phase stability of this binary is also essential for the understanding of the CoNiGa ternary, which has been recently identified as a potential High Temperature Shape Memory Alloy (HTSMA) [4]. Contrary to traditional SMAs, CoNiGa-based SMAs are designed as multi-phase systems, in which ductile fcc-based grain boundary precipitates are used to improve the ductility of the alloys [30]. This additional ductility, coupled to the great tunability of the M_s temperature through control of the composition of the austenite phase (B2 structure) make this alloys very promising alternatives to other higher cost SM systems. Further investigation of this important system requires a sound understanding of the phase stability of the constituent binary systems–the CoGa binary system has been recently re-assessed by our group [31]. The results of this work in combination with the available experimental data are currently being used to develop a thermodynamic model for the CoNiGa system over the entire composition and temperature ranges.

Control of phase constitution is not only essential for improving the properties of this system, but also to understand and prevent the precipitation of intermetalic phases which may negatively affect its performance. For example, it has been observed that the precipitation of the intermetallic Ni_5Al_3 significantly affects the SM properties of the closely related CoNiAl system [32], suppressing the martensitic transformation once it starts to precipitate. In the particular case of CoNiGa, experimental investigations show that the δ-Ni_5Ga_3 and ϵ-$Ni_{13}Ga_9$ phases penetrate into the ternary at increasing concentrations of cobalt [33], although the extent of this penetration and whether these phases take part in important equilibria involving the B2 and γ (fcc) phases is still uncertain. The stability of other binary intermetallic phases in the CoNiGa ternary has yet to be determined.

The NiGa binary system as modeled by Ipser et al. is shown in Fig 12 [34]. This model has been used to model the ternary CoNiGa system, which will be discussed in subsequent chapters.

In this system, the intermetallic compounds are : β (B2) NiGa, Ni_5Ga_3, Ni_3Ga_2, $Ni_{13}Ga_9$, Ni_2Ga_3, $NiGa_4$ and Ni_3Ga (L12). Both, the L12 and B2 phases are non-stoichiometric compounds and are modeled based on a two sublattice system. The other five compounds are stoichiometric compounds.

The important order-disorder transition between the ordered L12 phase Ni_3Ga and the disordered fcc phase was also incorporated in Ipser's model. Ni_3Ga was modeled as a non-stoichiometric phase by a two sublattice model: $(Ni,Ga)_{0.75}(Ga,Ni)_{0.25}$, Ni and Ga being the species occupying the two sublattices. This means that Ni and Ga occupy 75% of the first sublattice and 25% of the second sublattice [34]. Ideally, the Ni_3Ga phase with L12 structure (which has the Cu_3Au structure), has the face centered positions that are occupied by the Ni atoms and the corner positions that are occupied by the Ga atoms.

The NiGa phase has the B2 structure(CsCl structure), wherein one sublattice is occupied by antistructure defects and the other by vacancies. In this model, the va-

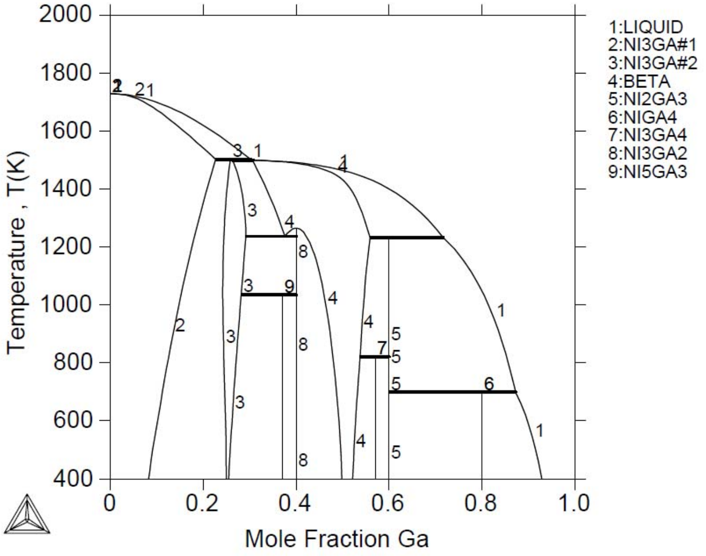

Fig. 12.: Binary NiGa phase diagram as calculated by Ipser et al. [34]

cancy was considered to be a component. This phase was modeled as follows:$(\mathrm{Ga,Ni})_{0.5}$ $(\mathrm{Ni,Va})_{0.5}$. This means that Ga and Ni occupy 50% of the first sublattice and Ni and Va occupy 50% of the second sublattice.

What makes the L12 and B2 phases interesting to study in this work, is their non-stoichiometry. Non-stoichiometry is a phenomenon where in compounds deviate from the law of definite proportions. Here, the compounds have elements which cannot be defined by a set of well defined natural numbers. These are due to defects in the crystal lattice such as substitutional point defects, i.e., when the 2 atoms Ni and Ga occupy the wrong sites in the L12 structure and triple defects seen in the B2 phase wherein antistructure defects are seen on one sublattice and vacancies are seen on the other [34]

C. Literature review

Despite being investigated–for a number of reasons– for over thirty years, [27,35–37], the details of the phase stability on the NiGa system have remained somewhat uncertain, particularly in compositions close to 100 % at. Ga. While Ducher et al. [27] have addressed the ambiguities in the Ni rich part, Ipser et al. [28] focussed on the study of the phases $NiGa_4$ and Ni_3Ga_7, along with other phases in the Ga-rich region of the phase diagram. In this work, we investigate the low temperature phase stability of the NiGa system through *ab initio* methods. High-throughput [13,38,39] techniques are used to search for the ground state of this system among hundreds of candidate crystal structures. These calculations, along with experimental data recently assessed by Ipser et al. [28] and Ducher [27] et al., formed the basis for comparison to corroborate the existence of all the binary phases in this work. The structure and formation energies of all the known intermetallic phases, including the recently reported Ni_3Ga_7 and $NiGa_5$ intermetallics is presented. The absence of $NiGa_4$ structure from the ground state is corroborated. Our results confirm the α'-Ni_3Ga(L12), δ-Ni_5Ga_3, Ni_2Ga, Ni_3Ga_7, Ni_2Ga_3 and ϵ-$Ni_{13}Ga_9$ phases as ground state structures, with the Ni_3Ga_4 being somewhat metastable with respect to the *ab initio* ground state. The stability of NiGa (B2), the central and dominant phase in this binary system, is also discussed.

The NiGa binary system has been previously investigated in several studies [28,34,35,40–46]. Ipser et al. [34] in their most recent work involving the thermodynamic modeling of the phase diagram, assessed the binary system over the entire composition range, through a combined CALPHAD and experimental approach. The phases considered were γ-Ni(fcc), γ'-Ni_3Ga(L12), β-NiGa (B2), δ-Ni_5Ga_3, Ni_3Ga_4, Ni_2Ga_3, $NiGa_4$ and ϵ-$Ni_{13}Ga_9$. In addition to the phases in the Ni-rich region as reported by Ipser, previous work [29, 35, 47, 48] carried out in the same composition range, found the $Ni_{13}Ga_7$ phase to be stable, although not at low temperatures (ground state). Ducher et al. [27] conducted Differential Scanning Calorimetry (DSC) experiments to understand the ambiguities involved in the stability among the phases δ, ϵ and β. The crystal structures of phases present in the low temperatures were observed using XRD.

Several studies have been performed in the Ga-rich region of the phase diagram, especially to address the uncertainty around the 70-80 at. % Ga, involving the existence of the phases $NiGa_4$ and Ni_3Ga_7 [28, 36, 47–57]. The work by Häussermann et al. [36] primarily focussed on addressing this issue. In the region between 70 and 80 at. % Ga, they confirmed the phase to be Ni_3Ga_7 instead of the $NiGa_4$ phase. Ipser et al. [28] reconfirmed the existence of the Ni_3Ga_7 phase, in addition to addressing other Ga-rich phases: $NiGa_5$, Ni_3Ga_7, Ni_3Ga_4, β, Ni_2Ga_3. They also performed calorimetric experiments in order to find the enthalpies of formation of the NiGa alloys within a temperature range of 1000-1400 °C. These, along with data from other experimental work have been compared with our calculations. For a more thorough review of the current state of knowledge on the phase stability of this system, the reader is referred to the most recent experimental investigations [27, 28].

Computational methods have made it easier nowadays to determine phase stability of alloys without relying on cumbersome experimental data, thus making computations more powerful as well as efficient.Stability of a phase is determined by its free energy which is the sum of configurational and vibrational free energies. Configurational entropy occurs due to atoms jumping from one site of the crystal to another and vibrational entropy occurs due to vibrations of the atoms about their equilibrium positions. These lattice vibrations have a profound effect on the stability of phases in a system. Configurational energy is assumed to be the energy of the system when all the atoms are fixed,i.e., do not move, at their positions at a prescribed temperature. In phase diagram calculations, it is important to study the effects of vibrations of the lattice [58]

The order-disorder transition in the L12 phase is of considerable importance for this study. As temperature decreases in the system, a transition from the disordered to the ordered phase can result due to vibrational entropy effects. However, metallic systems such as the one under study, has a larger configurational entropy difference due to disorder, as compared to vibrational entropy. When phase transition occurs, there is a change in heat capacity due to lattice vibrations. This can help calculate the vibrational entropy when disorder occurs [58].

In order to study the impact of vibrational effects on the stability of phases, it is necessary to understand the magnitude of vibrational entropy differences between phases in alloys [58].

The bonds between species that are dissimilar have a different stiffness when compared to those present between similar species. In an order-disorder transition, the overall stiffness of the alloy changes as the type of each bond in the alloy changes which results in a change in the vibrational entropy. In ordered transition, bonds between "unlike" atoms are favored than those between "like" atoms, thus making the system more stable and rigid. Disordering favors the opposite, i.e., bonds between "like" atoms and hence have large vibrational entropy and are soft [58].

D. Methodology

1. Ground state calculations in NiGa system

The electronic structure method: In the present work, Density Functional Theory [59] electronic structure calculations have been used. Specifically, the projector augmented plane wave code VASP [60,61] was used to calculate the total energies and the ground state properties of the phases. The exchange correlations corrections were addressed using LDA, PBE-GGA [62, 63] and PW91-GGA [64] approximations, each of which has its own advantages and limitations. By using these three approximations an attempt has been made to predict the phase properties as close to the realistic values as possible. Different k-points and cut-off energy values were used in each of the phases to ensure convergence of the calculations to within 1 meV. The LDA is implemented in VASP according to the Perdew–Zunger parameterizations [65] of the data by Ceperley and Alder [66], while the PW91 corrections have been used [67] in the GGA approximations.

Full relaxations were performed using the Methfessel–Paxton order 1 smearing method [68] followed by a final self-consistent static calculation with the tetrahedron smearing method with Blöchl corrections [69]. In the GGA-PW91 calculations, Ga-d potential having 13 valence electrons with an electronic configuration of $3d^{10}4s^{2}4p^{1}$ and an ENMAX (optimized value for the energy cutoff) value of 282.7 eV was used, while in the LDA and PBE calculations, a harder version of the Ga potential with 13 valence electrons but ENMAX of 404.7 eV was employed. In all the calculations the Ni potential with 16 valence electrons having electronic configuration of $3p^{6}3d^{8}4s^{2}$ and ENMAX of 367.9 eV was used.Accurate precision calculations were carried out with an energy cut off value (ENCUT) 1.3 times the ENMAX value in their respective potentials and k-point mesh size of 10,000 k-points per unit cell per reciprocal atom. Experimental thermodynamic data like enthalpy of formation (eV/atom) and the lattice parameters of the phases were compared with calculations done from first principles DFT calculations using the above mentioned approximations.

High-throughput DFT calculations: An extensive study of the ground state of all the phases present in the binary Ni-Ga system by first principles DFT calculations using the PBE-GGA approximation has been performed. These high-through put calculations were performed using the AFLOW package [70]. Through this package, the structures of hundreds of binary prototype structures from the Inorganic Crystal Structure Database (ICSD) [71] were selected and fully relaxed. The High-throughput calculations were performed within the PBE-GGA approximation [62,63]. All structures were fully relaxed with a convergence tolerance of 1meV/atom using dense reciprocal meshes of 3000-4000 k-points per reciprocal atom for the integrations over the Brillouin Zone. After the initial relaxation, a much denser grid of 10,000 k-points was used to get accurate charge densities and electronic densities of state. The Monkhorst-Pack scheme [72] was used for all the structures, except for hexagonal and rhombohedral cells, in which Γ-centered meshes were selected for faster convergence.

Generation of the $Ni_{13}Ga_7$ *structure:* The $Ni_{13}Ga_7$ phase with a $B8_1$-hexagonal structure was reported to be a solid solution phase by Ducher et al. [33]. In order to build a relevant structure with nearest composition for the first principle calculations, a 32-atom special quasi random structure (SQS) was constructed as described for hcp structure by Shin et al. [73] using ATAT [74, 75] package. In the calculations, the random mixing was restricted to the Ga sublattice and the resulting structures were fully relaxed.

2. Finite temperature thermodynamic calculations

Phase stability of a system is studied by calculating the free energy which is a sum of vibrational and configurational energies. [58] In order to study the effects of lattice vibrations on the free energy, one can take into consideration that the atoms are slightly perturbed from their equilibrium positions. Considering that the atom of mass M_i is displaced, a force f is exerted on it as shown by Eqn. 4.1 [58, 76]:

$$f(i) = \phi(i,j)u(j) \tag{4.1}$$

where $\phi(i,j)$ represent 3×3 matrices called force constant tensors. These represent the force acting on the atom i displacing atom j from its equilibrium position.

The origin of the force constant tensor is in the harmonic approximation of the Hamiltonian given by Eqn. 4.2 [76]:

$$\phi_{\alpha,\beta}(i,j) = \frac{\partial^2 E}{\partial u_\alpha(i)\partial u_\beta(j)} \tag{4.2}$$

A Fourier transform is then applied to the force constant tensor ϕ to give rise to the diagonalized matrix as shown in Eqn 4.3 [76]. The eigen values of the matrix, corresponding to the phonons (modes of oscillation) of the structure, give rise to the frequencies of the phonons.

$$D = \left[\frac{\phi(i,j)}{\sqrt{M_i M_j}}\right] \tag{4.3}$$

The vibrational free energy is given by the distribution of the frequencies, g[ν(k)] as shown by Eqn.4.4 [76]:

$$F_{vib}(T) = k_B T \int_0^\infty ln\left[2\sinh\left(\frac{h\nu}{2k_B T}\right)\right] g[\nu(K)]d\nu \tag{4.4}$$

where k_B is the Boltzmann constant.

For a quasi-harmonic approximation where the frequencies are volume dependent, the total energy of a system under constant volume and temperature is given by Eqn. 4.5 [76]:

$$F(V,T) = E_{0K}(V) + F_{vib}(V,T) + F_{elec}(V,T) \tag{4.5}$$

where E_{0K}(V) is the free energy at 0 K as a function of volume, F_{vib}(V,T) is the vibrational free energy as a function of volume and temperature and F_{elec}(V,T) is the electronic free energy as a function of volume and temperature. Eqn. 4.5 does not take into consideration magnetic and configurational DOF. The volume dependency is brought about due to changes in the electronic density of states with volume.

The vibrational free energy can be calculated using Eqn. 4.4. The electronic free energy can be obtained by relating the electronic energy and entropy given by eqn. 4.6 [76]:

$$F_{elec} = E_{elec} - TS_{elec} \tag{4.6}$$

where E_{elec} is given by Eqn. 4.7 and S_{elec} is given by Eqn. 4.8:

$$E_{elec}(V,T) = \int n(\epsilon,V) f\epsilon d\epsilon - \int^{\epsilon F} n(\epsilon,V)\epsilon d\epsilon \tag{4.7}$$

$$S_{elec}(V,T) = -k_B \int n(\epsilon,V)\left[f ln f + (1-f) ln(1-f)\right] d\epsilon \tag{4.8}$$

where n(ϵ,V) is the electronic DOS and f is the fermi function.

The equilibrium volume V^*(T) at each temperature can be calculated by minimizing the total free energy from eqn. 4.5. The free energy can then be expressed as a function of temperature as follows (Eqn. 4.9 [76]):

$$F(T) = E(V^*(T)) + F_{vib}(V^*(T),T) + F_{elec}(V^*(T),T) \tag{4.9}$$

There are two methods to calculate the force constants. One is the Linear Response Theory (LRT) and the Super Cell (SC) methods. The supercell method is used in this study to calculate the force constants. In this method, a supercell is created from a fully relaxed primitive supercell. The force constants are calculated by generating a system of equations by relating the inter-atomic forces and displacements. For a specific supercell, there are only a certain finite number of perturbations that can be considered. For lower symmetry structures, larger the number of perturbations are required.

An important aspect to consider is that ab initio methods find the short range force constants to predict an accurate measurement of thermodynamic properties in metals. The properties are averages that are taken over all the phonon modes. For solids consisting of pairwise harmonic interactions only, these force constant tensors are symmetric between a pair of atoms. [58]

Quasiharmonic analysis is the method used to calculate the vibrational thermodynamic properties. The quasi-harmonic approximation is used to take into account the effect of volume thermal expansion on the vibrational properties. In this approximation, the phonon frequencies are volume dependent which results in the force constant tensors to also be volume dependent. Thus, this method is a collection of harmonic calculations at different volumes.

VASP software was used for the calculations and a script using ATAT was used to perform static calculations, relax the structures and find the thermodynamic properties. VASP (Vienna Ab-initio Simulation Package) is a package that is used to perform ab-initio quantum mechanical molecular dynamics calculations using pseudo potentials and a plane wave basis set. It is based on a local density approximation that has free energy as its variational quantity and calculates the instantaneous ground state at each molecular dynamics time step.

There are four basic input files in VASP:

1. INCAR- It is the input file of vasp that contains lines of syntax, some of them

with default values, if they are not specified.

2. KPOINTS- It contains the co-ordinates and weights, or the mesh size for creating the grid.
3. POSCAR- This file contains the positions of the ions. This can be given in direct or cartesian co-ordinates.
4. POTCAR- It contains the pseudopotentials as well as information about the atoms such as mass, valency etc.

In this work, the thermodynamic properties of L12 and B2 phases of the NiGa system were evaluated using density functional theory (DFT), by taking into consideration the vibrational effects and the electronic degrees of freedom. The actual force constants were calculated using the Alloy Theorated Automated Toolkit (ATAT) method. Since first principles thermodynamic calculations take a lot of time when performed manually, ATAT has been used to make the process faster by doing the calculations automatically. Computationally, first principles lattice dynamics calculations are very intensive due to the very large number of configuration of atoms. The results are faster using ATAT.

3. Script used for calculation

On running the script, it generates the necessary input files of VASP and monitors the jobs being sent to the supercomputing facility. These jobs are sent to calculate the thermodynamic properties of the two structures within the quasiharmonic approximation method, which is implemented by ATAT [58]. In this approximation, the lattice dynamic properties of the structure are calculated by determining the force constants that relates the atomic displacements to the interatomic forces. As mentioned before, these constants are analogous to the spring constants, considering that the atoms are connected by springs, relating to a mass-spring system.

After determining these force constants, the dynamical matrix is generated. The dynamical matrix consists of elements of the force constants divided by the square root of the product of the pair ions. These pair ions are assumed to be connected by springs. A fourier transform is then applied to this matrix to get a diagonalized matrix. These Eigenvalues are the normal independent phonons.

In the script, ATAT first generates the volumes necessary for the quasiharmonic approximation. For each of the volumes generated, the degrees of freedom are relaxed at constant volume to perform self-consistent static calculations. ATAT then generates the perturbations needed to evaluate the force constants from the interatomic forces calculated by VASP. After the forces have been evaluated, ATAT then fits the spring mass system. The mass-spring system is then diagonalized to result in the Eigenvalues. For each of these volumes, the script extracts the phonon density of states. Contributions due to electronic degrees of freedom are incorporated as well.

A free energy surface which is a function of volume and temperature is then generated. At each temperature, the volume at which the free energy is minimum is found (for stability). This minimum energy-volume path on the surface of free energy is used to derive the thermal expansion for the structure. Zero pressure thermodynamic properties are then evaluated by finding the projection of the free energy surface along this path. Finally, the thermodynamic properties like enthalpy, entropy, specific heat are calculated by taking the partial derivatives of the free energy with respect to temperature.

E. Results

1. Ground state calculation of the phases in the NiGa system

The free energies and other ground state properties of the phases found in the NiGa binary are tabulated in Table II and III along with the differences as compared to experiments, in % .

Table II.: Comparison of the lattice parameters calculated using the LDA, PBE and GGA approximations with the experimental results. Error in % is included in parenthesis and the ground state phases are in bold

Phase	Prototype	Pearson Symbol	Lattice parameters (Å)				
		Space Group		Exp	GGA(%err)	PBE(%err)	LDA(%err)
Ni$_3$Ga	Al$_3$Zr	tI16	a	-	3.646	3.640	3.559
	(Tetragonal)	139	b	-	13.772	13.748	13.436
	L12	cP4	a	3.585 [116]	3.579(0.17)	3.573(0.33)	3.481(2.9)
	(Cubic)	221					
Ni$_2$Ga	Co$_2$Si	oP12	a	-	5.055	5.043	4.91
	(Orthorhombic)	62	b	-	3.782	3.777	3.682
			c	-	7.404	7.389	7.203
	Ni$_2$In	hP6	a	-	4.043	4.038	3.937
	(Hexagonal)	194	c	-	5.03	5.017	4.881

Continued on next page

TableII–Continued

Phase	Prototype	Pearson Symbol	Lattice parameters (Å)				
		Space Group		Exp	GGA(%err)	PBE(%err)	LDA(%err)
$\mathbf{Ni_5Ga_3}$	$\mathbf{Pt_5Ga_3}$	oC16	a	7.53 [27]	7.537(0.09)	7.52(0.13)	7.324(2.73)
	(Orthorhombic)	65	b	6.79 [27]	6.77(2.94)	6.755(0.51)	6.576(3.15)
			c	3.74 [27]	3.724(0.42)	3.736(0.10)	3.644(2.56)
$\mathbf{Ni_{13}Ga_9}$	$\mathbf{Pt_{13}In_9}$	C12/m1	a	13.838 [27]	13.912(0.53)	13.91(0.52)	13.62(1.54)
	(Monoclinic)		b	7.9 [27]	7.910(0.12)	7.904(0.05)	7.713(2.36)
			c	8.52 [27]	8.506(0.16)	8.498(0.25)	8.286(2.74)
NiGa	CsCl (Cubic)	cP2 221	a	2.87 [28]	2.916(1.62)	2.835(1.21)	2.905(1.21)
$\mathbf{Ni_3Ga_4}$	$\mathbf{Ni_3Ga_4}$	cI112	a	11.558 [28]	11.484(0.64)	11.462(0.83)	11.168(3.3)

Continued on next page

TableII–Continued

Phase	Prototype	Pearson Symbol	Lattice parameters (Å)				
		Space Group		Exp	GGA(%err)	PBE(%err)	LDA(%err)
	(Cubic)	230					
$\mathbf{Ni_2Ga_3}$	$\mathbf{Ni_2Al_3}$	hP5	a	4.05 [28]	4.075(0.61)	4.064(0.34)	3.955(2.34)
	(Trigonal)	164	c	4.89 [28]	4.906(0.32)	4.899(0.18)	4.783(2.18)
	Bi_2Te_3	hR5	a	-	2.847	2.831	2.754
	(Hexagonal)	166	c	-	29.643	29.675	28.886
$NiGa_2$	FeS_2	cP12	a	-	5.7	5.684	5.534
	(Cubic)	205					
$\mathbf{Ni_3Ga_7}$	$\mathbf{Ir_3Ge_7}$		a	8.43	8.469(0.46)	8.447(0.20)	8.222(2.46)
	(Cubic)	229					
$NiGa_4$	Cu_5Zn_8	I23	a	8.429 [117]	8.931(5.94)	8.884(5.39)	8.605(2.08)

Continued on next page

TableII–Continued

Phase	Prototype	Pearson Symbol	Lattice parameters (Å)				
		Space Group		Exp	GGA(%err)	PBE(%err)	LDA(%err)
	(Cubic)	197					
NiGa$_5$	PdGa$_5$	tI24	a	6.312 [28]	6.37(0.91)	6.33(0.28)	6.333(0.33)
	(Tetragonal)	141	c	9.721 [28]	9.760(0.40)	9.748(0.27)	9.748(0.27)
			a	6.326 [28]	6.37(0.69)	6.33(0.06)	6.333(0.11)
			c	9.741 [28]	9.760(0.19)	9.748(0.07)	9.748(0.7)
Ni$_{13}$Ga$_7$	NiAs	B8$_1$	a	4.005 [27]	-	-	-

Continued on next page

TableII–Continued

Phase	Prototype	Pearson Symbol	Lattice parameters (Å)				
		Space Group		Exp	GGA(%err)	PBE(%err)	LDA(%err)
	(Hexagonal)	194	c	5.018 [27]	-	-	-

Table III.: Enthalpy of formation calculated with LDA, PBE and GGA approximations and comparison with experimental results

Phase	Structure	H_f(J/mol)				
		GGA	PBE	LDA	DQMC	Other Work
Ni_3Ga	Al_3Zr	-26919	-27594	-32901	-28057	-27800(298 K) [40][1]
						-23191.5(300 K) [57][2]
						-33883(873 K) [80][3]
						-33064.4(1223 K) [79][3]
						-28138.7(298 K) [77][2]
	L12	-26726	-27594	32226	-	-
Ni_2Ga	Co_2Si	-32322	-33384	-39269	-33943	-
	Ni_2In	-30200	-31164	-36664	-	-
Ni_5Ga_3	**Pt_5Ga_3**	-34349	-35699	-41971	-36423	-35500(298 K) [40][1]
						-40080(298 K) [77][2]
$Ni_{13}Ga_9$	**$Pt_{13}In_9$**	-36182	-37537	-43611	-	-40425(300 K) [57][2]
						-45193.6(298 K) [77][2]

Continued on next page

TableIII–Continued

Phase	Structure	H$_f$(J/mol)				
		GGA	PBE	LDA	DQMC	Other Work
						-37200(298 K) [40][1]
NiGa	CsCl	-32322	-34541	-41585	-36230	-38500(298 K) [40][1]
						-38297.9(300 K) [57][2]
						-48829.8(873 K) [80][3]
						-49893.7(1023 K) [78][2]
Ni$_3$Ga$_4$	**Ni$_3$Ga$_4$**	-35603	-37725	-44576	-	-35700(298 K) [40][1]
Ni$_2$Ga$_3$	**Ni$_2$Al$_3$**	-37243	-39173	-45541	-19605	-33600(298 K) [40][1]
						-45106.4(300 K) [57][2]
						-50341.1(873 K) [80][3]
	Bi$_2$Te$_3$	-16209	-18428	-22191	-	-
NiGa$_2$	Fm-3m	-28752	-29910	-34927	-31126	-
Ni$_3$Ga$_7$	**Ir$_3$Ge$_7$**	-29235	-31261	-35989	-	-33830(300 K) [57][2]
NiGa$_4$	Cu$_5$Zn$_8$	10710	8587	10710	83160	-24300(298 K) [40][1]
						-22127.7(300 K) [57][2]

Continued on next page

TableIII–Continued

Phase	Structure	H_f(J/mol)				
		GGA	PBE	LDA	DQMC	Other Work
$NiGa_5$	$PdGa_5$	-13990	-16788.4	-19682.9	-	
$Ni_{13}Ga_7$	NiAs	26516.5	21407.6	26157.58	-	-

---

[1] Calculated
[2] Experimental-Calorimetry
[3] Experimental-emf

These tables show a comparison of enthalpy of formation (eV/atom) and the lattice parameters (Å) of the different binary phases present, with experimental data. Table III, shows that different approximations (GGA, PBE and LDA) predict slightly different enthalpies of formation. In general, a relatively small difference of $\sim$ -1 kJ/Mol exists between the GGA and PBE approximations. When compared to the LDA calculations, the difference in energy is about 5 kJ/mol-atom. As is usually the case, the LDA calculations overestimated the formation energies, relative to the gradient-corrected approximations. When comparing the calculated and experimental lattice parameters, it was observed that the largest error corresponded to the LDA approximations. While the GGA-based calculations outperformed the LDA predictions of the structural parameters of the phases studied in this work, the LDA calculations seem to be closer (on average) to the most recent thermochemical measurements in this system, particularly in the central composition range. Note that the experimental data are extrapolations to room temperature and the calculations do not take finite temperature effects. However, from previous theoretical work carried out by Arróyave et al. [76] on the chemically similar Ni-Al system and coupled with experimental findings in literature,it is assumed that the variation in the enthalpy of formation with temperature is in the order of a few kJ/mol-atom for 1000 K rise in temperature. Hence taking this into consideration, the variations in the current ground state calculations to actual values at 300K could be negligible, justifying the comparison between the ground state and the experimental calculations in the range of 300 K.

As reported by Ipser [28], the Ni_3Ga_7 phase is observed to belong to the ground state in all approximations. Along with this structure, other ground state phases identified through this work are Ni_3Ga (with the L12 structure),Ni_2Ga (with the P63mmc structure), $Ni_{13}Ga_9$, Ni_5Ga_3 and Ni_2Ga_3 (with the Ni_2Al_3 structure). The above phases were found to be in the ground state using all the three exchange correlation approximations. A comparison of the enthalpy of formation under the GGA, LDA and PBE exchange correlation approximations with experimental data, is made in Figs. 13, 14 and 15. These figures show that most of the experimental data [77–79], with the results by Martosudirjo and Pratt [57] and Bird and Pratt [80] under and overestimate the mean formation enthalpies in this system, particularly in the central regions of the phase diagram. In fact, close to the 50-50 composition, the experimental scatter is around 10 kJ/mol-atom.

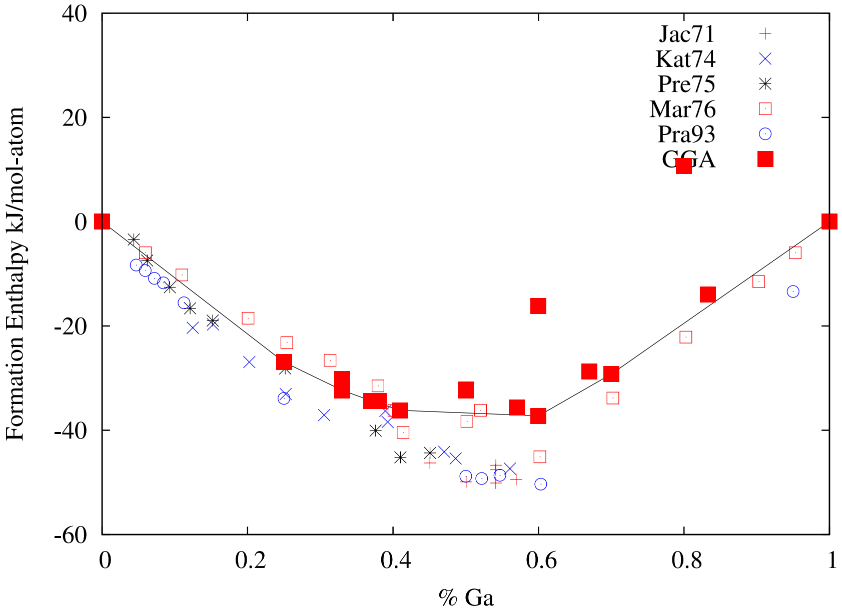

Fig. 13.: Enthalpies of formation (kJ/mol-atom) in the Ni-Ga system. Comparison between experimental measurements [57, 77–80] and DFT-GGA calculations.

As mentioned above, over the past decades there has been considerable controversy regarding the existence of the $NiGa_4$ and Ni_3Ga_7 phases [28, 36, 47–57]. The calculations in this study, support experimental observations that place Ni_3Ga_7 in the

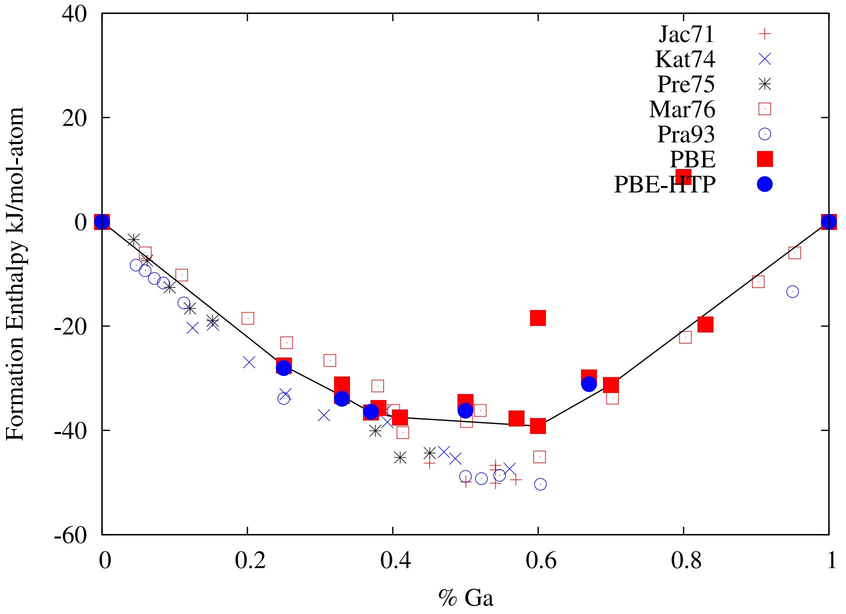

Fig. 14.: Enthalpies of formation (kJ/mol-atom) in the Ni-Ga system. Comparison between experimental measurements [57, 77–80] and DFT-PBE calculations. The results from the High-throughput calculations are also included for comparison.

ground state of this binary. At the same time, the present calculations confirm recent experiments [28] that have ruled out the presence of $NiGa_4$ in the equilibrium phase diagram of NiGa. In fact, the calculations (see Table III) suggest that this phase has a positive enthalpy of formation relative to the constituent elements. Figs. 13, 14 and 15. illustrate that this phase is well-above the ground state and is therefore highly unlikely to be present in NiGa, even under metastable conditions.

While $NiGa_4$ had been recognized to be the structure with the highest concentration of Ga in the NiGa binary, Ipser et al. [28] report a new phase with the $NiGa_5$ stoichiometry and with the $PdGa_5$ structure (space group:I4/mcm) as its prototype. In the experiments, samples with about 80% at. Ga were prepared, and quenched

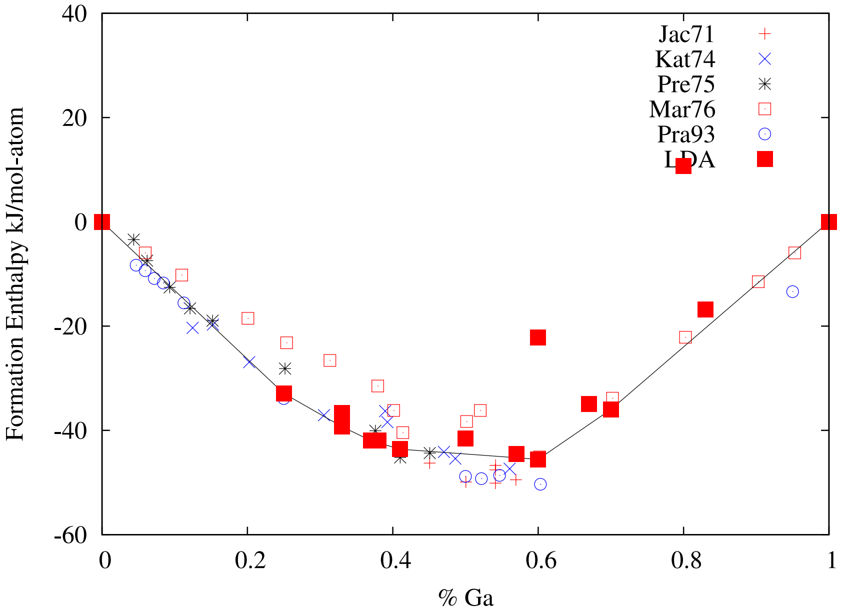

Fig. 15.: Enthalpies of formation (kJ/mol-atom) in the Ni-Ga system. Comparison between experimental measurements [57, 77–80] and DFT-LDA calculations.

from 340^0C. This temperature places the alloy above the proposed peritectic reaction involving a Ga-rich liquid as well as Ni_3Ga_7. When the XRD pattern was analyzed and after structure refinement, the structure was assigned to be of the prototype $PdGa_5$. The experiments were not able to produce large amounts of this phase, as it always occurred in the presence of Ni_2Ga_3, with the formation of Ni_3Ga_7—the phase that would be at equilibrium with $NiGa_5$—possibly prevented due to kinetics. Larger amounts of Ga (83.3% at.) yielded samples with Ni_3Ga_7, Ni_2Ga_3 and small amounts of $NiGa_5$. The XRD patterns for this structure were observed to disappear at about 125^0C. The small amounts of $NiGa_5$ produced, and the fact that this quantity is smaller in the annealed samples compared to the ones directly quenched, suggests that this phase is either metastable or that the kinetics of the formation reaction around $100^0 C$ is so slow that it is not possible to attain thermodynamic equilibrium conditions. In all the three approximations used, the calculations in the present work suggest (see Figs. 13, 14 and 15) that this structure lies slightly above the ground state, which is consistent with the experimental observations [28].

The Ni_2Ga_3 phase with trigonal symmetry was found to be in the ground state and these results agree with the experimental results of Ipser et al. [28] who found the phase to be stable. However, Ni_2Ga_3 with the hexagonal symmetry was not found to be in the ground state from the calculations. The phases $Ni_{13}Ga_9$ and Ni_5Ga_3 that appear in the ternary CoNiGa system, have been found to be in the ground state and these results match those reported by Ducher et al. [27] in their investigation of the Ni-region of the phase diagram. The ground state is relatively flat in the central region of the phase diagram and these phases are some of the most stable phases (at low temperatures). The preliminary phase-stability analysis of the CoNiGa system by Oikawa and collaborators suggest that these phases penetrate the ternary Gibbs triangle and take part in equilibria involving the Ni-rich $L1_2$ structure, suggesting that they can be further stabilized by substituting Co into the Ni sublattice.

The $Ni_{13}Ga_7$ with the $B8_1$-hexagonal structure, was reported to be a solution phase that stabilizes above 720 °C by Ducher et al. [27]. The calculations support this observation, which can be seen in the Figs. 13, 14 and 15. This phase is found to be well above the ground state (convex hull), with a positive value of enthalpy of formation at 0 K. Whether this phase becomes stable at higher temperatures due to anti-site defects, vacancies or a combination of both defect structures is beyond the scope of this work.

From the figures and the tabulated data, it can be seen that the calculations differ from the accepted phase diagrams [27,34,35,37,47] in that the β phase (NiGa) seems to be slightly above the ground state in all the three approximations considered in this work. In all three approximations, this structure lies between 2.5-5 kJ/mol-atom above the ground state segment formed by $Ni_{13}Ga_9$ and Ni_2Ga_3. Moreover, while the results from the High-throughput search did not consider the Ni_2Ga_3 with trigonal symmetry, these additional DFT-PBE calculations suggest that, at best, NiGa lies on a relatively flat ground state, involving 'competition' among four different phases, closely spaced in the composition space ($Ni_{13}Ga_9$, NiGa, Ni_3Ga_4 and Ni_2Ga_3). Since the HTP-PBE results do not vary much from the other PBE calculations (the largest difference being about 1-2 kJ/mol-atom) and are also consistent with the GGA and LDA approximations, the fact that NiGa in the B2 structure does not seem to lie on the ground state cannot be ascribed to numerical uncertainties of the DFT calculations. While it is certainly likely that the observed disagreement is due to limitations on the *ab initio* methods used, it is also possible (although less likely) that this phase actually decomposes at low temperatures and becomes stabilized at finite temperatures due to entropic effects. This structure has significant degrees of non-stoichiometry due to anti-site and vacancy point defects so configurational entropy definitely contributes to its stability at high temperatures. At lower temperatures, the stabilization would have to be due to vibrational effects since the thermal population of defects would be negligible. Unfortunately, for this explanation to be viable, the entropy of this phase relative to the equilibrium between $Ni_{13}Ga_9$ and Ni_2Ga_3 would have to be in the order 8 J/mol-atom/K. Such a large entropy difference at low temperatures does not seem to be reasonable. While it may be possible that there is another structure lower in energy than NiGa-B2 and that belongs to the *ab initio* ground state, in practice this is a question that cannot be addressed since by necessity the kinetics would be so slow that the chance of observing this hypothetical phase would be zero.

Table IV.: Total energies (eV) calculated using LDA and GGA methods

	Total energy using LDA (eV)	Total energy using GGA (eV)
NiGa	-11.120451	-9.161637
Ni_3Ga	-24.744645	-20.523712

2. Total energies of L12 and B2 phases compared using LDA and GGA methods

First, the structures were relaxed to find the optimum crystal structure to calculate further properties. GGA (General Gradient Approximation) and LDA (Local Density Approximation) methods were compared, as seen in Table IV.

When compared to LDA, General Gradient Approximations soften bonds, improve total and atomization energies. The LDA method was used before, as it was simpler and gave better descriptions of the atomic structures and other properties of systems, but was not as accurate in describing the energies of reactions. This led to the LDA over-estimating binding energies of molecular configurations and crystals. The GGA method however, was able to overcome such problems, giving a better description of the energy barriers. Hence, GGA method was used here, to perform further calculations.

a. NiGa (B2) calculations

INCAR file:

```
SYSTEM = NiGa
PREC = A
ENCUT = 350
EDIFF = 1E-6
ISTART = 1
```

```
ISMEAR = 1
SIGMA = 0.15
ISPIN=2
MAGMOM=2*1
NSW = 20
IBRION = 2
ALGO = Fast
NELMIN = 4
ISIF = 3
LCHARG = .FALSE
LWAVE = .TRUE.
```

ENCUT is the cut off energy for the plane wave basis set. Since this is a spin polarized calculation, IPSIN=2. There are 2 atoms, Ni and Ga, and hence MAGMOM= 2*1. ISIF=3 means that stress tensors and forces are calculated and the ions are relaxed.

KPOINTS file:

```
0
G
18 18 18
0 0 0
```

Here, the 0 in the first line indicates that the mesh is to be generated automatically, using a Gamma centered grid that has 18 subdivisions along each reciprocal vector. The 0s in the 4th line indicates that there is no additional shift of the mesh.

Ni has an fcc crystal structure and Ga, orthorhombic.

The POSCAR file is:

```
1.00000000000000
2.9162464926307812 0.0000000000000000 0.0000000000000000
0.0000000000000000 2.9161804025746894 0.0000000000000000
0.0000000000000000 0.0000000000000000 2.9161804025746894
1 1
Direct
0.0000000000000000 0.0000000000000000 0.0000000000000000
0.5000000000000000 0.5000000000000000 0.5000000000000000
0.00000000E+00 0.00000000E+00 0.00000000E+00
0.00000000E+00 0.00000000E+00 0.00000000E+00
```

The first line indicates the scaling factor. The next 3 lines give the lattice vectors that defines the unit cell. The fifth line gives us the number of atoms in each element. The atom positions are in direct coordinates.

The supercell of NiGa has 32 atoms and that of Ni_3Ga has 36 atoms. Supercells are repeating units of single cells that have primitive cells in them. Although the primitive cells of the supercell have different crystal structure, on perturbation of these cells, we get the supercell of another crystal structure, which then becomes the primitive cell of the whole system. This is specially helpful in computational methods.

b. Ni_3Ga (L12) calculations

INCAR file:

```
SYSTEM = Ni3Ga
PREC = A
ENCUT = 350
EDIFF = 1E-6
```

```
ISTART = 1
ISMEAR = 1
SIGMA = 0.15
ISPIN=2
MAGMOM=4*1
NSW = 20
IBRION = 2
ALGO = Fast
NELMIN = 4
ISIF = 3
LCHARG = .FALSE
LWAVE = .TRUE.
```

Here, since there are 4 atoms for the 2 species, MAGMOM= 4*1. The remaining parameters are the same.

KPOINTS file:

```
0
G
14 14 14
0 0 0
```

Here, 14 subdivisions are made for every vector between two positions.

The POSCAR file is:

```
1.00000000000000
3.5837275085361182 0.0000000000000000 0.0000000000000000
0.0000000000000000 3.5837275085361182 0.0000000000000000
0.0000000000000000 0.0000000000000000 3.5837275085361182
```

```
1 3
Direct
0.0000000000000000 0.0000000000000000 0.0000000000000000
0.5000000000000000 0.5000000000000000 0.5000000000000000
0.5000000000000000 0.0000000000000000 0.5000000000000000
0.5000000000000000 0.5000000000000000 0.0000000000000000

0.00000000E+00 0.00000000E+00 0.00000000E+00
0.00000000E+00 0.00000000E+00 0.00000000E+00
0.00000000E+00 0.00000000E+00 0.00000000E+00
0.00000000E+00 0.00000000E+00 0.00000000E+00
```

For both structures, the Pearson symbol crystal database was referred to generate the basis vectors. In Ni_3Ga, which has the Cu_3Au structure, there are additional 2 lines in the direct co-ordinate definition. This is because we now have 4 atoms in total. Hence, we also have 1 3 in the fifth line of this file.

3. Evaluation of thermodynamic properties

In the calculations of finite temperature thermodynamic properties, vibrational effects as well as the electronic degrees of freedom were taken into consideration. The thermodynamic properties evaluated for the L12 and B2 phases were:

1. Specific heat
2. Enthalpy
3. Entropy
4. Relative enthalpy

5. Co-efficient of thermal expansion

The properties are compared by including, quasiharmonic effects (Q), electronic degrees of freedom (Ele), and anharmonicity(Anh). The properties are then evaluated by examining which properties give better results at specific temperatures by including these effects. The trends of these properties are shown in Figs. 16a-19b. These include harmonic (har), harmonic plus electronic (har+elec), quasi-harmonic (q-h), quasi-harmonic plus electronic (q-h+elec) and quasi-harmonic plus electronic plus anharmonicity (q-h+elec+anh) approximations.

Quasi-harmonic approximations include include higher order effects as well, considering volume dependance of frequency and ignoring temperature effect on frequency.

Anharmonicity takes into account those high temperature dependent effects which were neglected by quasi-harmonic approximation.

Harmonic approximations consider that every atom is located within a harmonic potential. Therefore, to calculate vibrational properties, one has to take into account the interatomic forces that come into play between the interacting atoms. But at high temperatures, i.e., temperatures close to melting temperatures and higher, the ions move a lot. These perturbations thus cannot be calculated and the harmonic theory fails. Hence the harmonic approximation does not consider phonon interactions.

In Density Functional Theory (DFT), perturbations of the atoms in the ground state can be done over finite temperatures i.e., 0 K to 2/3 melting temperature of the solid.

In general, it is the ions that contribute to the degrees of freedom in a solid.

a. Specific heat or heat capacity

This is defined as the heat required to raise the temperature of unit mass of a substance by unit temperature. This heat capacity is 'specific' which means that it is a measurement of an intrinsic property,i.e., the mass of the substance must be 'specified'. For different approximations, the temperature dependent specific heat was calculated to generate the plot as shown in Figs 16a and 16b for B2 and L12.

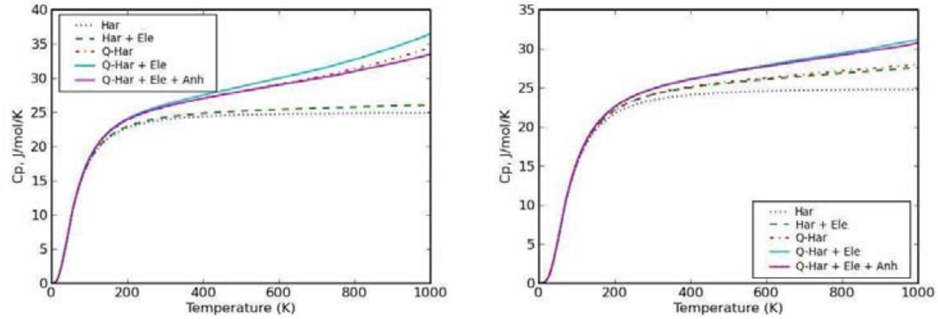

(a)

(b)

Fig. 16.: Specific heat of NiGa and Ni_3Ga as a function of temperature (J/mol/K).

There are several factors that affect the heat capacity of a substance. Molecules have different degrees of freedom that depend on the motions of the atoms. This affects heat capacity. Higher the temperature would mean that the atoms are excited to higher modes of vibration, thus increasing the capacity to store heat. The unit for specific heat is taken as per mole, due to the fact that, heat is stored by each atom in the substance and not the bulk material as a whole, and this affects heat capacity.

The quasiharmonic approximation helps in the calculation of specific heat. In this approximation, the force tensors are volume dependent due to the assumption that the phonon frequencies are volume dependent. With these approximations, reliable calculations of thermal expansion co-efficients can be made.

b. Enthalpy

It is the heat transfer that takes place at constant pressure in a closed system. It is also defined as the sum of the internal energy plus the product of pressure of the substance multiplied by its volume. H=U+PV

Enthalpy is a state variable, defined in terms of three other state variables. A state variable is a quantity which does not depend on the path the process takes in the system, but its value remains the same in the system. The units of enthalpy are J/mol.

Figs. 17a and 17b show the calculated finite temperature enthalpy for B2 and L12 for the different approximations.

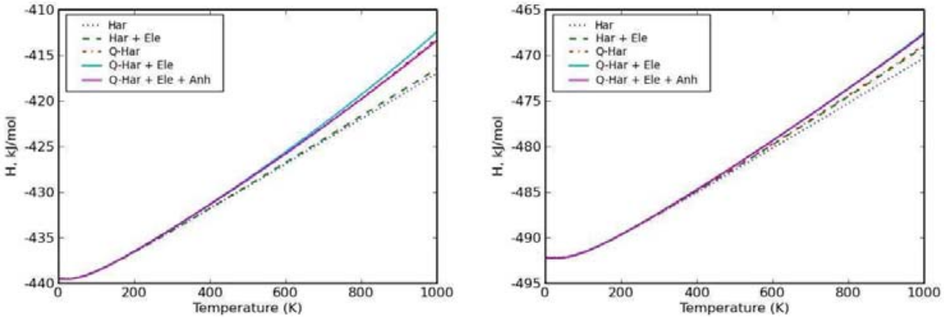

(a) (b)

Fig. 17.: Enthalpy of NiGa and Ni_3Ga as a function of temperature (kJ/mol).

c. Entropy

In general, entropy is a measure of how much energy is spread out in a process or system. Vibrational entropy is a measure of the stiffness of a substance. In this system, we have considered atoms connected by springs or harmonic oscillators. The entropy of the system depends on how the atoms oscillate. Larger the oscillation amplitude, greater is the entropy of the system. From the Gibbs free energy equation, we have: G=H-TS. Hence, larger entropies would mean lower free energy which results in a system becoming more stable.

Figs. 18a and 18b show the calculated entropy for B2 and L12 for the different approximations considered.

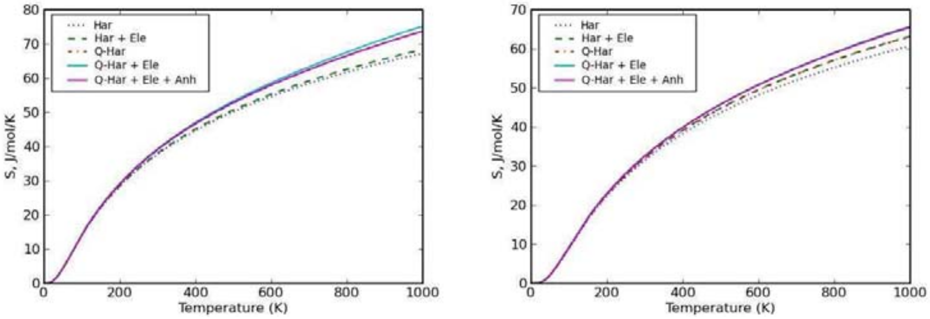

(a) (b)

Fig. 18.: Entropy of NiGa and Ni_3Ga as a function of temperature (J/mol/K).

d. Co-efficient of thermal expansion

The energy stored between intermolecular bonds changes as the temperature of the substance changes. As the energy in the bonds increases, the bonds change their length due to changes in temperature, resulting in a dimensional response to temperature change. This response is given by the co-efficient of thermal expansion. As the volume changes of a substance, so does the vibrational entropy. Hence we can say that this dependence results in thermal expansion. It has units of per Kelvin or per unit temperature. Within the quasiharmonic approximation, the bond stiffness vs bond length relationships help in determining the thermal expansion.

The coefficient of thermal expansion for B2 and L12 has been calculated as shown in Figs. 19a and 19b for the quasi-harmonic, quasi-harmonic plus electronic, quasi-harmonic plus electronic plus anharmonicity approximations.

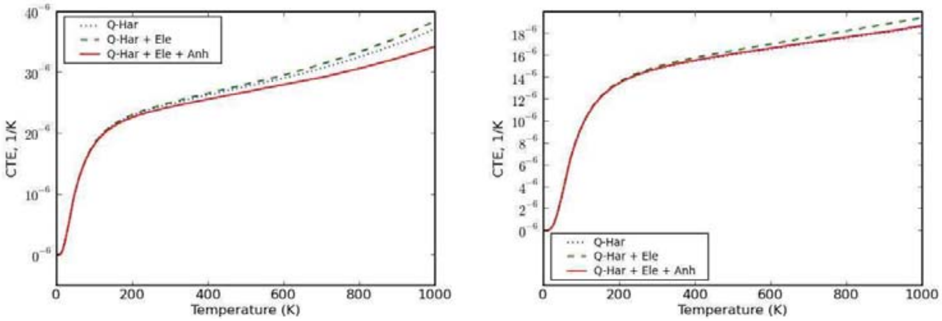

(a) (b)

Fig. 19.: Co-efficient of thermal expansion of NiGa and Ni_3Ga as a function of temperature (1/K).

F. Summary and conclusions

In this work, the structure and formation energies of all the known intermetallic phases, including the recently reported Ni_3Ga_7 and $NiGa_5$ intermetallics is presented. A high-throughput ground state search was combined with experimental data to generate a structure database that was studied in more detail using three DFT approximations. In general, the calculations compare well with the structural parameters determined for all the intermetallics and the calculated enthalpies of formation lie within the scatter in the published thermochemical measurements [57, 77–80]. The biggest discrepancy between experiments and calculations corresponds to the stability of the B2 phase, relative to $Ni_{13}Ga_9$ and Ni_2Ga_3. While it is possible that this phase in fact does not belong to the ground state, it is perhaps more likely that the fault lies in the DFT methods used.

During calculations of the thermodynamic properties of L12 and B2, it was seen that vibrational entropy differences are lesser than configurational entropy differences. This shows that vibrations have a smaller impact. The quasiharmonic model helps to model thermal expansion, and it overcomes limitations of standard harmonic approximations. The model also helps in determining the effects of lattice vibrations and anharmonicity in phase diagram calculations. The stiffness vs. bond length relationships can be determined from lattice dynamic calculations. The study of thermodynamic properties is important to evaluate the structure of the phases present as well as study the influence of the structure of the components. The evaluation of the thermodynamic properties of NiGa will help in the study of CoNiGa HTSMAs and their behavior later on. Computational techniques make it easier and less time consuming to arrive at the desired results.

CHAPTER V

THERMODYNAMIC MODELING OF THE CoGa BINARY SYSTEM THROUGH A COMBINED CALPHAD+AB-INITIO METHOD*

A. Overview

The thermodynamic properties and phase relations of the CoGa binary system are remodeled based on the CALPHAD approach. In this work, CoGa(β) is considered non-stoichiometric and $CoGa_3$ stoichiometric. The β phase is thermodynamically described by a 2 sublattice model $(Co,Ga)_{0.5}(Co,Va)_{0.5}$. The stability of the β phase is restricted in the low temperature regions by giving necessary driving force constraints. The lattice parameters and enthalpy of formation of the β and $CoGa_3$ phases have been compared with first-principles calculations based on density functional theory. The calculated CoGa phase diagram is compared to previously calculated ones.

B. Introduction

Shape Memory Alloys (SMA) are highly advanced materials that undergo reversible martensitic transformations upon the application of temperature, stress and/or magnetic field. Their unique shape memory properties (in some cases accompanied by significant pseudoelastic behavior)make SMAs very attractive functional materials widely used in the aerospace and medical device industries, as well as in more general applications in which the SM effect is used for the purposes of sensing and/or actuating. Recently, the CoNiGa system has emerged as the basis for very promising High Temperature Shape Memory Alloys (HTSMAs) [2,3]. Investigation of the phase sta-

---

*Reprinted from CALPHAD, 34, Arpita Chari, Andres Garay, Raymundo Arroyave, Thermodynamic remodeling of the Co-Ga system, 189-195, copyright(2010) with permission from Elsevier.

bility of this ternary system is essential for the further development of CoNiGa-based HTSMAs.

An accurate thermodynamic model for the CoGa system is essential for the development of reliable thermodynamic descriptions of the CoNiGa ternary. The focus of this study is to overcome the limitations found in previously developed models for the CoGa system, especially with regards to the stability of the β phase. The correct description of the β phase is very important, as it dominates the central region of the ternary CoNiGa system where the shape memory effect is observed [3]. Although the description for the β phase does not pose any difficulty in the binary thermodynamic model developed by Su and Tedenac [81](as only lower temperature description of the phases has been described), the extrapolation into the ternary CoNiGa is made difficult as the model incorrectly predicts the re-stabilization of the β phase as the temperature increases above the liquidus in the CoGa system. Resolving this un-physical behavior is one of the main reasons to remodel the CoGa system.

C. Comparison of the two models

We have compared two previously developed thermodynamic models for the CoGa system. The first one, developed by Gröbner [40], used insufficient experimental data to model the CoGa system. Also, they predicted that the β phase melts congruently, whereas in fact, according to experiments [47,82–84], the β phase melts incongruently. The next model we have used for comparison is the one developed by Su and Tedenac [81]. Su and Tedenac [81] have assessed an excellent thermodynamic model and the calculated results match very well with the experimental data. The CoGa system was modeled using all experimental data including activities in the beta and fcc regions, enthalpies of formation of the liquid alloys, intermediate phases and sublattice site fraction of vacancies of the β phase. Also, by using experimental data [47, 82–84] , their model was able to overcome the deficiencies of the model by Gröbner, with respect to the congruent melting of the β phase. Unfortunately, one of the problems we observed in the model developed by Su and Tedenac was that beginning at about 2000 K, the β phase became stable over a wide range of compositions. This extraneous artifact of the binary description, while of not much importance when examining the phase stability of the CoGa binary at low temperatures, was observed to dramatically affect the phase stability of the β phase in the ternary CoNiGa phase diagram. In addition, the description of the gas phase was not included in the previous study [81], and in fact, when the gas phase was included in that description, the β phase still dominated the high-temperature phase diagram, making the need for remodeling this system even more evident.

Although the model developed by Su and Tedenac (see Fig. 20) agreed very well with the published phase stability and thermodynamic data, the β phase appeared to be stable at high temperatures.

For the modeling of the phase stability of HTSMAs like the ternary CoNiGa, it is necessary to model the phase stability of the β phase with great accuracy as this phase is the one that undergoes the martensitic transformation responsible for the shape memory effect in these systems.

It is important to note that the optimized parameters calculated in this study have not changed much for the phases with respect to the parameters as calculated by Su [81], except for some variables corresponding to the mathematical description of the Gibbs energy of the liquid, β and fcc phases. The changes in these latter phases were due to the extra stability constraints (to be described below) imposed during the optimization to ensure that the β phase became metastable with respect to the

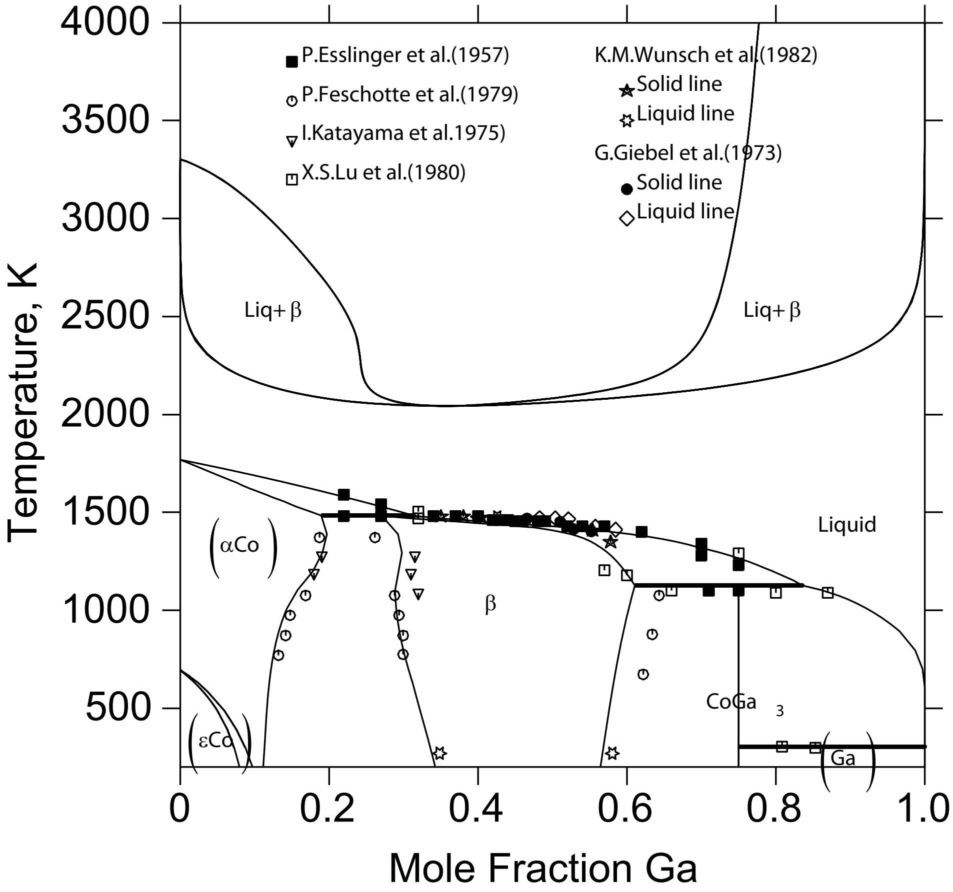

Fig. 20.: The model predicted by Su and Tedenac. [81]

liquid (or gas) phase at high temperatures.

D. The thermodynamic model

1. Unary phases

The Gibbs energy of the pure species as a function of temperature is given by the equation:

$$^{0}G_{\mathrm{i}}^{\phi}(T) -^{0} H_{SER}^{i}(298.15K) = a + bT + cT\ln(T) + \sum_{2}^{n} d_n T^n \qquad (5.1)$$

The left hand side of Eq. (5.1) is the Gibbs energy with reference to the standard element reference state(SER). The reference state is the most stable phase at 10^5Pa and 298.15 K. a, b, c and d are coefficients and n signifies a set of integers that can take values of 2, 3 and -1 [10]. i refers to the pure element. ϕ refers to the phases, liquid, fcc and ortho. The standard element reference for pure Co is hcp and ortho for pure Ga. In this study, the Gibbs energy functions have been taken from the SGTE data for pure elements [85].

2. Random substitutional phase

The gas phase is an ideal solution, based on a random substitutional model where the components can randomly mix in any space in the phase [10]. The description of the gas phase has been included in the calculations as it is more stable than the β phase at high temperatures [The description of the gas phase and its functions have been included in Table (V) and Appendix (A)].

3. Ordinary substitutional phases

The liquid, α-Co (fcc solid solution) and the ϵ-Co (hcp) phases are treated as ordinary substitutional solutions. The general form of the Gibbs energy function is described by Eq. (5.2) [10]:

$$^{0}G_{\mathrm{m}}^{\phi} = \sum_{i} x_i^0 G_i^{\phi} + RT\sum_{i} x_i \ln x_i +^{ex} G_{\mathrm{m}}^{\phi} \tag{5.2}$$

The Gibbs energy function for the phases is given by Eq. (5.3):

$$^{0}G_{\mathrm{m}}^{\phi} = x_{\mathrm{Co}}{}^{0}G_{\mathrm{Co}}^{\phi} + x_{\mathrm{Ga}}{}^{0}G_{\mathrm{Ga}}^{\phi} + RT(x_{\mathrm{Co}}\ln x_{\mathrm{Co}} + x_{\mathrm{Ga}}\ln x_{\mathrm{Ga}}) +^{ex} G_{\mathrm{m}}^{\phi} \tag{5.3}$$

where $^{0}G_{\mathrm{Co}}^{\phi}$and $^{0}G_{\mathrm{Ga}}^{\phi}$ are the molar Gibbs energies of cobalt and gallium in their pure standard states. $x_{\mathrm{Co}}$and x_{Ga} are the mole fractions of pure cobalt and gallium. $^{ex}G_{\mathrm{m}}^{\phi}$ is the excess Gibbs free energy of mixing. $^{ex}G_{\mathrm{m}}^{\phi}$ is given by Eq. (5.4) [86]:

$$^{ex}G_{\mathrm{m}}^{\phi} = x_{\mathrm{Co}}x_{\mathrm{Ga}}\sum_{i} L_{\mathrm{Co,Ga}}^{\phi}(x_{\mathrm{Co}} - x_{\mathrm{Ga}})^i \tag{5.4}$$

$^{i}L_{\mathrm{Co,Ga}}^{\phi}$ is called the interaction parameter between Co and Ga which is a function of temperature and is given by Eq. (5.5):

$$^{i}L_{\mathrm{Co,Ga}}^{\phi} = a + bT \tag{5.5}$$

In this work, the corresponding parameters are to be evaluated.

4. Stoichiometric intermetallic compounds

In the present study, we consider $\mathrm{CoGa_3}$ as a stoichiometric compound due to its small composition range [81].

The Gibbs energy is given by Eq. (5.6) :

$$G_{\mathrm{m}}^{\mathrm{CoGa_3}} = 0.25\,{}^0G_{\mathrm{Co}}^{\mathrm{hcp}} + 0.75\,{}^0G_{\mathrm{Ga}}^{\mathrm{ort}} + a_1 + b_1T \tag{5.6}$$

where $a_1$and $b_1$are the parameters that are evaluated.

5. Non-stoichiometric intermetallic compounds

The crystal structure of the β phase is of the CsCl, B2 type [87], which is an ordered cubic structure. The description of the β phase is extremely important in this study as it will be used for extrapolation at higher temperatures in the ternary CoNiGa system. Different chemical models were suggested [83, 88–91] to describe the β phase with point defects and vacancy concentration using a triple defect structure. The models suggest that this phase is a substitutional solid solution for higher compositions of Co and deviates from this substitutional behavior at higher compositions of Ga, in which large concentrations of vacancies are responsible for the observed deviations from non-stoichiometry. This model was used by Su and Tedenac where the cobalt and gallium atoms combined on the 1st sublattice and cobalt and vacancies combined on the 2nd sublattice. The two-sublattice model for the β phase is given by $(\mathrm{Co,Ga})_{0.5}(\mathrm{Co,Va})_{0.5}$. Incidentally, Yuan and Ipser [34] in their model for NiGa, have also described the β phase using the same description for its defect structure, which we will be using to model the ternary system. Gröbner did not use the triple defect model.

The Gibbs energy per mole is given by Eq. (5.7) [81]:

$$\begin{aligned} G^{\beta}_{\mathrm{m}} &= y'_{\mathrm{Co}}y''_{\mathrm{Co}}\,{}^{0}G^{\beta}_{\mathrm{Co:Co}} + y'_{\mathrm{Co}}y''_{\mathrm{Va}}\,{}^{0}G^{\beta}_{\mathrm{Co:Va}} \\ &\quad + y'_{\mathrm{Ga}}y''_{\mathrm{Co}}\,{}^{0}G^{\beta}_{\mathrm{Ga:Co}} + y'_{\mathrm{Ga}}y''_{\mathrm{Va}}\,{}^{0}G^{\beta}_{\mathrm{Ga:Va}} \\ &\quad + RT(y'_{\mathrm{Co}}\ln y'_{\mathrm{Co}} + y'_{\mathrm{Ga}}\ln y'_{\mathrm{Ga}} + y''_{\mathrm{Co}}\ln y''_{\mathrm{Co}} + y''_{\mathrm{Va}}\ln y''_{\mathrm{Va}}) \\ &\quad + y'_{\mathrm{Co}}y'_{\mathrm{Ga}}(y''_{\mathrm{Co}}\,{}^{0}L^{\beta}_{\mathrm{Co,Ga:Co}} + y''_{\mathrm{Va}}\,{}^{0}L^{\beta}_{\mathrm{Co,Ga:Va}}) \\ &\quad + y''_{\mathrm{Co}}y''_{\mathrm{Va}}(y'_{\mathrm{Co}}\,{}^{0}L^{\beta}_{\mathrm{Co:Co,Va}} + y'_{\mathrm{Ga}}\,{}^{0}L^{\beta}_{\mathrm{Ga:Co,Va}}) \end{aligned} \tag{5.7}$$

$y'_{\mathrm{Co}}$and $y'_{\mathrm{Ga}}$are the site fractions of Co and Ga in the first sublattice of the β phase, $y''_{\mathrm{Co}}$and $y''_{\mathrm{Va}}$are the site fractions of Co and Va in the second sublattice. ${}^{0}G^{\beta}_{\mathrm{Co:Co}}$is the Gibbs energy of pure cobalt with a bcc structure [81], ${}^{0}G^{\beta}_{\mathrm{Ga:Co}}$is the Gibbs energy of the β phase with a B2 structure, ${}^{0}G^{\beta}_{\mathrm{Co:Va}}$and ${}^{0}G^{\beta}_{\mathrm{Ga:Va}}$ are the Gibbs energies of pure cobalt and pure gallium respectively with a vacancy in the second sublattice. From Dupin's [90] work, the following relations were used for the description of the β phase [81]:

$${}^{0}G^{\beta}_{\mathrm{Co:Co}} = {}^{0}G^{\mathrm{bcc}}_{\mathrm{Co}} \tag{5.8}$$

$${}^{0}G^{\beta}_{\mathrm{Co:Va}} = {}^{0}G^{\beta}_{\mathrm{Co:Co}} + {}^{0}G^{\beta}_{\mathrm{Ga:Va}} - {}^{0}G^{\beta}_{\mathrm{Ga:Co}} \tag{5.9}$$

E. Experimental information

1. Phase diagram data

Researchers have studied the CoGa system using X-Ray diffraction studies [40], Differential Thermal Analysis (DTA) ,thermal, microscopic and magnetic methods [47, 82,83]. The liquidus and solidus have been calculated and reported by [47,82–84,92].

The phases in this system are liquid, the two sublattice β phase, the stoichiometric $CoGa_3$ phase, α-cobalt (fcc), ϵ-cobalt (hcp) and orthorhombic gallium.

The calculated liquidus is consistent with experimental results, while the solidus shows some differences [81]. The solidus measured by Geibel [92], Feschotte [47] and Wunsch [83] have been accepted [81]. The β phase has a wide homogeneity range and decomposes in the peritectic reaction Liq+fcc$\rightarrow\beta$. The temperature of this reaction is taken as 1483 K [47]. The other reported temperatures are 1450 K [82]and 1480 K [84]. The β phase description has been modified to allow stability of the phase only at lower temperatures.

The homogeneity of the β phase in the Ga-rich region which is controlled by this vacancy concentration was determined experimentally by Ommen [88] and other researchers [83, 89, 93]. The fraction of vacancies in the second sublattice site of the β phase was thus used as experimental data for the thermodynamic optimization.

In this study, $CoGa_3$ is taken as a stoichiometric compound with the crystal structure tP16 which decomposes in the peritectic reaction Liq+$\beta\rightarrow CoGa_3$. The temperature at which this reaction takes place is taken as 1120 K. The other reported temperatures are 1106 K [82], 1111 K [84] and 1128 K [47].

2. Thermodynamic data

Thermodynamic properties of the CoGa system has been studied by many researchers. The enthalpies of formation of the liquid alloys were measured by Haddad [94] using a high temperature calorimeter ($\triangle_{mix}H_m^0$=-16 kJ/mol with x_{Co}=0.45) at temperatures ranging from 1524 to 1694 K. Also, from Figs. 21 and 22, it can be seen that the enthalpies are temperature independent with a minimum of -15.9 kJ/mol at x_{Ga}=0.55 [81, 94].

The enthalpies of formation of the intermediate phases were studied by Predel [96]

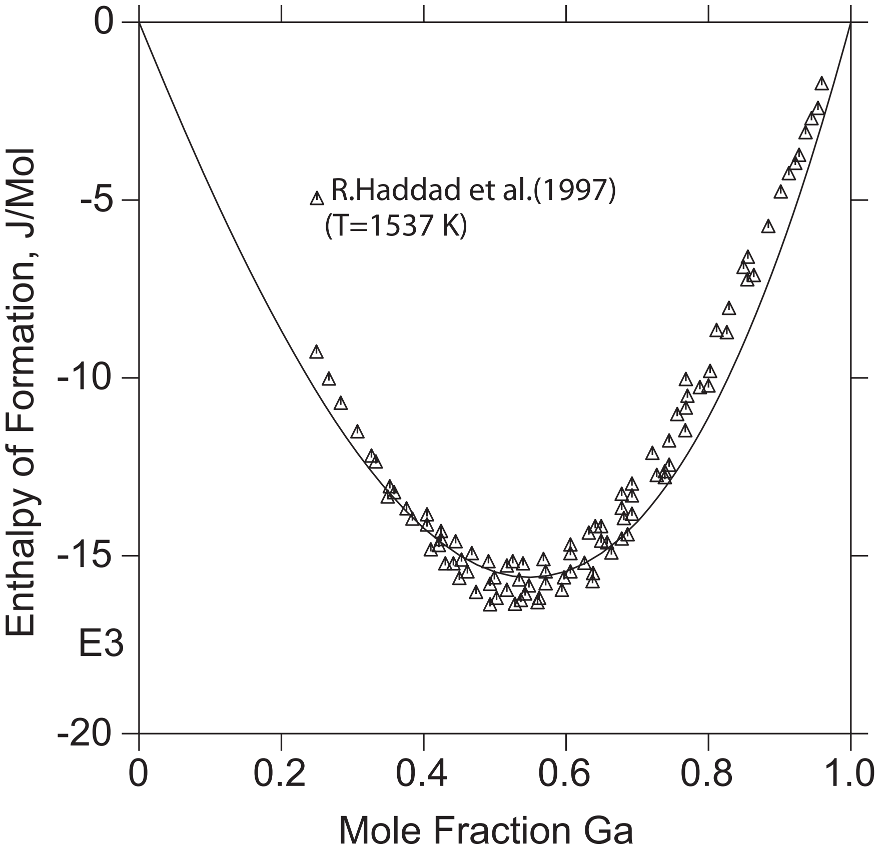

Fig. 21.: Calculated enthalpies of formation for the CoGa liquid alloys at 1537 K compared with experimental data.

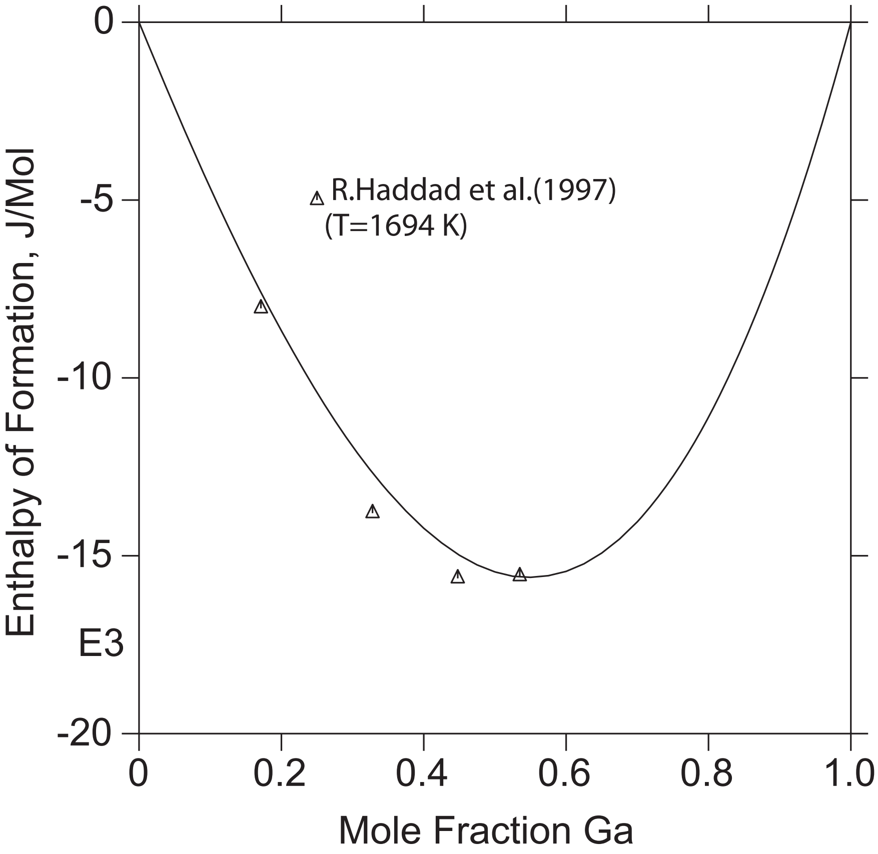

Fig. 22.: Calculated enthalpies of formation for the CoGa liquid alloys at 1694 K compared with experimental data.

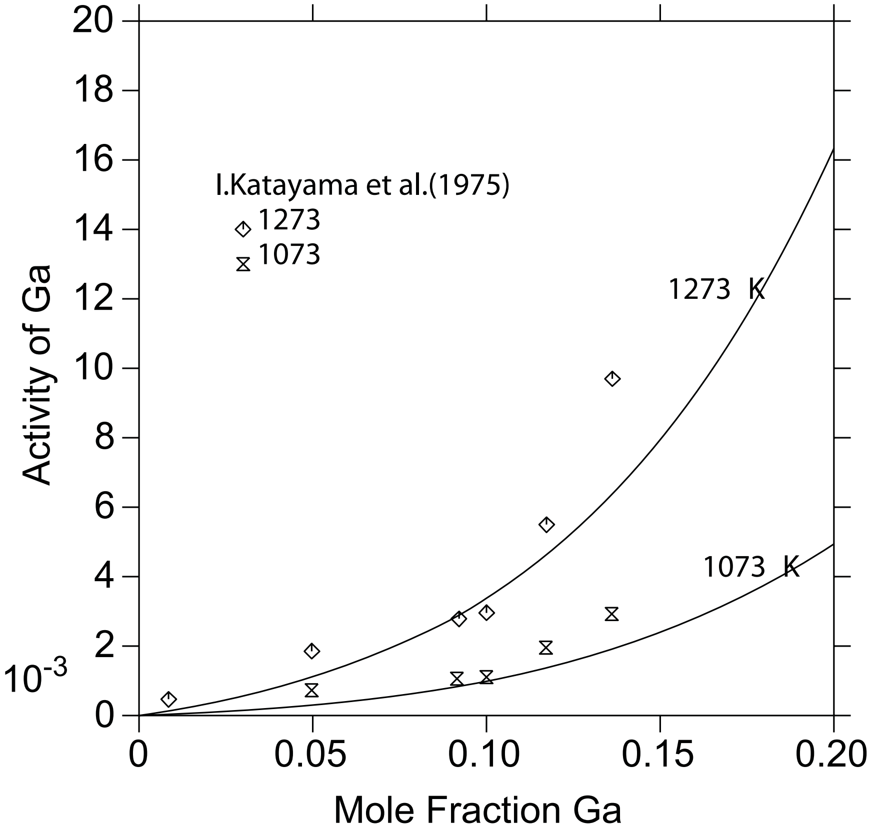

Fig. 23.: Calculated activities of the fcc solid solutions with experimental data. Reference state: liquid gallium.

and Henig [97]. We see that Predel's values do not match with the data reported by Henig and that Predel's values are more negative.

The activities of gallium for the fcc solid solutions were studied by Katayama [95] and compared with the calculated results (see Fig. 23).

F. Thermodynamic assessment of data

The thermodynamic parameters including those for the Gibbs energy functions and interaction parameters for all the phases, were optimized using the Thermo-Calc software package. The experimental data were given weights depending on the level of accuracy needed to perform the calculations and the estimated uncertainty of the measurements. As the calculations were being carried out, the weights of the experiments were modified (increased or decreased) in order to steer the optimization and ensure accurate self-consistent results. All the model parameters were optimized together, starting with a small number of optimization iterations and increasing this number as the optimization progressed. The starting values for the parameters of the model were obtained from the study of Su and Tedenac [81]. These parameters were optimized using all experimental thermodynamic, phase diagram and defect constitution data. The three invariant reactions experimentally determined in this binary system were assigned the highest statistical weights. The coefficient $\mathrm{b_i}$ for the interaction parameter ${}^{1}L^{\mathrm{Liq}}_{\mathrm{Co,Ga}}$ was almost zero at the end of the optimization process and was finally taken as zero.

Due to the large solubility of the fcc solid solution, two interaction parameters were used to describe the phase [81]. The parameters for the β phase were optimized again, giving higher weights for the experimental data for sublattice site fractions of the vacancies of the β phase measured by Ommen [88]. The composition sets of the β phase were explicitly defined while optimizing the variables.

In order to prevent the β phase from stabilizing for a second time at temperatures above the liquidus, stability constraints were used. The stability constraints are defined in terms of the driving force for precipitation of the β phase under metastable equilibria conditions involving the liquid and/or gas phases. Specifically, the non-stability of the β phase over the entire composition range at high temperatures was enforced by establishing that the driving force (DGMR) for the precipitation of this phase was negative at high temperatures at all compositions. We used these stability constraints as experiments and gave them higher weights during optimization. Using

Thermo-Calc, the stability constraint (for the β phase) is given as follows:

EXPERIMENT DGMR(beta)<0:1e^{-3}

The driving force was calculated within an error of 1e^{-3}

Only through the imposition of these driving force (or stability) constraints, was it possible to prevent the β phase from becoming stable at high temperatures. During the optimization, further stability constraints were employed to prevent the stabilization of other phases in regions in which their absence has been positively demonstrated through experimental investigations.

Here we would like to note the fact that many thermodynamic models published in the past have suffered from these types of artifacts. The main reason for this is that in most cases, optimization of thermodynamic model parameters is focused on low temperature regions of the phase diagram. The parameters are thus optimized to minimize the error between predictions and 'positive' experimental results, without taking into account 'negative' results (i.e. the absence of phases in ranges of temperature and composition) which can further constrain the optimization. While this may not be much of a problem in most instances, anomalous re-stabilization of phases may become problematic when attempting to extrapolate these descriptions to higher-order systems.

G. Results and discussion

The optimized parameters of all the phases for the CoGa system have been listed in Table V.

The calculated binary phase diagram with all the experimental data is shown in Fig. 24.

The calculated phase diagram is compared with experimental data measured

Table V.: Optimized parameters for the phases in the CoGa system

Gas	${}^0G^{\mathrm{Gas}}_{\mathrm{Co}}$	$F6985T + RTln(1 * 10^{-5}P)$
	${}^0G^{\mathrm{Gas}}_{\mathrm{Ga}}$	$F9633T + RTln(1 * 10^{-5}P)$
	${}^0G^{\mathrm{Gas}}_{\mathrm{Ga2}}$	$F9695T + RTln(1 * 10^{-5}P)$
Liquid	${}^0L^{\mathrm{Liq}}_{\mathrm{Co,Ga}}$	$-61807 + 7.985T$
	${}^1L^{\mathrm{Liq}}_{\mathrm{Co,Ga}}$	12605.5
Fcc	${}^0L^{\mathrm{fcc}}_{\mathrm{Co,Ga}}$	$-125202 + 54.131T$
	${}^1L^{\mathrm{fcc}}_{\mathrm{Co,Ga}}$	$30657 - 25.625T$
Hcp	${}^0L^{\mathrm{hcp}}_{\mathrm{Co,Ga}}$	$-87051 + 22.438T$
$\mathrm{CoGa_3}$	${}^0G^{\mathrm{CoGa_3}}_{\mathrm{Co:Ga}} - 0.25{}^0G^{\mathrm{hcp}}_{\mathrm{Co}} - 0.75{}^0G^{\mathrm{ort}}_{\mathrm{Ga}}$	$-30770 + 3.043T$
B2-CoGa(β)	${}^0G^{\beta}_{\mathrm{Co:Co}} = {}^0G^{\mathrm{bcc}}_{\mathrm{Co}}$	${}^0G^{\mathrm{hcp}}_{\mathrm{Co}} + 2938 - 0.7138T$
	${}^0G^{\beta}_{\mathrm{Ga:Co}} - 0.5{}^0G^{\mathrm{ort}}_{\mathrm{Ga}} - 0.5{}^0G^{\mathrm{hcp}}_{\mathrm{Co}}$	$-42125 + 9.519T$
	${}^0G^{\beta}_{\mathrm{Ga:Va}}$	$0.5{}^0G^{\mathrm{ort}}_{\mathrm{Ga}} + 7250 - 6.35T$
	${}^0G^{\beta}_{\mathrm{Co:Va}}$	${}^0G^{\beta}_{\mathrm{Co:Co}} +^0 G^{\beta}_{\mathrm{Ga:Va}} -^0 G^{\beta}_{\mathrm{Ga:Co}}$
	${}^0L^{\beta}_{\mathrm{Co:Co,Va}}$	$-6847 + 0.6913T$
	${}^0L^{\beta}_{\mathrm{Ga:Co,Va}}$	$-24462 + 9.677T$
	${}^0L^{\beta}_{\mathrm{Co,Ga:Co}}$	$-11752 + 3.505T$
	${}^0L^{\beta}_{\mathrm{Co,Ga:Va}}$	$-7557 - 0.3907T$

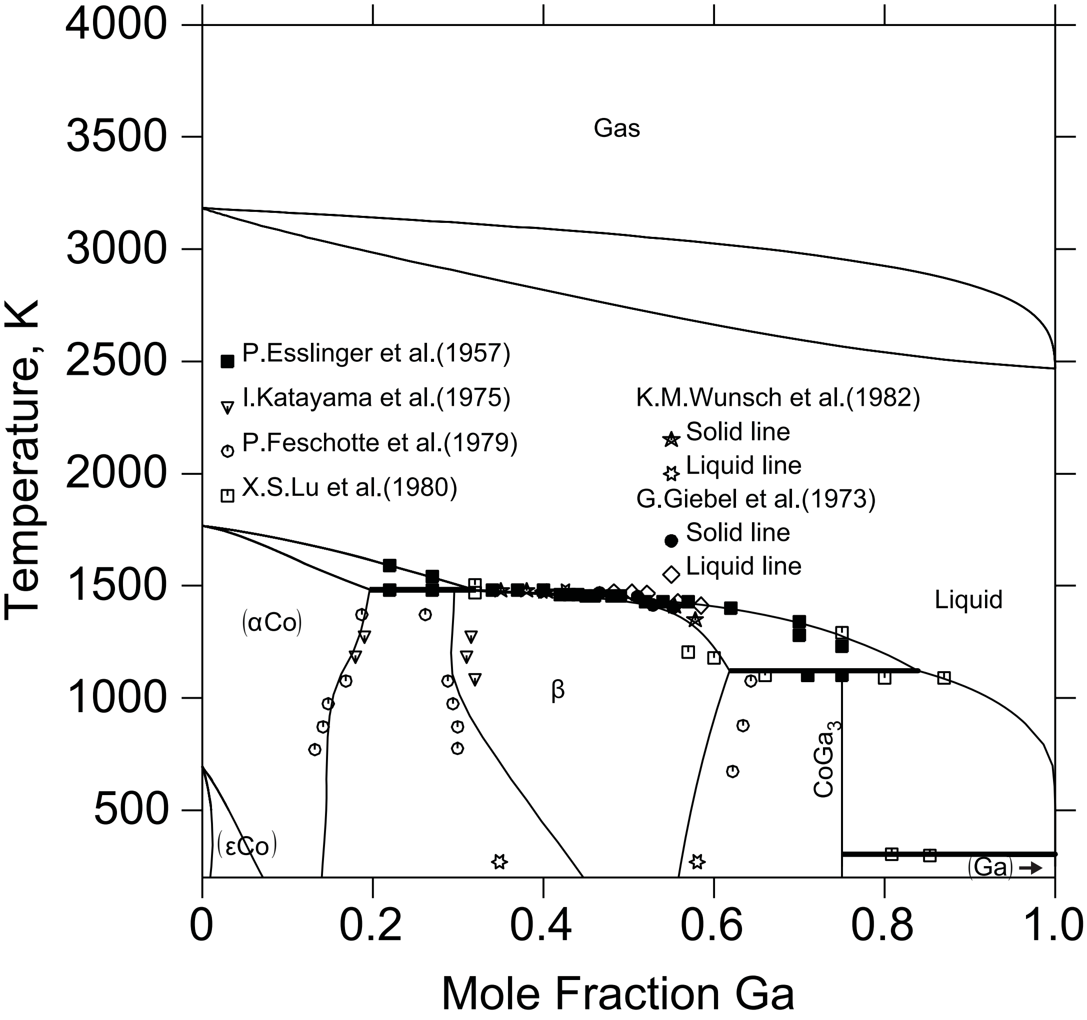

Fig. 24.: Calculated CoGa phase diagram compared with experimental data.

by [47, 82–84, 92, 95]. The solidus of the fcc phase shows good agreement with the data reported by Feschotte [47]. The liquidus agrees well with the experimental results [47,83,84,92]. The solidus of the β phase calculated in this work is more Ga-rich when compared to the curves calculated by Esslinger [84] and Lu [81, 82], and is less Ga-rich than those predicted by Wunsch [83] and Geibel [92]. The solubility of gallium in fcc agrees better with the data reported by Katayama [95] and Feschotte [47] as compared to the model by Su [81].

The total energies of the intermetallic compounds β and $CoGa_3$ and end members of the β phase with the $Pm\bar{3}m$ symmetry in the CoGa system were calculated using DFT [59] within the LDA and GGA approximations, with projector augmented-wave (PAW) pseudo-potentials, as implemented in the Vienna ab initio simulation package (VASP) [60, 61]. The LDA is implemented in VASP according to the Perdew–Zunger parameterization [65] of the data by Ceperly and Alder [66]. In the case of GGA, the PW91 corrections have been used [67]. Brillouin zone integrations were performed using a Monkhorst–Pack mesh [72]. Full relaxations were performed using the Methfessel–Paxton order 1 smearing method [68] and a final self-consistent static calculation with the tetrahedron smearing method with Blöchl corrections [69] was performed. The energy cutoff and k-point mesh used ensured convergence in the total energies calculated within less than 1 meV. Table VI shows the resulting enthalpies of formation. The DFT calculations for the β and $CoGa_3$ phases were excluded from the optimization process.

The lattice parameters of the β and $CoGa_3$ phases were measured by DFT calculations, using LDA and GGA approximations. It was found that the GGA approximations for the calculations of 'a', came closer to the experimental results by 0.073(Å) for the β phase and 0.16(Å) for $CoGa_3$ phase. It was also found that there was a slight tetragonal distortion in $CoGa_3$, and hence the lattice parameter 'c' was not equal to a.

Table VI.: Comparison of the calculated (at 298 K) enthalpies of formation(J/mol-atom) of the β and $CoGa_3$ phases with first principles DFT calculations

Phase	GGA	LDA	Model
β (Ga:Co)	-26900	-39400	-37833
β (Ga:Va)	7700	8600	7250
$CoGa_3$	-25900	-32400	-28666

Table VII.: Comparison of calculated lattice parameters from DFT calculations with experimental data

Phase	Lattice Parameters(Å)	LDA	GGA	Experiments
β	a	2.813	2.886	2.880 [98]
$CoGa_3$	a	6.106	6.260	6.242 [99]
	c	6.295	6.471	6.442 [99]

The tabulated results compared to the results reported by Whittle [98]and Meyer [99] are as shown in Table VII.

We used the first principles results for the end members of the β phase and the enthalpy of formation for the $CoGa_3$ phase to verify the thermodynamic model (i.e. these calculations did not enter into our model). The first-principles calculations yielded results consistent with the thermodynamic model. The enthalpy of formation for the β phase predicted through the model agreed somewhat better with the results obtained from the DFT-LDA approximation, whereas the predicted enthalpy of formation for the $CoGa_3$ phase lies half way between the LDA and GGA calculations. An error of $\backsim$(-2) kJ/mol-atom has been accepted for comparing results.

It is important to re-state the fact that the calculated enthalpies of formation did not enter into the thermodynamic optimization but were rather used as a sanity check for the self-consistency of the thermodynamic model. A further check can be done by comparing the enthalpy of formation of the hypothetical end-member with Gibbs energy function ${}^{0}G^{\beta}_{\mathrm{Ga:Va}}$. This structure has the same symmetry (Pm$\bar{3}$m) as the β phase, but has only the 0,0,0 site occupied by Ga. We performed (full relaxation) calculations within the LDA and GGA approximations, and found that the enthalpy of this end member calculated with F-P was 7700-8600 J/mol depending on whether the LDA or GGA approximation was used. The (enthalpy) model parameter ${}^{0}G^{\beta}_{\mathrm{Ga:Va}}$ relative to orthorhombic Ga is 7250 J/mol (relative to 1 mole of β phase), which agrees perfectly with the F-P results. Again, the F-P calculations corroborate the thermodynamic consistency of the model and reinforce the present model's reliability.

The enthalpies of formation for the intermediate phases at 298 K are shown in Fig. 25 . Results from Predel [96] and Henig [97] do not agree with each other. The calculated values agree well with those reported by Henig [97], specially above Ga compositions of 0.5 when compared to those predicted by Predel [96]. The reference states were taken as hcp for cobalt and orthorhombic for gallium. The predictions from the model and the first-principles calculations seem to suggest that the results from Predel [96] are not reliable at all.

There is very good agreement of the calculated values of enthalpies of formation of liquid alloys, with the results reported by Haddad [94]. In fact, the parameters responsible for entropic contributions to the mixing Gibbs energy of the liquid were very small, resulting in a very small temperature dependence of the mixing (formation) enthalpies of the liquid phase, as is suggested by experimental results.

The invariant reactions and the temperatures obtained in this work is compared with previous work in Table VIII.

For the peritectic reaction involving the decomposition of the β phase, our result

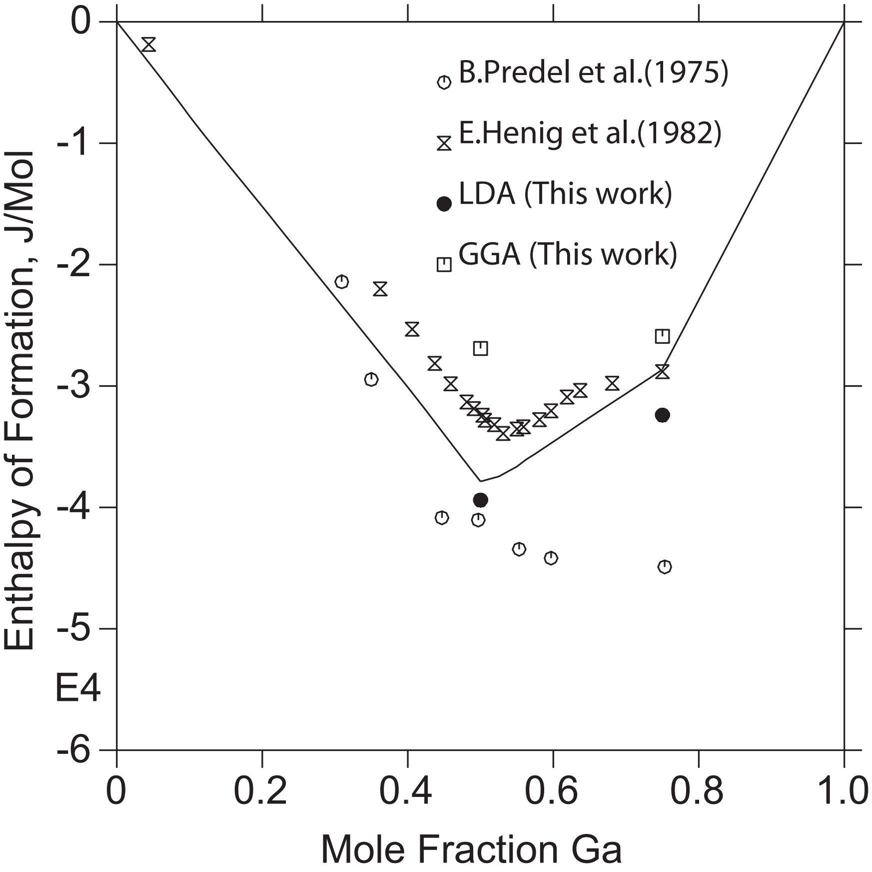

Fig. 25.: Calculated enthalpies of formation for the CoGa intermediate phases at 298 K compared with experimental data. The reference states taken are hcp for cobalt and orthorhombic for gallium.

Table VIII.: Invariant reactions in the CoGa binary system

Reaction	Temperature (K)	Composition (at.% Ga)			Reference
Liq.+fcc↔β	1482	31.85	19.66	29.52	This work
	1483	31.36	18.97	27.05	[81]-Assessment
	1483	26.50	19.00	26.50	[47]-Experimental
	1480	∽30.0	∽13.0	27.50	[84]-Experimental
	1450	∽51.0	∽33.0	∽36.0	[82]-Experimental
Liq.+β ↔fcc	1120	83.97	61.86		This work
	1128	83.55	61.03		[81]-Assessment
	1128	80.00	64.50		[47]-Experimental
	1111	∽80.0	∽65.0		[84]-Experimental
	1106	∽85.0	∽63.0		[82]-Experimental
Liq.+$CoGa_3$ →Orthorhombic Ga	302.9	100	75	100	This work
	303.5	100	75	100	[47]-Experimental

is closer to that obtained by Su and Tedenac [81] and for the invariant reaction involving the decomposition of the $CoGa_3$ phase, our result agrees well with the reported result of Esslinger et al. [84].

The chemical activity of Ga (ref. state: liquid) in the β phase at 1073, 1173 and 1273 K are shown in Fig. 26. A good agreement exists between the calculated and experimental results. The activities agree better with the results reported by Katayama [95]. The chemical activity of Ga (ref. state: liquid) for the fcc solid solutions at 1073 and 1273 K are shown in Fig. 23. The activities at 1073 K show a better compatibility with experimental results reported by Katayama [95], when compared to those at 1273 K.

Figs. 27 and 28 show the calculated sublattice site fractions of vacancies in the second sublattice of the model $(Co,Ga)_{0.5}(Co,Va)_{0.5}$ of the β phase as a function of temperature and composition.

In Fig. 27, there is good agreement with the experimental results as given by Ommen [88] at various compositions of Co. In Fig. 28, the calculated values for the Co-rich side of the β phase have higher values and compare better with results as reported by Ommen and Berner [89,93] when compared to those given by Wunsh [83].

H. Conclusions

Phase relations and consistent thermodynamic properties of the CoGa system based on all experimental information have been evaluated. Thermodynamic parameters have been optimized. In this work, the β phase description has been modified by specifying certain driving force constraints. This model is successful in determining the stability of the β phase at different temperatures. Also, the gas phase has been included. The β phase has been described by a two sublattice model $(Co,Ga)_{0.5}(Co,Va)_{0.5}$ and

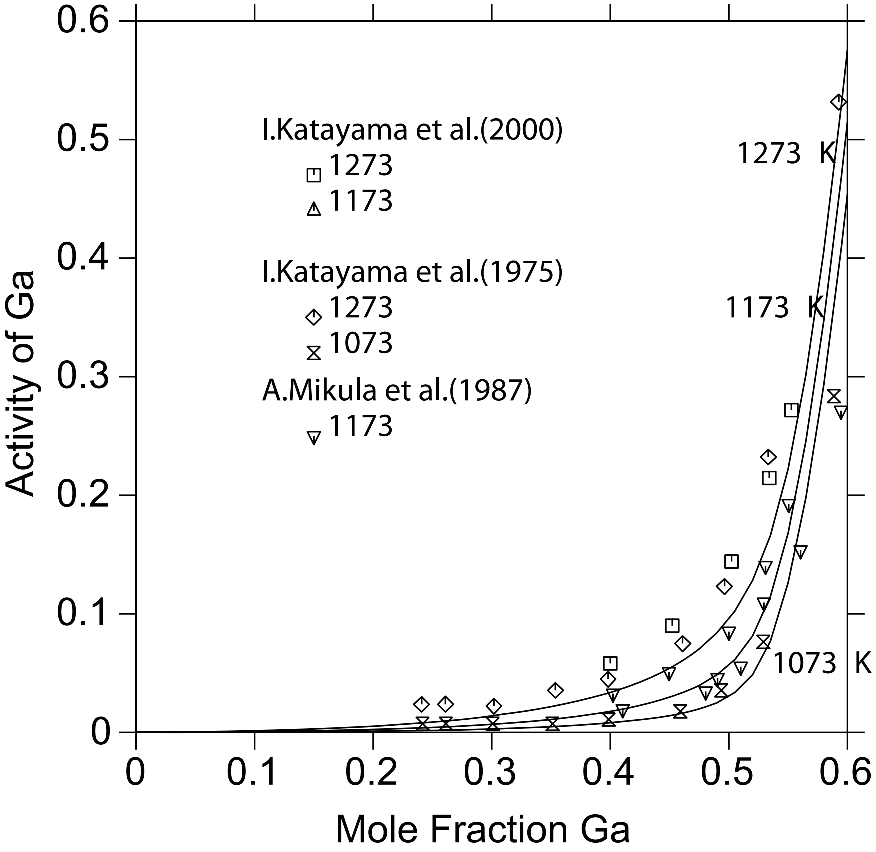

Fig. 26.: Calculated activities in the β phase at 1073, 1173 and 1273 K with experimental data. Reference state: liquid gallium.

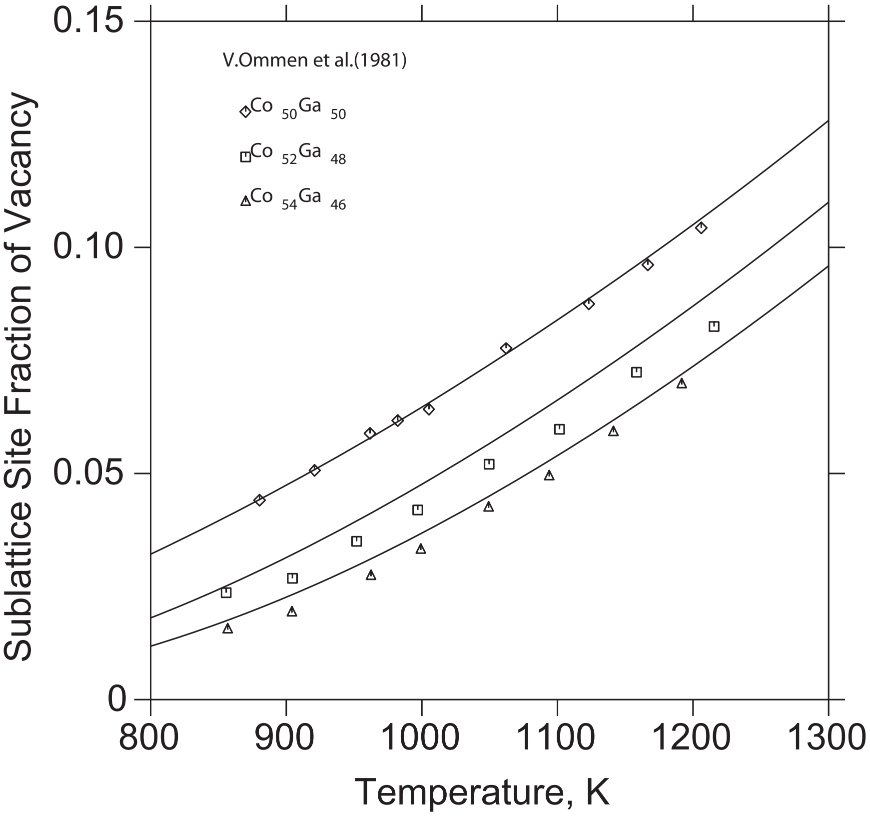

Fig. 27.: Calculated sublattice site fractions of vacancy in the second sublattice of the model $(Co,Ga)_{0.5}(Co,Va)_{0.5}$ of the β phase as a function of temperature at compositions 50, 52, 54 at. % Co with experimental data.

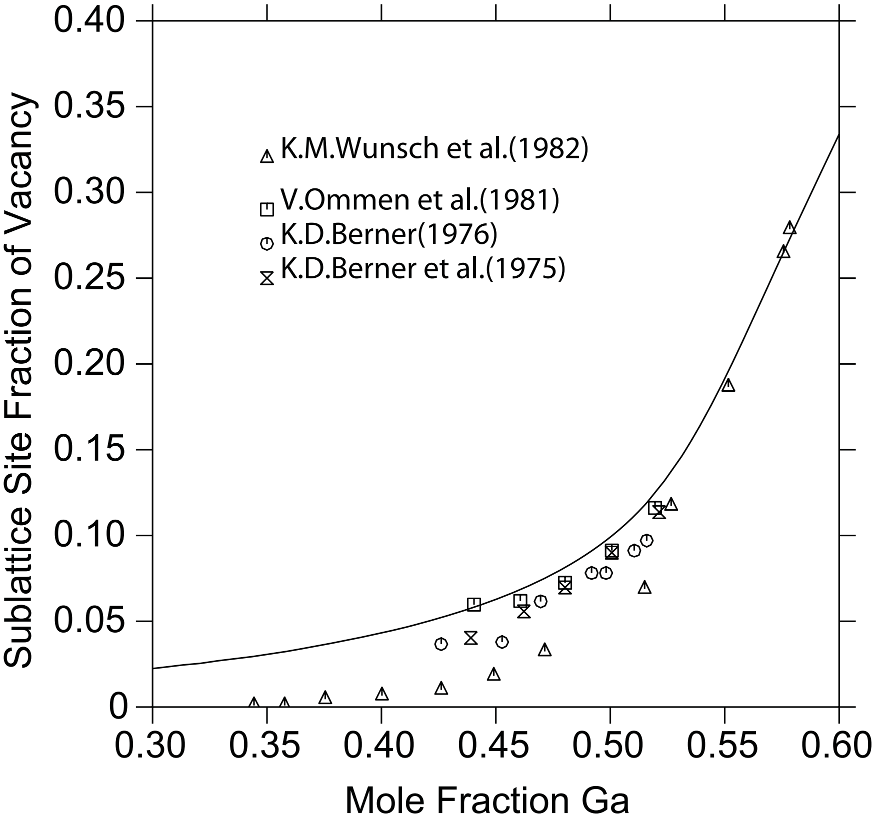

Fig. 28.: Calculated sublattice site fractions of vacancy in the second sublattice of the model $(Co,Ga)_{0.5}(Co,Va)_{0.5}$ of the β phase as a function of composition at 1173 K with experimental data.

the $CoGa_3$ phase is considered to be stoichiometric. The lattice parameters and enthalpies of formation of the β and $CoGa_3$ phases have been verified by first principles DFT calculations. With the set of optimized variables, the thermodynamic phase diagram was assessed successfully and all the thermodynamic properties were compared with experimental results.

CHAPTER VI

THERMODYNAMIC MODELING OF THE CoNiGa SYSTEM

A. Overview

The CoNiGa ternary system has recently emerged as a promising alternative to currently used high temperature Shape Memory Alloys, with possible applications in the aerospace and automotive industries. In this work, thermodynamic modeling is used based on the CALPHAD approach to investigate the thermodynamic properties, phase stability and shape memory properties of these alloys. The thermodynamic model parameters have been obtained by fitting experimental and ab initio data. In order to investigate the martensitic transformation, the parameters describing the Gibbs free energy of the martensite (tetragonal) phase were optimized through the use of experimentally determined Ms temperatures. The stability of the β phase at high temperatures was enforced accurately by remodeling the CoGa system. Also, the phase stabilities of Ni_5Ga_3 (δ) and $Ni_{13}Ga_9$ (ϵ) were determined as they are known to cause detrimental effects in the ternary at low temperatures.

B. Introduction

Recent alternatives to the conventional Heusler Ni_2MnGa alloys have been the CoNiAl and CoNiGa systems [4]. These alloy systems have shown to exhibit shape memory and pseudoelastic properties at low temperatures. Also, CoNiGa alloys are commercially important as SMAs operating at temperatures above 250 °C. Limited experimental information is available for this system for a wide range of composition, and temperature regions [4, 5, 9] A reliable and consistent thermodynamic model of the CoNiGa system has not been calculated using a computational approach thus far, and it would be useful to have a complete description of phase stability over a wide range of compositions and temperatures.

It was shown that the ductility of the brittle CoNiGa β alloys can be improved by the addition of the γ (fcc) phase [4]. Hence, the study of the stability of the β phase (which undergoes the martensitic transformation in the ternary and has a wide range of stability in the NiGa and CoGa binaries), along with the existence of the two-phase $\beta + \gamma$ equilibrium in the Co-rich and Ni-rich regions in the binaries, is important in this investigation in order for the ternary alloy system to be used as a ductile ferromagnetic Shape Memory Alloy.

The CoGa binary model developed by Su and Tedenac [81] was described accurately for low temperatures and it was seen that the β phase became stable at temperatures higher than 1000 °C. Although this artifact does not pose a difficulty in the binary, the extrapolation to the ternary CoNiGa system becomes difficult. This behavior was resolved in our previous work [31], and the CoGa system was remodeled with the β phase becoming stable at only lower temperatures. In this work, the binary phase descriptions of the CoGa [31], NiGa [34] and CoNi [100] systems have been used from previously developed models, for the modeling of the ternary. The thermodynamic parameters obtained in the binary become useful when trying to calculate the properties of the ternary system. But a simple extrapolation of these models cannot be performed, due to the effect of higher order ternary interaction parameters in the system. The ternary system was hence modeled using the data available from experiments and information from the lower order binary systems.

In the present work, a self-consistent thermodynamic model of the CoNiGa Shape Memory Alloy has been obtained using a combined CALPHAD and Ab-Initio method. The binary interaction parameters were obtained from previous models [31, 34, 100] while the ternary interaction parameters were derived using experimental information in the optimization module 'Parrot' of the ThermoCalc package. The ternary model was then used to calculate isothermal sections at various temperatures, activities, enthalpy of formation and vertical sections. Experiments were conducted to corroborate the results obtained from the calculated thermodynamic model.

The main aim of this work is to develop a model for the Shape Memory Alloy with accurate descriptions of the Gibbs energies of its phases. This system should then be able to demonstrate required characteristics such as perfect Shape Memory Effect(SME) and pseudoelasticity (PE) for temperatures of 500 °C and above, have a broad range of M_s temperatures, high Curie Temperature (T_c) and provide a better understanding of how the martensitic transformation temperature M_s changes with composition.

C. Literature review

There have been several reports on Ni_2MnGa alloys being used as ferromagnetic shape memory materials. The main disadvantage found in these Heusler type alloys is that they are brittle in the polycrystalline state. This prevents them from being used as Ferromagnetic Shape Memory Alloys (FSMAs). Studies by Ishida et al. [101] showed that the ductility of the brittle CoNiGa β alloys can be improved by the introduction of γ phase (disordered fcc A1) of Ni solid solution on the grain boundaries of the β phase. This was also reported by Liu et al. and Oikawa et al [4, 102]. A two-stage annealing process was found to be an effective method in order to develop such a microstructure, among other methods [4, 9, 102] for this alloy. This type of microstructural control was also developed in several other Shape Memory Alloys such as CoNiAl [103, 104], NiFeAl [105, 106] and NiFeGa alloys [33, 107, 108]. Studies by Prusik et al. [30] showed that the precipitation of γ particles on the grain boundaries had a positive effect to increase ductility as compared to when the particles were dispersed inside the grains of the matrix. Another advantage of the CoNiGa Shape Memory Alloys is that their Curie temperature (T_c)is higher, thus having higher magnetization when compared to Ni_2MnGa alloys.

The equilibria among the phases in the CoNiGa system are similar to that in the CoNiAl system because Al and Ga belong to the same group IIIb in the periodic table. Also, the β phase has a wide homogeneity range and an equilibrium exists with the γ phase in the Co-rich and Ni-rich compositions [4, 5, 109]. Mikula et al. [110], showed through their XRD studies that the β phase has a B2 structure at 900 °C. This was also reported by Booth et al. [111] at 550 °C and 830 °C. They concluded that Ni atoms occupy Co sites in the β phase and the Co atoms that were displaced in the Co sublattice move to the Ga sublattice.

The β phase and γ phases occupy a wide concentration range of the phase diagram and it is known that the β phase is the one that undergoes the martensitic transformation to the $L1_0$ phase [33, 108]. It is thus important to correctly ascertain the composition region where this martensitic phase is stable. Ducher et al. [33, 112, 113] performed the diffusion triple technique to determine the phase equilibria in the ternary at isothermal sections of 700 °C and 1000 °C. Their study focussed on the Ni-rich composition regions where the martensitic transformations are observed. Equilibrium concentrations (at. %)for the two temperatures were accurately determined, which was used for the present work. At temperatures of 700 °C and below, Ducher et al. [27] and Ipser et al. [34] reported the presence of the δ-Ni_5Ga_3 and ϵ-$Ni_{13}Ga_9$ phases, in their models of the NiGa binary system. It was found that these phases penetrate into the ternary, continuing in the CoGa direction parallel to CoNi. Also, these phases are known to cause detrimental effects in the ternary. Vertical sections of 20 at. % Ni with varying compositions of Co and Ga was calculated by Ducher et al. [33]. This section forms a basis for the microstructural control in the CoNiGa SMA.

The crystal structure of the ternary β phase is an ordered cubic, B2-type structure. Different chemical models were suggested [83,88–91] to describe the β phase with point defects and vacancy concentration using a triple defect structure in the binary CoGa and NiGa subsystems. The models suggest that this phase is a substitutional solid solution for higher compositions of Co and deviates from this substitutional behavior at higher compositions of Ga, in which large concentrations of vacancies are responsible for the observed deviations from non-stoichiometry. This model was used by Su and Tedenac [81] in their binary CoGa system, where the cobalt and gallium atoms combined on the 1st sublattice and cobalt and vacancies combined on the 2nd sublattice. The two-sublattice model for the β phase is given by $(\mathrm{Co,Ga})_{0.5}(\mathrm{Co,Va})_{0.5}$. We also incorporated the same defect structure for the β phase while remodeling the CoGa system [31] Incidentally, Yuan and Ipser [34] in their model for NiGa, have also described the β phase using the same description for its defect structure, which we have used to model the ternary system. Gröbner [40] did not use the triple defect model.

However, limited information exists in literature on the thermodynamic properties and vacancy concentration of the ternary intermetallic β phase which exhibits triple defects. Mikula et al. [110] through their emf studies were able to predict these properties for a wide range of concentration. They calculated the activity curves and enthalpy of formation of the ternary alloy for varying at.% Ga. They were also able to predict the thermodynamic properties of the β phase (in the temperature range of 800-1000 °C) that showed triple-defects in the NiGa and CoGa binary systems. These calculations were also extended to the ternary. Three sections with constant ratios of x_{Co}/x_{Ni} taken as 3:1, 1:1 and 1:3 with varying Ga content of 40,45,50,55 and 60 at.% were studied by Mikula et al. [110]. The emfs obtained through their experiments were used to calculate the activity and partial molar enthalpy. The data for the partial molar enthalpy and activities were then used as data points to check the consistency of the model by comparing the experimental data and the values predicted in the present work.

The order-disorder transformation phenomenon between the γ and γ' phases has not been included in the present work as it is known to hinder the shape memory performance characteristics [5, 107, 114] and Magnetic Field-Induced Strain (MFIS) [5, 115]. This will be incorporated in future work.

1. Two-phase tie-lines

Tie lines are those that connect the composition of phases whose chemical potentials μ_i are the same. Compositions of the β, γ and γ' phases were taken from the experimental investigations of Oikawa et al. and Ducher et al. [4,9,33], in order to optimize the model parameters and calculate the equilibria among the phases.

The experimental information for these tie lines were obtained from the work of Ducher et al. [33] who used the diffusion triple (DT) method to determine phase equilibria over a wide composition range at 700 °C and 1000 °C. Oikawa et al. [4] measured the composition of the β and γ phases in equilibrium for a temperature range of 1000-1300 °C using energy dispersion X-ray spectroscopy (EDX). The experimental tie-lines indicate an equality in chemical potential of the element that is common to the two binary subsystems [22].

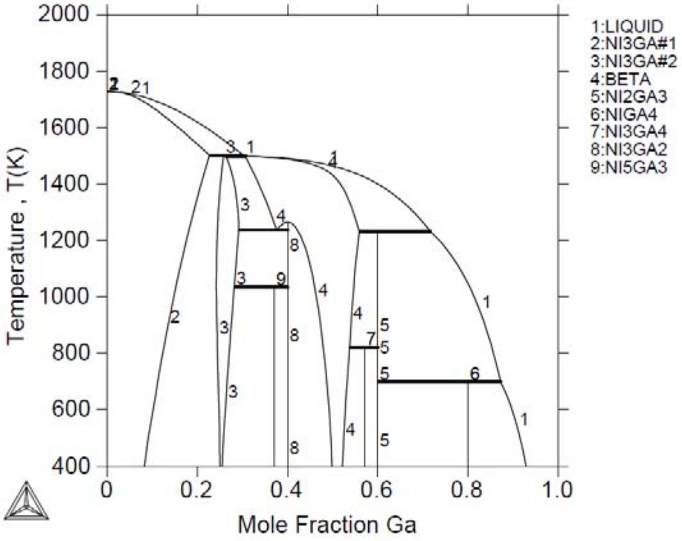

Fig. 29.: Binary NiGa phase diagram as calculated by Ipser et al. [34]

D. Thermodynamic model

1. Binary sub-systems

The phase description of the binary systems that make up the ternary have been taken from the work of Ipser et al. [34] (Fig. 29) for the NiGa binary, Chari et al. [31] (Fig. 30) for the CoGa system and the thermodynamic description of the CoNi system has been taken from the SGTE solution database (Fig. 31).

The thermodynamic phase description of the CoGa system by Chari et al. [31] is a remodeled system based on the previous work by Su and Tedenac [81]. The re-assessment was necessary to account for the stability conditions of the β phase at higher temperatures. The remodeled phase diagram is shown in Fig. 30.

Ipser et al. [34] described the order-disorder transformation between the non stoichiometric Ni_3Ga-(γ') and fcc(γ) phases, while modeling the NiGa system. In

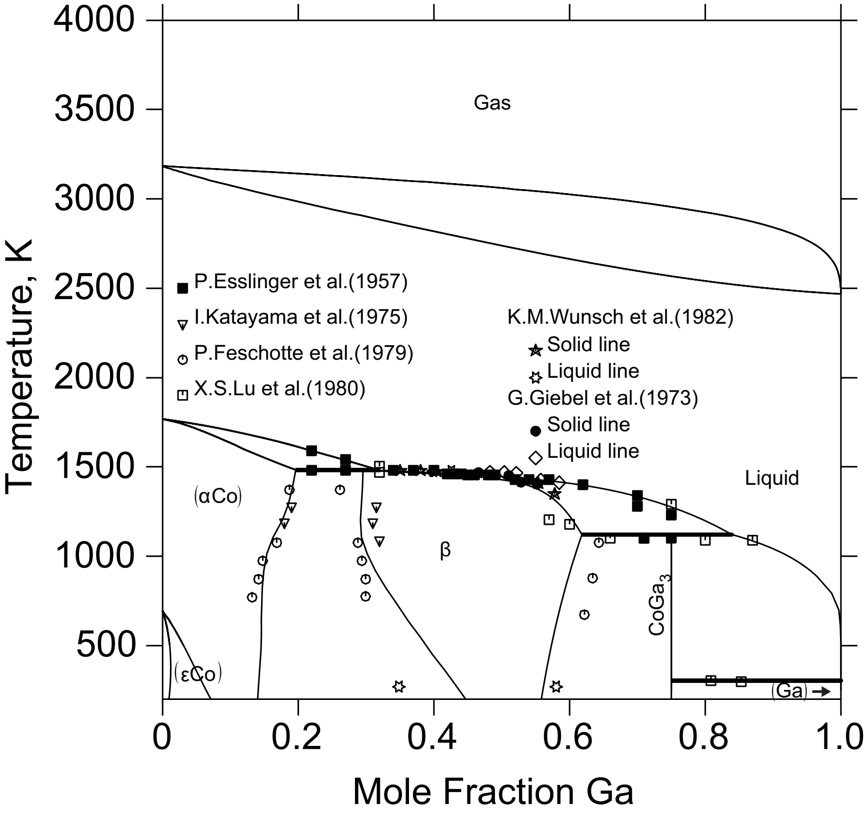

Fig. 30.: Calculated CoGa phase diagram compared with experimental data.

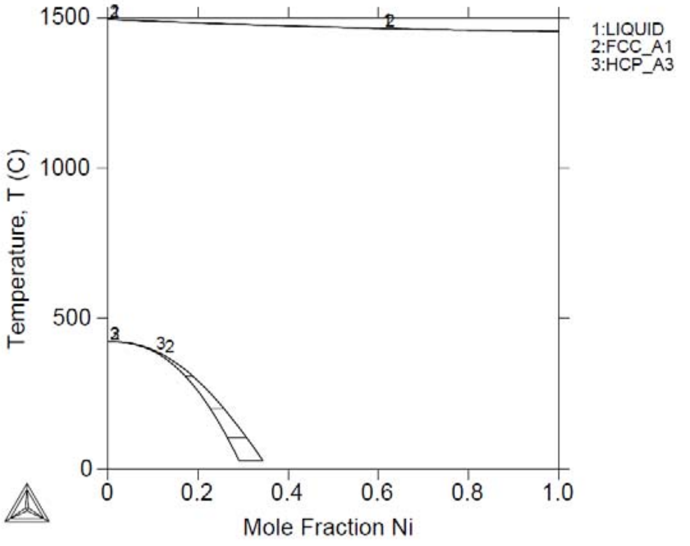

Fig. 31.: Binary CoNi phase diagram taken from the SGTE solution database of ThermoCalc.

order to consistently model the ternary, this phenomenon has not been taken into consideration. The Ni_5Ga_3 (δ) and Ni_3Ga_2 (ϵ) phases were modeled as stoichiometric phases entering into the ternary. They were modeled as non-stoichiometric phases as given by the experimental description of these phases by Ducher et al. [33] at 700 °C and this could be incorporated in future work.

E. Experimental procedure

In order to validate the thermodynamic model for the CoNiGa ternary system, Dr. Karaman's group performed heat treatments on different CoNiGa alloy compositions (in at.%). These were prepared using vacuum arc-melting of 99.9% purity Co, 99.95% Ni and 99.999% purity Ga. The compositions were chosen from different regions of the ternary system. These alloys were prepared in the form of arc melted buttons. The expected phases according to the thermodynamic model and experimentally observed phases at certain temperatures have been listed in Table IX.

Table IX.: Heat treatments performed for six chosen alloys to corroborate phase stability in the calculated phase diagram

Composition	Temperature	Duration	Expected Phases	Observed Phases	γ phase volume fraction (%)
$Co_{0.05}Ni_{0.62}Ga_{0.33}$	1127 °C	1 day	β	β,γ',hcp ($Ni_{1.235}Ga_{0.665}$)	0
	+1200 °C	1 day	β	β	0
	+300 °C	1 week	γ',γ,Ni_5Ga_3	β,hcp ($Ni_{1.235}Ga_{0.665}$)	
$Co_{0.15}Ni_{0.8}Ga_{0.05}$	1200 °C	4 hours	γ	γ	100
$Co_{0.2}Ni_{0.65}Ga_{0.15}$	1127 °C	1 day	γ	γ	100
	300 °C	1 week	γ,γ'	γ	
$Co_{0.3}Ni_{0.45}Ga_{0.25}$	1077 °C	1 day	β, γ	β, γ	50
	300 °C	1 week	γ,Ni_5Ga_3	β,γ	
$Co_{0.6}Ni_{0.1}Ga_{0.3}$	1027 °C	1 day	β	β	0
$Co_{0.8}Ni_{0.15}Ga_{0.05}$	1200 °C	4 hours	γ		

Continued on next page

TableIX–Continued

	1200 °C	4 hours	γ	hcp (Co_3Ni)	

The microstructural evolution and chemical analysis were examined using a digital Keyence VH-Z100 optical microscopy (OM) and a Cameca SX50 scanning electron microscopy (SEM) equipped with four wavelength dispersive X-Ray spectrometers (WDS). The samples examined using OM were etched in 50% hydrochloric acid, 33% ethanol, 8.5% copper sulfate and 8.5% water solution. Crystal structure of different phases were determined using a Bruker-AXS D8 X-ray diffractometer (XRD)with CuK_α (0.15406 nm) radiation.

F. Optimization procedure

Experimental data including activities, volume fractions, tie-lines, triple points and partial molar enthalpies [4, 5, 9, 33, 110] were included in the optimization process, which was performed using the software ThermoCalc. The software uses a technique of global minimization of Gibbs energy to assess the thermodynamic model parameters such as the Gibbs energy functions and interaction parameters. The binary system parameters were taken from previously developed models of the NiGa and CoGa systems [31, 34] and these values remained fixed throughout the optimization process. Initial weights were given to the experimental data based on the accuracy required for the calculations. The weights were increased as the optimization process continued, depending if the results evaluated were within the uncertainty of the measurements. This was to ensure that self-consistent results were obtained.

All the model parameters were optimized together, starting with a small number of optimization iterations and increasing this number as the optimization progressed. Negative driving force constraints for some phases were enforced in regions of the ternary to prevent their stability in those regions.

The starting values of the ternary interaction parameters were given by a trial and error method, till a reasonable fit was obtained with respect to the experimental data. The experimental data for vertical sections and volume fractions were given low weights throughout the optimization process, with higher weights given to the triple points and tie lines. As the optimization process progressed, the weights for the triple points were increased.

In order for the binary system parameters to enter into the ternary, it was necessary to include ternary interaction parameters as well as the enthalpies of formation for the Gibbs energy functions of the end members of the Ni_3Ga, Ni_5Ga_3 and Ni_3Ga_2 phases. The enthalpies were calculated using first-principles within the GGA approximation with projector augmented-wave (PAW) pseudo-potentials, as implemented in the Vienna ab initio simulation package (VASP) [60, 61]. In the case of GGA, the PW91 corrections have been used [67]. Brillouin zone integrations were performed using a Monkhorst–Pack mesh [72]. Full relaxations were performed using the Methfessel–Paxton order 1 smearing method [68] and a final self-consistent static calculation with the tetrahedron smearing method with Blöchl corrections [69] was performed. The energy cutoff and k-point mesh used ensured convergence in the total energies calculated within less than 1 meV. The DFT calculations for the end members were included in the optimization process.

G. Results and discussion

1. Isothermal sections at 700 °C, 1000 °C and 1200 °C

a. Microstructure and two-phase equilibrium

The ternary phase diagram was optimized for a wide range of temperatures and the isothermal sections are shown in Figs. 32, 33 and 34 as compared with experimental data. Equilibrium concentrations of the γ, β and γ' phases at 700 °C, 1000 °C and

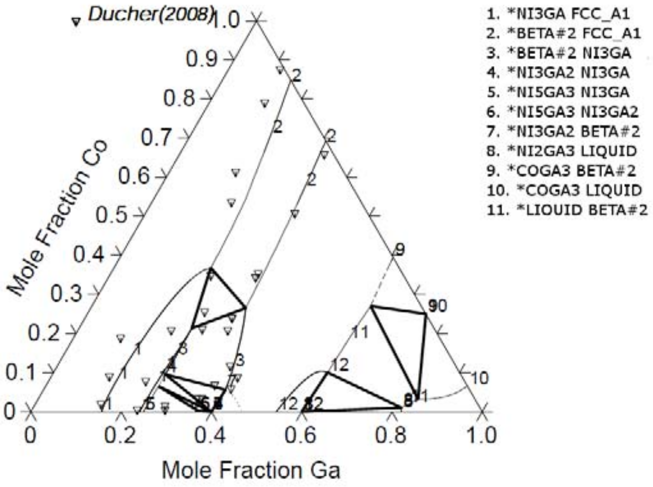

Fig. 32.: Isothermal section schematic phase diagram of the CoNiGa ternary system at 700 °C.

1200 °C have been listed in Table (X). The optimized binary and ternary interaction parameters, including the Gibbs energy functions have been calculated using the model and listed in Table (XI)

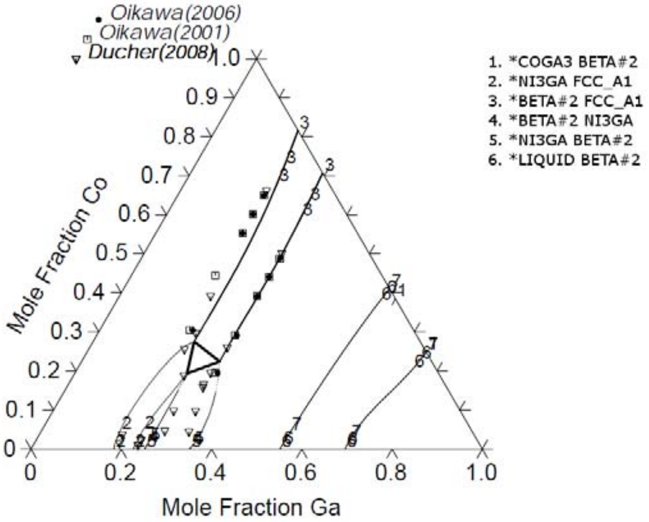

Fig. 33.: Isothermal section schematic phase diagram of the CoNiGa ternary system at 1000 °C.

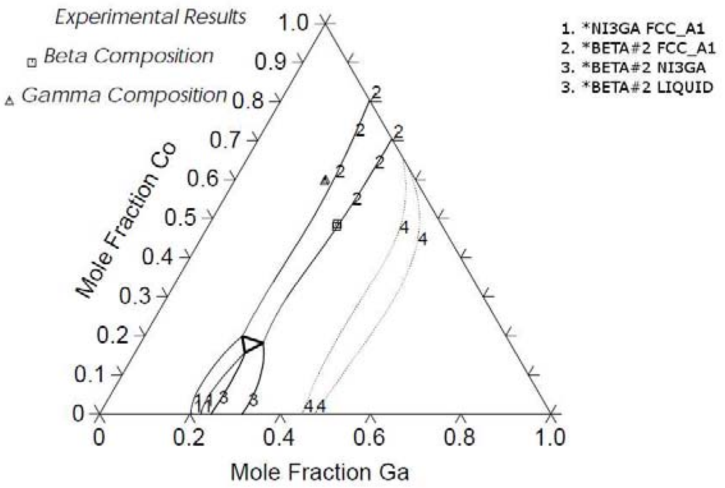

Fig. 34.: Isothermal section schematic phase diagram of the CoNiGa ternary system at 1200 °C.

Table X.: Composition of β, γ and γ' phases at various temperatures in the CoNiGa system, compared with experimental data. Values of the experimental data are in brackets

T, °C	β Phase		γ Phase		γ' Phase		Ref.
	At. % Co	At. % Ga	At. % Co	At. % Ga	At. % Co	At. % Ga	
700 °C	33.10 (34.4)	33.54 (32.6)	49.70 (53.6)	21.42 (17.6)	-	-	[33]
	34.61 (35.4)	33.30 (32.7)	54.53 (61.3)	20.53 (14.7)	-	-	
	51.21 (50.8)	32.39 (33.1)	71.74 (79.1)	17.18 (12.3)	-	-	
	67.21 (65.8)	30.25 (32.1)	80.49 (87.6)	16.22 (11.4)	-	-	
	-	-	7.45 (9.00)	15.29 (12.9)	6.54 (2.56)	23.64 (25.7)	
	-	-	2.02 (2.00)	15.46 (14.5)	5.08 (2.12)	23.34 (27.4)	
	21.03 (20.8)	36.01 (33.2)	-	-	19.22 (20.8)	25.45 (20.7)	
1000 °C	25.56 (19.6^1,19.49^2)	30.44 (31.0^1,31.6^2)	35.82 (30.5^1,30.4^2)	23.01 (20.0^1,20.672)	-	-	[4]^1, [9]^2

Continued on next page

TableX–Continued

	28.58	30.46	39.14	22.63	-	-	[4]^1, [9]^2
	(29.2^1,29.1^2)	(30.5^1,31.06^2)	(44.40^1,53.31^2)	(18.61,10.10^2)			
	38.54	30.57	51.21	22.45	-	-	[4]^1, [9]^2
	(39.1^1,39.08^2)	(30.6^1,30.58^2)	(55.4^1,55.34^2)	(19.2^1,19.21^2)			
	43.37	30.70	56.34	21.92	-	-	[4]^1, [9]^2
	(44.0^1,44.01^2)	(30.80^1,30.77^2)	(60.2^1,60.17^2)	(19.1^1,19.11^2)			
	48.80	30.54	61.47	21.40	-	-	[4]^1, [9]^2
	(48.9^1,48.88^2)	(30.7^1,30.72^2)	(64.9^1,64.85^2)	(19.2^1,19.17^2)			
	-	-	4.13 (3.70^3)	17.97	2.32	21.93	[33]^3
				(18.40^3)	(1.00^3)	(23.20^3)	
	-	-	2.32 (1.50^3)	17.85	0.51	22.58	[33]^3
				(18.90^3)	(2.30^3)	(23.30^3)	
	9.26 (9.70^3)	34.76	-	-	10.17	25.65	[33]^3
		(31.60^3)			(9.80^3)	(26.70^3)	

Continued on next page

TableX–Continued

	4.73 (4.40[3])	34.48 (32.80[3])	-	-	5.34 (4.70[3])	25.51 (27.30[3])	[33][3]
1200 °C	49.1 (48.65)	28.35 (28.36)	58.46 (59.8)	22.14 (20.19)	-	-	Exp
	47.89 (48.13)	28.19 (28.4)	57.85 (59.36)	22.19 (20.08)	-	-	Exp

Table XI.: Optimized parameters for the phases in the ternary

Gas	$^0G^{\text{Gas}}_{\text{Co}}$	$F6985T + RTln(1 * 10^{-5}P)$
	$^0G^{\text{Gas}}_{\text{Ga}}$	$F9633T + RTln(1 * 10^{-5}P)$
	$^0G^{\text{Gas}}_{\text{Ga2}}$	$F9695T + RTln(1 * 10^{-5}P)$
Liquid	$^0L^{\text{Liq}}_{\text{Co,Ga}}$	$-61807 + 7.985T$
	$^1L^{\text{Liq}}_{\text{Co,Ga}}$	12605.5
	$^0L^{\text{Liq}}_{\text{Co,Ga,Ni}}$	$66048.054 + 3.162T$
	$^0L^{\text{Liq}}_{\text{Co,Ni}}$	1331
	$^0L^{\text{Liq}}_{\text{Ga,Ni}}$	$-122488.59 + 35.72 * T$
	$^1L^{\text{Liq}}_{\text{Ga,Ni}}$	$-29685 + 14 * T$
	$^2L^{\text{Liq}}_{\text{Ga,Ni}}$	$-30751.9 + 22.1 * T$
Fcc	$^0L^{\text{fcc}}_{\text{Co,Ga}}$	$-125202.28 + 54.131T$
	$^1L^{\text{fcc}}_{\text{Co,Ga}}$	$30657 - 25.625T$
	$^0L^{\text{fcc}}_{\text{Co,Ga,Ni}}$	$-1.7622 - 38.595T$
	$^1L^{\text{fcc}}_{\text{Co,Ga,Ni}}$	$0.8857 - 1.176T$
	$^2L^{\text{fcc}}_{\text{Co,Ga,Ni}}$	$0.45 - 53.406T$

Continued on next page

TableXI–Continued

	${}^{0}L^{\mathrm{fcc}}_{\mathrm{Co,Ni}}$	$-800 + 1.2629T$
	${}^{0}L^{\mathrm{fcc}}_{\mathrm{Ga,Ni}}$	$-130526 + 40T$
Hcp	${}^{0}L^{\mathrm{hcp}}_{\mathrm{Co,Ga}}$	$-87051 + 22.438T$
	${}^{0}L^{\mathrm{hcp}}_{\mathrm{Co,Ni}}$	$-1620 - 0.385T$
$\mathrm{CoGa_3}$	${}^{0}G^{\mathrm{CoGa_3}}_{\mathrm{Co:Ga}} - 0.25{}^{0}G^{\mathrm{hcp}}_{\mathrm{Co}} - 0.75{}^{0}G^{\mathrm{ort}}_{\mathrm{Ga}}$	$-30770 + 3.043T$
B2(β)	${}^{0}G^{\beta}_{\mathrm{Co:Co}} = {}^{0}G^{\mathrm{bcc}}_{\mathrm{Co}}$	${}^{0}G^{\mathrm{hcp}}_{\mathrm{Co}} + 2938 - 0.7138T$
	${}^{0}G^{\beta}_{\mathrm{Ga:Co}} - 0.5{}^{0}G^{\mathrm{ort}}_{\mathrm{Ga}} - 0.5{}^{0}G^{\mathrm{hcp}}_{\mathrm{Co}}$	$-42125 + 9.519T$
	${}^{0}G^{\beta}_{\mathrm{Ni:Co}} - 0.5{}^{0}G^{\mathrm{bcc}}_{\mathrm{Ni}} - 0.5{}^{0}G^{\mathrm{bcc}}_{\mathrm{Co}}$	39.147
	${}^{0}G^{\beta}_{\mathrm{Co:Ni}} - 0.5{}^{0}G^{\mathrm{bcc}}_{\mathrm{Ni}} - 0.5{}^{0}G^{\mathrm{bcc}}_{\mathrm{Co}}$	$4850.934 - 8.378T$
	${}^{0}G^{\beta}_{\mathrm{Ga:Ni}} - 0.5{}^{0}G^{\mathrm{bcc}}_{\mathrm{Ga}} - 0.5{}^{0}G^{\mathrm{bcc}}_{\mathrm{Ni}}$	$-54030.75 + 16.5 * T$
	${}^{0}G^{\beta}_{\mathrm{Ni:Ni}}$	${}^{0}G^{\mathrm{bcc}}_{\mathrm{Ni}}$
	${}^{0}G^{\beta}_{\mathrm{Co:Va}}$	$0.5{}^{0}G^{\mathrm{hcp}}_{\mathrm{Co}} + 52313 - 16.5828 * T$
	${}^{0}G^{\beta}_{\mathrm{Ga:Va}}$	$0.5{}^{0}G^{\mathrm{ort}}_{\mathrm{Ga}} + 7250 - 6.35T$
	${}^{0}G^{\beta}_{\mathrm{Ni:Va}}$	${}^{0}G^{\mathrm{bcc}}_{\mathrm{Ni:Va}}$
	${}^{0}L^{\beta}_{\mathrm{Co,Ga:Co}}$	$-11752 + 3.505T$

Continued on next page

TableXI–Continued

	${}^{0}L^{\beta}_{\mathrm{Co,Ni:Co}}$	$68.236 - 0.5264T$
	${}^{0}L^{\beta}_{\mathrm{Co:Co,Va}}$	$-6847 + 0.6913T$
	${}^{0}L^{\beta}_{\mathrm{Co:Co,Ni}}$	$-14.586 + 1.7T$
	${}^{0}L^{\beta}_{\mathrm{Ga,Ni:Co}}$	$-50.724 - 5.817T$
	${}^{0}L^{\beta}_{\mathrm{Ga:Co,Va}}$	$-24462 + 9.677T$
	${}^{0}L^{\beta}_{\mathrm{Co,Ga:Ni}}$	$-12540.193 + 0.2745T$
	${}^{0}L^{\beta}_{\mathrm{Ga,Ni:Ni}}$	$-8724 - 2.38T$
	${}^{0}L^{\beta}_{\mathrm{Ga:Ni,Va}}$	$-35016.42 + 20.31T$
	${}^{0}L^{\beta}_{\mathrm{Ni:Ni,Va}}$	$-35016.42 + 20.31T$
	${}^{0}L^{\beta}_{\mathrm{Co,Ga:Va}}$	$-7557 - 0.3907T$
	${}^{0}L^{\beta}_{\mathrm{Ga,Ni:Va}}$	$-8724 - 2.38T$
$\mathrm{Ni_2Ga_3}$	${}^{0}G^{\mathrm{Ni_2Ga_3}}_{\mathrm{Ni:Ga}} - 0.4{}^{0}G^{\mathrm{fcc}}_{\mathrm{Ni}} - 0.6{}^{0}G^{\mathrm{ort}}_{\mathrm{Ga}}$	$-47426.09 + 8.94T$
$\mathrm{Ni_3Ga}$	${}^{0}G^{\mathrm{Ni_3Ga}}_{\mathrm{Co:Co}}$	${}^{0}G^{\mathrm{fcc}}_{\mathrm{Co}}$
	${}^{0}G^{\mathrm{Ni_3G}}_{\mathrm{Ga:Co}}a - 0.25{}^{0}G^{\mathrm{hcp}}_{\mathrm{Co}} - 0.75{}^{0}G^{\mathrm{ort}}_{\mathrm{Ga}}$	9116.964
	${}^{0}G^{\mathrm{Ni_3Ga}}_{\mathrm{Co:Ga}} - 0.75{}^{0}G^{\mathrm{hcp}}_{\mathrm{Co}} - 0.25{}^{0}G^{\mathrm{ort}}_{\mathrm{Ga}}$	-5758.22

Continued on next page

TableXI–Continued

	${}^{0}G^{\mathrm{Ni_3Ga}}_{\mathrm{Ga:Ga}}$	${}^{0}G^{\mathrm{fcc}}_{\mathrm{Ga}}$
	${}^{0}G^{\mathrm{Ni_3Ga}}_{\mathrm{Ni:Ga}} - 0.75{}^{0}G^{\mathrm{fcc}}_{\mathrm{Ni}} - 0.25{}^{0}G^{\mathrm{fcc}}_{\mathrm{Ga}}$	$-27789 + 5.24T$
	${}^{0}G^{\mathrm{Ni_3Ga}}_{\mathrm{Co:Ni}} - 0.75{}^{0}G^{\mathrm{hcp}}_{\mathrm{Co}} - 0.25{}^{0}G^{\mathrm{fcc}}_{\mathrm{Ni}}$	314
	${}^{0}G^{\mathrm{Ni_3Ga}}_{\mathrm{Ga:Ni}} - 0.75{}^{0}G^{\mathrm{fcc}}_{\mathrm{Ga}} - 0.25{}^{0}G^{\mathrm{fcc}}_{\mathrm{Ni}}$	3200
	${}^{0}G^{\mathrm{Ni_3Ga}}_{\mathrm{Ni:Ni}}$	${}^{0}G^{\mathrm{fcc}}_{\mathrm{Ni}}$
	${}^{0}L^{\mathrm{Ni_3Ga}}_{\mathrm{Co,Ni:Ga}}$	-24445.144
	${}^{0}L^{\mathrm{Ni_3Ga}}_{\mathrm{Ga,Ni:Ga}}$	$-25578 + 3T$
	${}^{0}L^{\mathrm{Ni_3Ga}}_{\mathrm{Ga,Ni:Ni}}$	$-25578 + 3T$
	${}^{0}L^{\mathrm{Ni_3Ga}}_{\mathrm{Ga,Ni:Co}}$	$-25578 + 3T$
	${}^{1}L^{\mathrm{Ni_3Ga}}_{\mathrm{Ga,Ni:Ga}}$	$14040 - 8T$
	${}^{1}L^{\mathrm{Ni_3Ga}}_{\mathrm{Ga,Ni:Ni}}$	$14040 - 8T$
	${}^{1}L^{\mathrm{Ni_3Ga}}_{\mathrm{Ga,Ni:Co}}$	$14040 - 8T$
	${}^{1}L^{\mathrm{Ni_3Ga}}_{\mathrm{Ga:Ga,Ni}}$	$7841.97 - 4.133T$
	${}^{1}L^{\mathrm{Ni_3Ga}}_{\mathrm{Ni:Ga,Ni}}$	$7841.97 - 4.133T$
	${}^{1}L^{\mathrm{Ni_3Ga}}_{\mathrm{Co:Ga,Ni}}$	$7841.97 - 4.133T$

Continued on next page

TableXI–Continued

$\mathrm{Ni_3Ga_2}$	${}^0G^{\mathrm{Ni_3Ga_2}}_{\mathrm{Ni:Ga}} - 0.4{}^0G^{\mathrm{ort}}_{\mathrm{Ga}} - 0.6{}^0G^{\mathrm{fcc}}_{\mathrm{Ni}}$	$-39753.31 + 5.55T$
$\mathrm{Ni_3Ga_4}$	${}^0G^{\mathrm{Ni_3Ga_4}}_{\mathrm{Ni:Ga}} - 0.57{}^0G^{\mathrm{ort}}_{\mathrm{Ga}} - 0.43{}^0G^{\mathrm{fcc}}_{\mathrm{Ni}}$	$-47790.8 + 9.04T$
$\mathrm{Ni_5Ga_3}$	${}^0G^{\mathrm{Ni_5Ga_3}}_{\mathrm{Ni:Ga}} - 0.37{}^0G^{\mathrm{ort}}_{\mathrm{Ga}} - 0.63{}^0G^{\mathrm{fcc}}_{\mathrm{Ni}}$	$-37658.61 + 5.34T$
	${}^0G^{\mathrm{Ni_5Ga_3}}_{\mathrm{Co:Ga}} - 0.37{}^0G^{\mathrm{ort}}_{\mathrm{Ga}} - 0.63{}^0G^{\mathrm{hcp}}_{\mathrm{Co}}$	-15746.6
$\mathrm{NiGa_4}$	${}^0G^{\mathrm{NiGa_4}}_{\mathrm{Ni:Ga}} - 0.8{}^0G^{\mathrm{ort}}_{\mathrm{Ga}} - 0.2{}^0G^{\mathrm{fcc}}_{\mathrm{Ni}}$	$-24367.51 - 2.71T$

It can be observed from the three isothermal sections of the ternary that there are two distinct phases present: γ and β. This two-phase region extends into the ternary over a wide range of composition, from the CoGa side towards the Ni-rich side. The γ phase is present in the Co and Ni rich regions and the β phase is present in the central region of the ternary. The γ' phase can be observed at compositions up to 30 at. % Ni. Additional phases δ and ϵ are also observed at 700 °C (Fig. 32). These intermetallic phases are observed below 700 °C between 30-40 at.% Ga as also reported by Ducher et al. [33]. The single phase regions are parallel to the CoNi region, with no solubility change in Ga. The β+γ two-phase region agrees well with the results reported by Ducher [33]. At 1000 °C (Fig 33), the concentrations at the two-phase β+γ phase boundaries compare well with the experimental results by Oikawa et al. [4, 9]. The equilibrium data obtained between the β,γ and γ' phases(three-phase triple point region) is in agreement with the results by Ducher [33]. At 1200 °C , it can be seen that the β and γ phase compositions compare well with our experimental work (Fig 34). It is observed that the two-phase β+γ region widens with decreasing temperature as also reported by Oikawa [4, 9].

b. Experimental results

Fig. 35 displays an optical micrograph of the $Co_{0.30}Ni_{0.45}Ga_{0.25}$ sample after homogenization at 1077 °C for 24 hrs followed by water quenching indicating two phase microstructure (β+γ).

Figures 36a-37b show X-ray diffraction pattern of $Co_{0.20}Ni_{0.65}Ga_{0.15}$,$Co_{0.30}Ni_{0.45}$ $Ga_{0.25}$, $Co_{0.80}Ni_{0.15}Ga_{0.05}$ and $Co_{0.05}Ni_{0.62}Ga_{0.33}$ alloys, respectively.

Overall, there is a good agreement between expected and observed phases at given temperatures (Table IX). According to the thermodynamics model the stable phase at 1200 °C for $Co_{0.05}Ni_{0.62}Ga_{0.33}$ and at 1127 °C for $Co_{0.20}Ni_{0.65}Ga_{0.15}$ is β and γ

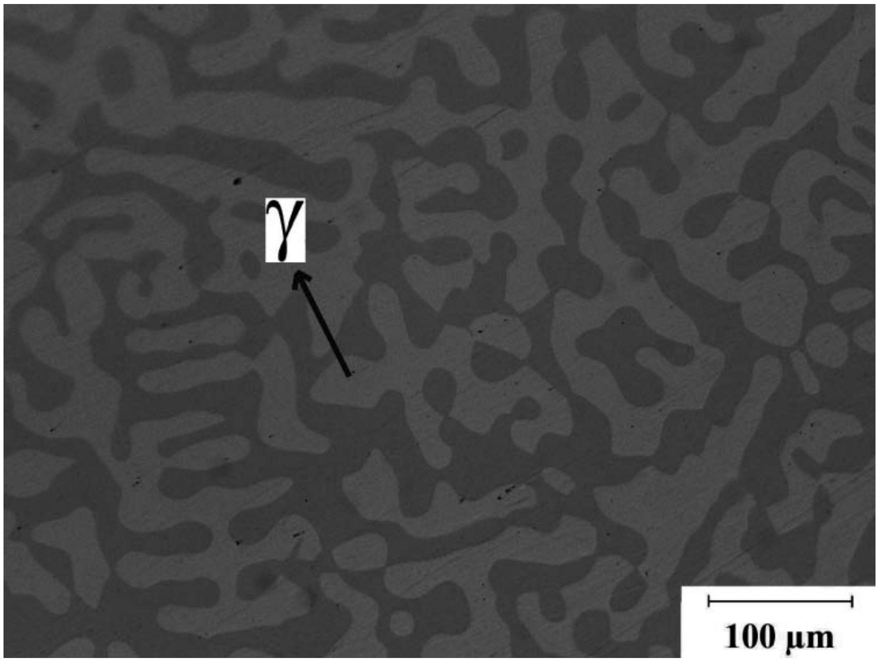

Fig. 35.: Optical micrograph of $Co_{0.30}Ni_{0.45}Ga_{0.25}$ sample after homogenization at 1077 °C for 24 hrs followed by water quenching indicating two phase microstructure (β+γ).

phase respectively, which agree well with experimental results. For $Co_{0.20}Ni_{0.65}Ga_{0.15}$, the thermodynamic model indicates two phase microstructure γ and (γ') phases at 300 °C but ageing at 300 °C for 1 week does not change the microstructure and stable structure is only γ phase. For $Co_{0.30}Ni_{0.45}Ga_{0.25}$, the X-Ray diffraction pattern (Fig. 36b) reveals two phase microstructure of β and γ phases, which has a good agreement with the model for 1077 °C. Again there is an inconsistency with the model which indicates Ni_5Ga_3 formation from β structure and γ phase when the sample is aged at 300 °C. However, aging at 300 °C for one week does not change the microstructure and the constitutive phases Fig. 36b. The discrepancy between the model and the experiment for 300 °C could be because one week is not enough to form such precipitates or thermodynamics model should be revised for this temperature. The expected

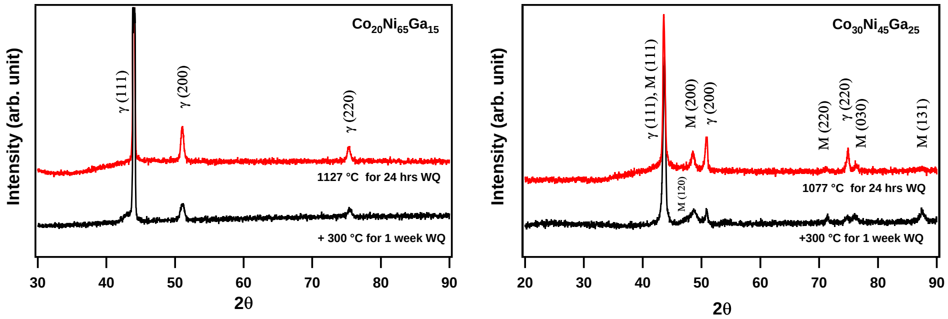

(a) (b)

Fig. 36.: X-ray diffraction pattern of the two samples (a) $Co_{0.2}Ni_{0.65}Ga_{0.15}$ and (b) $Co_{0.3}Ni_{0.45}Ga_{0.25}$ indicating the structures of the constitutive phases after different heat treatments. M: L10 martensite (B2), γ: A1 structure (disordered fcc), γ': L12 structure (ordered from fcc), hcp: A3 structure.

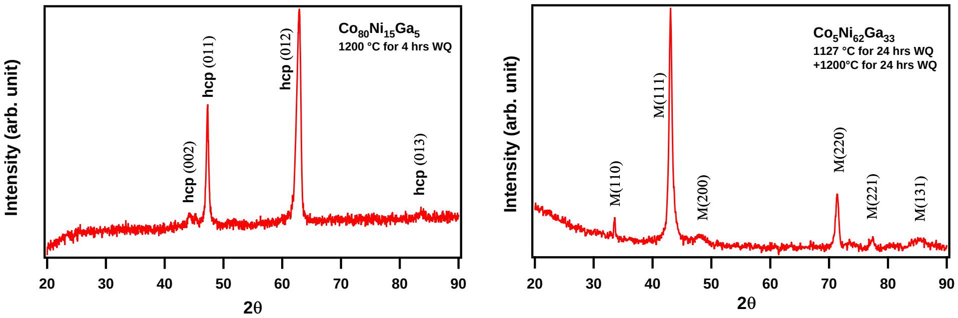

(a) (b)

Fig. 37.: X-ray diffraction pattern of the two samples (a) $Co_{0.8}Ni_{0.15}Ga_{0.05}$ and (b) $Co_{0.05}Ni_{0.62}Ga_{0.33}$ indicating the structures of the constitutive phases after different heat treatments. M: L10 martensite (B2), γ: A1 structure (disordered fcc), γ': L12 structure (ordered from fcc), hcp: A3 structure.

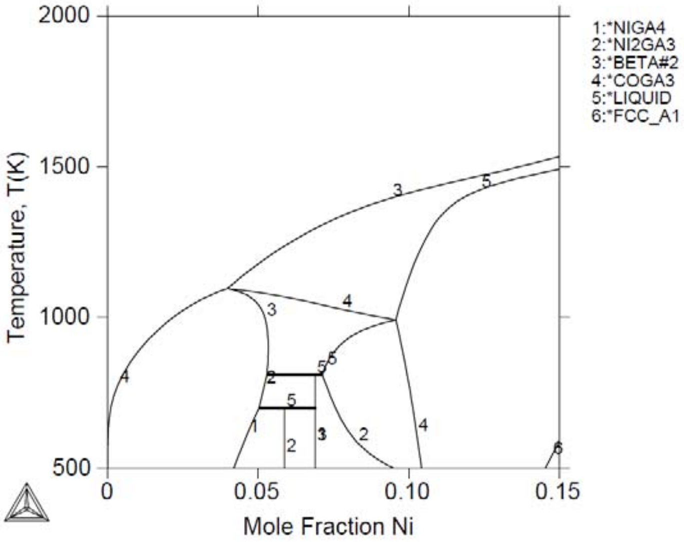

Fig. 38.: Vertical section of the CoNiGa system at x_{Co}/x_{Ni}=3:1 and 900 °C.

phase at 1200 °C for $Co_{0.80}Ni_{0.15}Ga_{0.05}$ alloy is single γ phase structure however hcp phase has been observed Fig. 37a.

2. Vertical sections, activities and partial enthalpy plots for different alloy compositions

Three vertical sections at 900 °C were calculated at constant x_{Co}/x_{Ni} 3:1,1:1 and 1:3 and can be seen in Figs. 38, 39 and 40.

The chemical activity of Ga (Ref.State:Liquid) in the ternary β phase was determined for varying compositions of Ga and temperature=900 °C and can be seen in Figs. 41, 42 and 43. It can be observed that the values of activities agree well with the results by Mikula et al. [110] for 40, 45 and 50 at.% Ga. Deviations are seen at 55 and 60 at.% Ga.

The partial enthalpy of the ternary β phase was determined for varying compo-

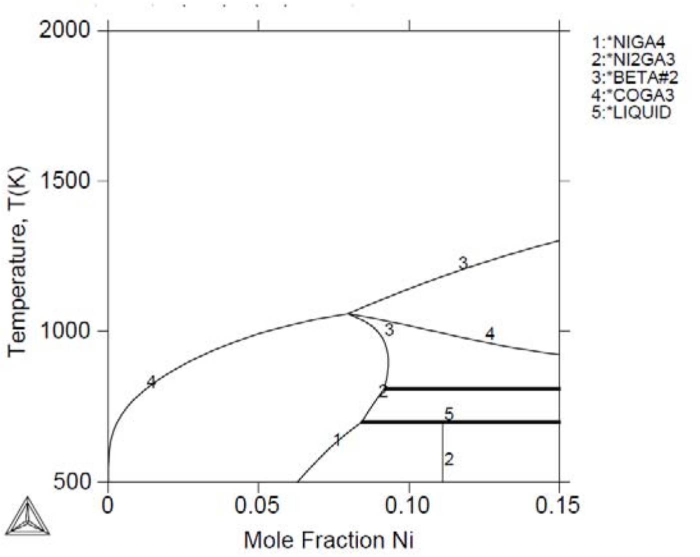

Fig. 39.: Vertical section of the CoNiGa system at x$_{Co}$/x$_{Ni}$=1:1 and 900 °C.

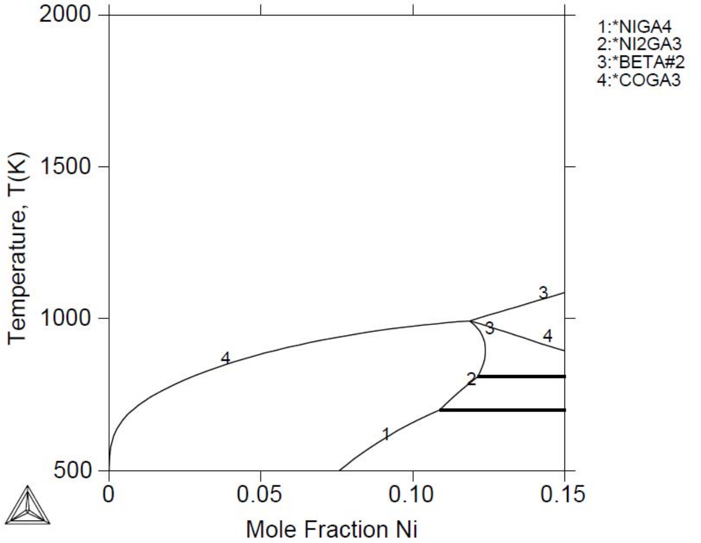

Fig. 40.: Vertical section of the CoNiGa system at x$_{Co}$/x$_{Ni}$=1:3 and 900 °C.

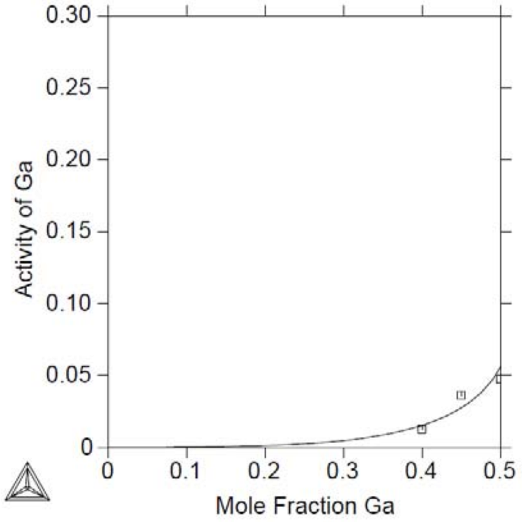

Fig. 41.: Activity of Ga in the β phase at x_{Co}/x_{Ni}=3:1 and 900 °C.

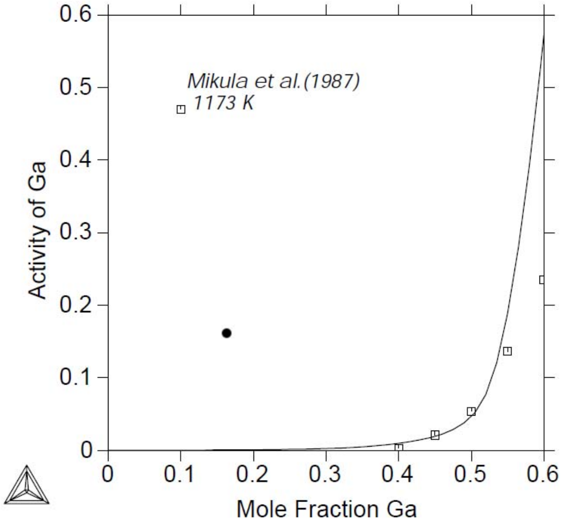

Fig. 42.: Activity of Ga in the β phase at x_{Co}/x_{Ni}=1:3 and 900 °C.

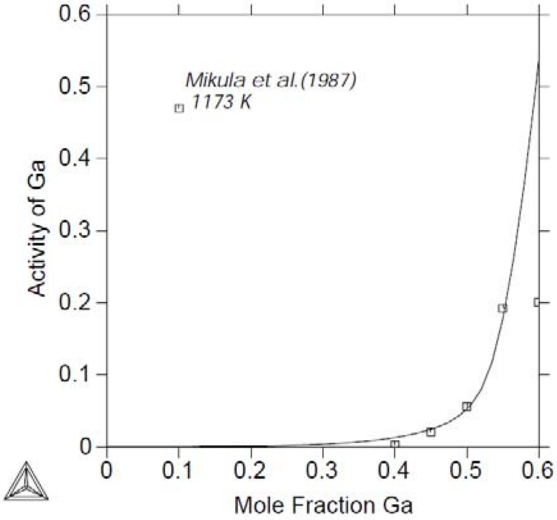

Fig. 43.: Activity of Ga in the β phase at x_{Co}/x_{Ni}=1:1 and 900 °C.

sitions of Ga and temperature=900 °C and can be seen in Figs. 44, 45 and 46. It can be observed that the partial enthalpies agree well with the results by Mikula et al. [110] for 50, 55 and 60 at.% Ga. Deviations are seen at 40 and 45 at.% Ga.

Mikula et al. [110] through their emf studies of the β phase, noticed considerable deviations of partial enthalpy and activity of Ga at 40 and 60 at. % when compared to theoretical calculations. A conclusion was hence made that that the phase boundary of the β phase in the ternary, could be close to or below 55 at. % Ga. In the present work, the β phase boundaries were found between 38 and 55 at. % Ga, hence agreeing with the experimental work by Mikula.

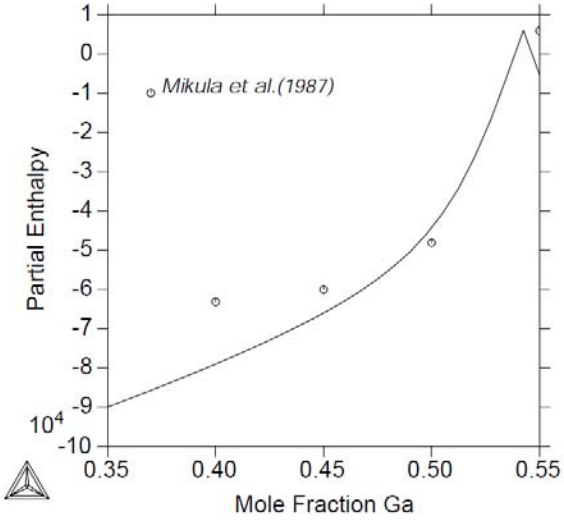

Fig. 44.: Partial enthalpy of β phase at x_{Co}/x_{Ni}=3:1 and 900 °C.

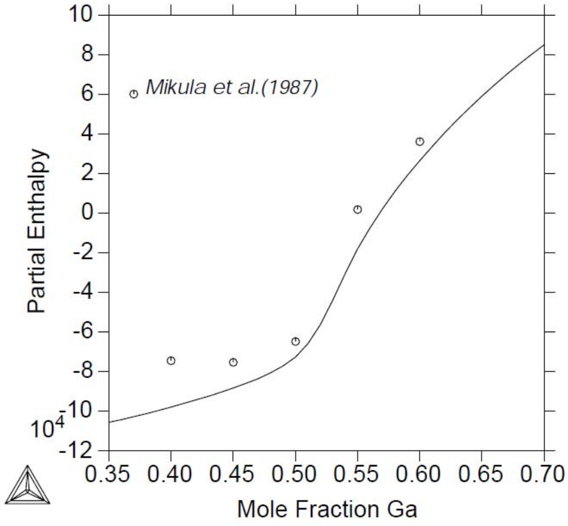

Fig. 45.: Partial enthalpy of β phase at x_{Co}/x_{Ni}=1:3 and 900 °C.

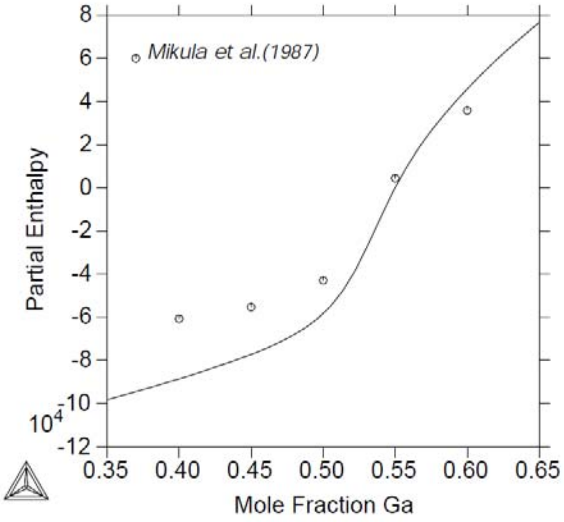

Fig. 46.: Partial enthalpy of β phase at x_{Co}/x_{Ni}=1:1 and 900 °C.

H. Conclusions

The phase equilibria among the γ (fcc), β, γ' (Ni_3Ga), δ (Ni_5Ga_3) and ϵ ($Ni_{13}Ga_9$) were determined at various temperatures using a computational (CALPHAD) approach coupled with experimental results in the CoNiGa High Temperature Shape Memory Alloy. The β phase was found to be observed in the central region of the ternary, parallel to the two-phase $\gamma+\beta$ region over a wide range of compositions, extending from the CoGa side to the NiGa side as seen in the CoNiAl system and it decreases in width with an increase in temperature. The phases expected from the thermodynamic model compared well with the observed phases from the experimental work. Activities and partial enthalpies calculated from the model compare well with experimental results. This model can be improved in future work by including order-disorder of the γ and γ' phases.

CHAPTER VII

CONCLUSION

The thermodynamic model of the ternary CoNiGa HTSMA was evaluated using a combined CALPHAD and Ab-Initio approach. ThermoCalc was used for the analysis. Thermodynamic properties like enthalpies, activities, phase fractions, site fractions of vacancies in the β phase, etc were calculated and compared with experimental data. The results compared well with the experimental data used, thus corroborating the present work. The same defect structure of the β phase in the binary CoGa and NiGa systems was used in the ternary. Similar results were obtained in the ternary while calculating site fractions of vacancies of the β phase, possibly due to point defects existing in the ternary (which controls martensitic transformation) leading to a conclusion that the ternary has a similar defect structure when compared to the corresponding binary systems.

The phase stability of the β, γ and γ' phases were determined over a wide range of compositions and temperatures. It was observed that the β phase exists in the central part of the ternary, over a wide range of composition, extending from the CoGa side to the NiGa side as seen in the CoNiAl system and it decreases in width with an increase in temperature. The phases expected from the thermodynamic model compared well with the observed phases from the experimental work. Since the β phase is the one that undergoes matensitic transformation, it is important to know it's stability in the ternary CoNiGa system. It was found that the β phase was incorrectly re-stabilizing above the liquidus in the binary CoGa system, thus making the extrapolation of the phase into the ternary difficult. Hence the CoGa system was remodeled to account for this artifact. The results obtained in the remodeled binary compared well with previously developed models of the CoGa system.

The thermodynamic properties of the B2 and L12 phases in the NiGa binary system were calculated using lattice dynamics. The study of thermodynamic properties is important to evaluate the structure of the phases present as well as study the influence of the structure of the components in the CoNiGa ternary. The low temperature phase stability of the NiGa system throughout the composition range via *ab initio* methods were also investigated in this work. The ground state of the NiGa binary was determined through a DFT-based high-throughput ground state search [13] over hundreds of possible binary crystal structures. The calculations were compared using three approximations namely LDA,GGA and PBE. The low temperature phase study and ground state calculations of the binary NiGa system helped to understand their behavior in the study of CoNiGa HTSMAs.

A. Future work

Martensitic transformation (M_s) is an important phenomenon in SMAs and this needs to be incorporated in the design of the system, for future work. A focus on how M_s changes with composition over a wide composition range would be useful to understand change in phase stability and kinetics of ductile and secondary phase precipitation in the system.This model can then also be used for alloy design. It would be desirable to incorporate the 1st order transition of order-disorder in the design although it is not a fundamental flaw or limitation in the design. It would definitely help to compare other similar systems with the same transition effects.

REFERENCES

[1] A.C. Kneissl, E. Unterweger, G. Lojen, I. Anzel, Microscopy and Microanalysis. 11 (2005)1704-1705.

[2] J. Pons, E. Cesari, C. Segu, F. Masdeu, R. Santamarta, Mater. Sci. Eng. A 57-65 (2008)481-482.

[3] C. Craciunescu, Y. Kishi, T.A. Lograsso, M. Wuttig, Scr. Mater. 47 (2002)285-288.

[4] K. Oikawa, T. Ota, F. Gejima, T. Ohmori,R. Kainuma, K. Ishida, Mater. Trans. 42 (2001)2472-2475.

[5] J. Liu, H. Xie, Y. Huo, H. Zheng, J. Li, J Alloys Comp. 420 (2006)145-157.

[6] J. Liu, M. Xia, Y. Huang, H. Zheng, J. Li, Effect of annealing on the microstructure and martensitic transformation of magnetic Shape Memory Alloys CoNiGa, J. Alloys Compd. 417 (2006)96-99.

[7] J. Dadda, H.J. Maier, I. Karaman, H.E. Karaca, Y.I. Chumlyakov, Pseudoelasticity at elevated temperatures in [001] oriented $Co_{49}Ni_{21}Ga_{30}$ single crystals under compression, Scripta Mater. 55(2006)663-666.

[8] K. Otsuka, H. Sakamoto, K. Shimizu, Successive stress-induced martensitic transformations and associated transformation pseudoelasticity in CuAlNi alloys, Acta Metallurgica 27(1979)585-601.

[9] K. Oikawa, T. Ota, Y. Imano, T. Omori, R. Kainuma, K. Ishida, J.Phase Equilib. Differ. 27(2006)75-82.

[10] N. Saunders, P. Miodownik, CALPHAD: Calculation of phase diagrams, in: Pergamon Materials Series, 1998.

[11] WebElements, (1993). Retrieved May 21, 2011, from http://www.webelements.com/.

[12] NASA Glenn, (2003). NASA Glenn Research & Technology. Retrieved May 21, 2011, from http://www.grc.nasa.gov/WWW/RT/RT2002/5000/5120noebe.html.

[13] W. Setyawan, S. Curtarolo, High-throughput electronic structure calculations: challenges and tools, Comp. Mater. Sci. 49(2010)299-312.

[14] S. Curtarolo, Duke University. (2008)

[15] N. Srivastava, G.J. Weng, J. Appl. Phys. 99(5)(2006)54-103.

[16] K. Otsuka, C.M. Wayman, Shape Memory Materials, London: Cambridge University Press, ISBN: 0521663849, 9780521663847, (1999)300.

[17] D.C. Lagoudas, C. Dimitris, Shape Memory Alloys: Modeling and engineering applications, SpringerLink, ISBN:0387476849. (2008)435.

[18] S.G. Braun, D.J. Ewins, S.S. Rao, Appl. Mech. Rev. 55(3)(2002)B45.

[19] P. Thomson, G.J. Balas, P.H. Leo, Smart Mater. Struct. 4(1995)36-42.

[20] S.K. Bhaumik, R.V. Krishnan, Proceedings of the SPIE. 5062(2003)879.

[21] J. Ryhänen. Biocompatibility evaluation of nickeltitanium shape memory metal alloy, University of Oulu. (1999)29.

[22] H. Lukas, S.G. Fries, B. Sundman, Computational thermodynamics:The CALPHAD method, ISBN:978-0-521-86811-2, 2007.

[23] B. Sundman, B. Jansson, J.O. Andersson, CALPHAD. 9(2)(1985)153-190.

[24] B. Jansson, B. Jönsson, B. Sundman, J. Agren, Thermochim. Acta. 214(1)(1993)93-96.

[25] B. Sundman, P. Shi, Electromchem. Soc. Proc. 97-39(1997)52-59.

[26] Thermo-Calc AB, Thermo-Calc user's manual, Version M. (1999).

[27] R. Ducher, R. Kainuma, K. Ishida K, Intermetallics. 15(2007)148-153.

[28] Clemens Schmetterer, Hans Flandorfer, L. Lengauer Christian, Jean-Pierre Bros, Herbert Ipser. 18(2010)277-285.

[29] S.Y. Lee, P. Nash. Phase diagrams of binary nickel alloys. Materials Park Ohio: ASM International (1991)133-40.

[30] K. Prusik, B. Kostrubiec, Goryczka, Dercz, P. Ochin, Morawiec, Mater. Sci. Eng. A 481-482(2008)330-333.

[31] A. Chari, A. Garay, R. Arroyave, CALPHAD. 34(2010)189-195.

[32] G.S. Firstov, J. Van Humbeeck, Y.N. Koval, High temperature Shape Memory Alloys: Problems and prospects, J. Intel. Mater. Sys. Struct. 17(12)(2006)1041-1047

[33] R. Ducher, R. Kainuma, K. Ishida, J Alloys Comp. 466(2008)208-213.

[34] W.X. Yuan, Z.Y. Qiao, H. Ipser, G. Eriksson, J. Phase Equilib. Diffu. 25 (2004)68-74.

[35] K. Micke, S.L. Markovski, H. Ipser, F.J.J. Van Loo, Ber Bunsen-Ges Phys Chem. 102(9)(1998)1240-4.

[36] U. Häussermann, M. Elding-Pontén, C. Svensson, C. Lidin, Chem Eur J. 102(1998)1240.

[37] T.B. Massalski, H. Okamoto, P.R. Subramanian, L. Kacprzak, Binary alloy phase diagrams. ASM International, ISBN: 978-0-87170-403-0, (1996)1829.

[38] S. Curtarolo, D. Morgan, K. Persson, J. Rodgers, G. Cedar, Phys. Rev. 91(2003)1355031-1335504

[39] O. Levy, G.L.W. Hart, S. Curtarolo, Uncovering compounds by synergy of cluster expansion and high-throughput methods, Journal of the American Chemical Society. 132(13)(2010)4830-4833.

[40] J. Gröbner,R. Wenzel, G.G. Fischer, R. Schmid-Fetzer, J. Phase Equilib. 20(6)(1999)615.

[41] H. Ipser, A. Mikula, W. Schuster, Monatsh Chem. 120(1989)283.

[42] X.Y. Zheng, J.C. Lin, D. Sweonson, K.C. Hsieh, Y.A. Chang, Mater Sci Eng B. 5(1)(1989)63.

[43] A. Guerin Rm Guivarc'h, J Appl Phys 66(5)(1989)2122.

[44] M.C. Le Clanche, S. Deputier, J.C. Jegaden, R. Guérin, Y. Ballini, A. Guivarc'h, J Alloys Compd. 206(1994)21.

[45] C. Wang, Z. Qiao, X. Xing, Y. Xie, Trans Nonferrous Met Soc China. 8(1)(1998)126.

[46] T. Ikeda, Y. Nosé, T. Korata, H. Numakura, M. Koiwa, J Phase Equilib. 20(6)(1999)626.

[47] P. Feschotte, P. Eggimann, J. Less-Common Met. (1979) 6315.

[48] E. Hellner, Z Metallkd. 41(1950)480-4.

[49] A.K. Niessen, A.R. Miedema, F.R. De Boer, R. Boom, Physica B. 152(3)(1988)303.

[50] E. Hellner, F. Laves, Z Naturfosch Teil. A 2(1947)177.

[51] R. Hultgren, P.D. Desai, D.T. Hawkins, M. Gleiser, K.K Kelley, American Society of Metals. (1973)918.

[52] D. Swenson, Mater. Res. Soc. Symp. Proc. 453(1997)367.

[53] J.N. Pratt, J.M. Bird, Martosudirjo, SUSNTI. AD Rep., no 786609/8GA 1(1974).

[54] L. Jingkui, X. Sishen, Sci. Sin. 26(1983)1305.

[55] T. Yamazaki, K. Terayami, T. Shimazaki, J Mater Sci Lett. 16(1997)1357.

[56] S.V. Yakovleva, S.T. Rogova, G.Z. Obukhova, R.N. Morzheedova, D.M. Karal'nik, USSR, Nauchnye Trudy, Gosudarstvennyi Nauchno-Issledovatel'skii Proektnyi Institut Redkometallicheskoi Promyshlennosti 57(1974)45.

[57] S. Martosudirjo, J.N. Pratt, ThermoChim. Acta. 17(1976)183.

[58] A. Van de Walle, G. Ceder, The effect of lattice vibrations on substitutional alloy thermodynamics, Reviews of Modern Physics. 74(1)(2002)11.

[59] W. Kohn, L.J. Sham, Self-consistent equations including exchange and correlation effects, Phys. Rev. 140(1965)A1133-A1138.

[60] G. Kresse, J. Furthmuller, Efficient iterative schemes for ab initio total-energy calculations using a plane-wave basis set, Phys. Rev. B 54(1996)11169.

[61] G. Kresse, J. Furthmuller, Efficiency of ab-initio total energy calculations for metals and semiconductors using a plane-wave basis set, Comput. Mater. Sci. 6(1996)15-50.

[62] J.P. Perdew, K. Burke, M. Ernzerhof, Phys Review Letters. 77(1996)3865.

[63] J.P. Perdew, K. Burke, M. Ernzerhof, Phys Review Letters. 78(1997)1396.

[64] Wang Perdew, Phys Rev. B 45(1992)13244.

[65] J.P. Perdew, A. Zunger, Self-interaction correction to density-functional approximations for many-electron systems, Phys. Rev. B 23(1981)5048-5079.

[66] D.M. Ceperley, B.J. Alder, Ground state of the electron gas by a stochastic method, Phys. Rev. Lett. 45(1980)566-569.

[67] J.P. Perdew, Y. Wang, Accurate and simple analytic representation of the electron-gas correlation energy, Phys. Rev. B 45(1992)13244-13249.

[68] M. Methfessel, A.T. Paxton, High-precision sampling for brillouin-zone integration in metals, Phys. Rev. B 40(1989)3616-3621.

[69] P.E. Blöchl, O. Jepsen, O.K. Andersen, Improved tetrahedron method for brillouin-zone integrations, Phys. Rev. B 49(1994)16223-16233.

[70] S. Curtarolo, G. L. W. Hart, W. Setyawan, M. Mehl, M. Jahnatek, R.V. Chepulskii, O. Levy, D. Morgan, AFLOW: Software for high-throughput calculation of material properties. (2009).

[71] A. Belsky, M. Hellenbrandt, V.L. Karen, P. Luksch, New developments in the inorganic crystal structure database (ICSD): accessibility in support of materi-

als research and design, Acta Crystallographica Section B: Structural Science. 58(3)(2002)356-369.

[72] H.J. Monkhorst, J.D. Pack, Special points for brillouin-zone integrations, Phys. Rev. B 13(1976)5188-5192.

[73] D. Shin, R. Arróyave, Z.-K. Liu, Phys. Rev. B 74(2006)024204-6.

[74] A. Van De Walle, M. Asta, G. Ceder, The alloy theoretic automated toolkit: A user guide, CALPHAD. 26(4)(2002)539-553.

[75] A. Van De Walle, Multicomponent multisublattice alloys, nonconfigurational entropy and other additions to the Alloy theoretic automated toolkit, CALPHAD. 33(2)(2009)266-278.

[76] R. Arroyave, D. Shin, Z.K. Liu, Acta Materialia. 53(2005)1809-1819

[77] B. Predel, W. Vogelbein, U. Schallner, Thermochim. Acta. 12(1975)367 (in German).

[78] H. Jacobi, D. Stöckel, H.L. Lukas, Z. Metallkd. 62(1971)305.

[79] I. Katayama, S. Igi, Z. Kozuka, Trans. JIM. 15(1974)447.

[80] J.N. Pratt, J.M. Bird, J Phase Equil. 14(1993)465.

[81] Su Xuping, J.-C. Tedenac, Intermetallics 13(5)(2005)467-473.

[82] X.S. Lu, J.K. Liang, D.F. Zhangm, Acta. Phy. Sin. 29(5)(1980)557.

[83] K.M. Wunsch, E. Watchel, Z. Met.kd. 73(1982)311.

[84] P. Esslinger, K. Schubert, Z. Met.kd. 48(1957)126.

[85] A.T. Dinsdale, CALPHAD 15(4)(1991)317.

[86] O. Redlich, A.T. Kister, Ind. Eng. Chem. 40(1948)345-348.

[87] K. Schubert, H.L. Lukas, H.G. Meissner, S. Bahn, Z. Met.kd. 50(1959)534.

[88] A.H. Van Ommen, A.A.H.J. Waegemaekers, A.C. Moleman, H. Schlatter, H. Bakker, Acta Metall 29(1981)123.

[89] D. Berner, Thesis, University of Stuttgart. (1976).

[90] N. Dupin, I. Ansara, Z. Met.kd. (1999)9076.

[91] E. Wachtel, V. Linse, V. Gerold, Phys Chem Solids. 34(1973)1461.

[92] G. Geibel, Diplomarbeitm Universitat Stuttgart; (1973).

[93] D. Berner, G. Geibel, Z.V. Gerold, E. Wachtel, Phys. Chem. Solids 36(1975)221.

[94] R. Haddad, M. Gaune-Escard, J.P. Bros, J. Alloys Compd. 247(1997)240.

[95] I. Katayama, N. Kemori, Z. Kosuka, Trans. Jpn. Inst. Met. 16(1975)423.

[96] B. Predel, W. Volgelbein, Thermocim. Acta. 13(1975)133.

[97] E.T. Henig, H.L. Lukas, G. Petzow, Z. Met.kd. 73(1982)87.

[98] G.L. Whittle, P.E. Clark, R. Cywinski, J. Phys. F: Metal Phys. 10(1980)2093.

[99] H. Meyer, M. Ellner, J. Alloys Compd. 26(1997)250-253.

[100] T. Nishizawa, K. Ishida, T.B. Massalski, Binary alloys phase diagrams. ASM International. (1990)1214.

[101] K. Ishida, R. Kainuma, N. Ueno0, T. Nishizawa, Metall. Trans. 22A(1991)441-446.

[102] J. Liu, J.G. Li, Scripta Mater. 56(2007)109-112.

[103] R. Kainuma, M. Ise, C.C. Jia, H. Ohtani, K. Ishida, Intermetallics. 4(1996)S151-S158.

[104] Y. Tanaka, K. Oikawa, Y. Sutou, T. Omori, R. Kainuma, K. Ishida, Mater. Sci. Eng. A 438-440(2006)1054-1060.

[105] R. Kainuma, K. Ishida, T. Nishizawa, Mater. Sci. Eng. 23A(1992)1147-1153.

[106] N. Ono, A. Tuskahara, R. Kainuma, K. Ishida, Mater. Sci. Eng. A 273-275(1999)420-424.

[107] T. Omori, N. Kamiya, Y. Sutou, K. Oikawa, R. Kainuma, K. Ishida, Mater. Sci. Eng. A 372(2004)403.

[108] K. Oikawa, T. Ota, T. Ohmori, Y. Tanaka, H. Morito, A. Fujita, R. Kainuma, K. Fukamichi, K. Ishida, Appl. Phys. Lett. 81(2002)5201.

[109] K. Oikawa, L. Wulff, T. Iijima, F. Gejima, T. Ohmori, A. Fujita, K. Fukamichi, R. Kainuma, K. Ishida, Appl. Phys. Lett. 43(2001)3290-3292.

[110] Mikula, W. Schuster, Y.A. Chang, E.T. Henig, Z. Met.kd. 78 (1987) 172.

[111] J.G. Booth, R. Cywinski, P.G. Prince, J. Magn. Mater. 7(1978)127-130.

[112] S.M. Hao, T. Takayama, K. Ishida, T. Nishizawa, Metall. trans. A 15A(1984)1819.

[113] J.C. Zhao, J. Mater. Sci. 39(2004)3913-3925.

[114] Y. Tanaka, T. Omori, K. Oikawa, R. Kainuma, K. Ishida, Mater. Trans. 45(2004)427.

[115] J. Liu, H.X. Zheng, Y.L. Huang, M.X. Xia, J.G. Li, Scripta Mater. 53(2005)29.

[116] D.B. Ingerly, D. Swenson, C.H. Jan, Y.A. Chang, J Appl. Phys. 80(1)(1996)543-550.

[117] D. Swenson, Y.A. Chang, J Phase Equlib. 16(6)(1995)510-515.

APPENDIX A

FUNCTIONS IN THE GAS PHASE DESCRIPTION

F6985:

$418307.916 - 34.9920304T - 20.82348TlnT - .00804072T^2 + 1.94275e^{-6}T^3$

$+69435.55T^{-1}$ $(298.14 < T < 600.00)$

$417194.563 - 4.48128666T - 25.91852TlnT - 3.2169625e^{-4}T^2 + 1.22796583e^{-8}$

$T^3 + 69799.8T^{-1}$ $(600.00 < T < 1600.00)$

$405652.322 + 60.9499874T - 34.4754TlnT + .0022698485T^2 - 1.11742517e^{-7}$

$T^3 + 2845478T^{-1}$ $(1600.00 < T < 5300.00)$

$616085.763 - 445.433806T + 24.5681TlnT - .00520688T^2 + 6.847335e^{-8}T^3$

$-1.3989465e^{8}T^{-1}$ $(5300.00 < T < 10000.00)$

F9633:

$259072.278 + 88.0130706T - 38.71057TlnT + .01053784T^2 - 9.86907833e^{-7}$

$T^3 + 338489.2T^{-1}$ $(298.14 < T < 600.00)$

$263812.519 + 33.4871435T - 30.75007TlnT + .00537745T^2 - 5.46534e^{-7}$

$T^3 - 150942.65T^{-1}$ $(600.00 < T < 1400.00)$

$270292.501 - 28.1810494T - 21.9834TlnT + 3.192416e^{-4}T^2 - 1.46299133e^{-8}$

$T^3 - 992093T^{-1}$ $(1400.00 < T < 6000.00)$

$340110.007 - 140.262257T - 9.704267TlnT - 4.5138725e^{-4}T^2 - 1.13427367e^{-8}$

$T^3 - 68387950T^{-1}$ $(6000.00 < T < 10000.00)$

F9695:

$422882.385 - 36.0787973T - 33.72863TlnT - .009368525T^2 + 7.62775167e^{-7}$

$T^3 - 19520.385T^{-1}$ $(298.14 < T < 1100.00)$

$419324.178 + 8.33965897T - 40.33555TlnT - .00418541135T^2 + 2.679565e^{-8}$

$T^3 + 312119.6T^{-1}$ $(1100.00 < T < 2500.00)$

VITA

Arpita Ramesh Chari received her Bachelor of Engineering degree in mechanical engineering from M.S.Ramaiah Institute of Technology, Bangalore, India. She entered the Master of Science program in mechanical engineering at Texas A&M University in August 2008 and received her degree in August 2011. Her research was based on computational thermodynamics, focussing on the study of high temperature Shape Memory Alloys such as CoNiGa. She has published a paper on the remodeling of the CoGa system and has 2 other papers ready to publish based on her research.

She may be reached at Texas A&M University, Department of Mechanical Engineering, 3123 TAMU, College Station TX 77843, USA. Her email address is arpita.chari @neo.tamu.edu.